CHARACTERIZATION OF *IN VITRO* TRANSCRIBED MRNA FOR OPTIMAL EXPRESSION IN THERAPEUTIC APPLICATIONS

A Dissertation
Presented to
The Academic Faculty

by

Jonathan Lee Kirschman

In Partial Fulfillment
Of the Requirements for the Degree
Doctor of Philosophy in Biomedical Engineering in the
Wallace H. Coulter Department of Biomedical Engineering

Georgia Institute of Technology
Emory University
August, 2017

CHARACTERIZATION OF *IN VITRO* TRANSCRIBED MRNA FOR OPTIMAL EXPRESSION IN THERAPEUTIC APPLICATIONS

Approved by:

Dr. Philip Santangelo, Ph.D., Advisor
Department of Biomedical Engineering
Georgia Institute of Technology

Dr. Garrett Stanley, Ph.D.
Department of Biomedical Engineering
Georgia Institute of Technology

Dr. Krishnendu Roy, Ph.D.
Department of Biomedical Engineering
Georgia Institute of Technology

Dr. Thomas Barker, Ph.D.
Department of Biomedical Engineering
University of Virginia

Dr. Loren Williams, Ph.D.
School of Chemistry and Biochemistry
Georgia Institute of Technology

Date Approved: July 12th, 2017

ACKNOWLEDGEMENTS

This PhD work would not have been possible without the kind guidance and support from other lab members in the Santangelo lab. My advisor Philip Santangelo of course played an important part of my entire graduate career, and I'll always appreciate that he continued to be supportive when unfortunate real life events put me in a tough spot. I'd also like to thank Jinmo Gu from the Cho lab at Emory, Clarissa Whitmire from the Stanley lab at Georgia Tech, and the folks at Axion Biosystems. Finally, friends and family provided unconditional support and encouragement that I could not have done without.

TABLE OF CONTENTS

LIST OF TABLES

LIST OF FIGURES

LIST OF SYMBOLS AND ABBREVIATIONS

2-AP	2-aminopurine
5meC	5-methylcytosine
5moC	5-methoxycytosine
5moU	5-methoxyuridine
C16	Imidazole-oxindole
DNA	deoxyribonucleic acid
dsRNA	double-stranded ribonucleic acid
EGFP	enhanced green fluorescent protein
EIF4E	eukaryotic initiation factor 4E
FBS	fetal bovine serum
FISH	fluorescent in situ hybridization
HPLC	high-performance liquid chromatography
IM	intramuscular
Ifnβ1	interferon-beta 1
Il1β	interleukin-1 beta
IPS-1	interferon-beta promoter stimulator 1
IVT mRNA	in vitro transcribed messenger ribonucleic acid
L2K	Lipofectamine-2000
M1Y, 1MY	N^1-Methylpseudouridine
MDA5	melanoma differentiation-associated protein 5
MTRIP	multiply-labeled tetravalent ribonucleic acid imaging probes

NF-κB	nuclear factor-κB
OAS	2'-5'-oligoadenylate synthetase
PAMP	pathogen-associated molecular pattern
PBS	Phosphate-buffered saline
PEI	polyethylenimine
PKR	protein kinase RNA-activated
PLA	proximity ligation assay
PRR	pathogen recognition receptor
qRT-PCR	quantitative reverse transcription polymerase chain reaction
RBP	RNA-binding protein
RIG-I	retinoic acid-inducible gene 1
RISC	RNA-induced silencing complex
RNA	ribonucleic acid
RNP	ribonucleoprotein
SG	stress granule
siRNA	silencing ribonucleic acid
ssRNA	single-stranded RNA
TLR	toll-like receptor
UTR	untranslated region
Ψ, Y	pseudouridine, pseudoU

SUMMARY

The use of synthetic messenger ribonucleic acid (mRNA) to express proteins is a highly promising therapeutic and vaccine approach that avoids many safety issues associated with viral or DNA-based systems. However, in order to optimize mRNA designs and delivery, technology advancements are required to study fundamental mechanisms of mRNA uptake and localization at the single-cell and tissue level. Here, we present a single RNA sensitive fluorescent labeling method which allows us to label and visualize synthetic mRNA without significantly affecting function. This approach enabled single cell characterization of mRNA uptake and release kinetics from endocytic compartments, the measurement of mRNA/protein correlations, and motivated the investigation of mRNA induced cellular stress, all important mechanisms influencing protein production. Using protein expression and cellular stress as metrics, messenger RNA was rationally designed through incorporation of chemically modified nucleotides, variations in UTRs, incorporation of cell-type specific micro RNA sites, and co-delivery with small molecules. In addition, we demonstrated this approach can facilitate near-infrared imaging of mRNA localization in vivo and in ex-vivo tissue sections, which will accelerate mRNA trafficking studies in pre-clinical models. Last, I demonstrate the effectiveness of this labeling approach through the expression of opsins, light-sensitive ion channels, in primary rat cortical neurons and cardiomyocytes. Overall, the ability to study fundamental mechanisms necessary to optimize delivery and therapeutic strategies was demonstrated, in order to design the next generation of novel mRNA therapeutics and vaccines.

CHAPTER 1

INTRODUCTION

Background

Messenger RNA (mRNA) therapeutics show great potential as a method of gene delivery for the expression of therapeutic proteins and vaccines. In vitro transcribed (IVT) mRNA is a platform technology, such that both native cellular proteins as well as novel protein designs can be specifically determined by sequence, allowing the rapid generation of new therapeutic strategies. Compared to DNA-based therapeutics, IVT mRNA has distinct advantages in safety, attributable to its inability to integrate into genomes as well as the temporary nature of RNA expression. Additionally, by eliminating the intracellular transcription step, the amount of protein expressed and the temporal initiation of expression is better controlled.

However, despite the enthusiasm for RNA-based therapeutics based on their potential, and even a number of clinical trials in progress, there are barriers which need to be traversed before RNA-based therapeutics can successfully be brought to the clinic. Due to the lack of intracellular transcription as an amplification step, the amount of protein expression is limited by the amount of mRNA delivered to a target cell. Furthermore, a successfully delivery strategy must also encompass the effects of innate immune activation. Delivering higher amounts of mRNA in order to improve protein expression must account for the possibility of activation of cellular defense mechanisms, which is not only counterproductive, as one of the consequences is global translational arrest, but this also

may trigger unwanted side effects and even cellular apoptosis. Cellular innate immune mechanisms have evolved over millennia to combat viruses, and in turn, viruses have evolved to counteract these mechanisms. IVT RNA therapeutics must follow this example and also evolve in order to successfully function.

Differences between IVT mRNA and endogenous mRNAs.

Endogenous mRNA is transcribed in the nucleus and undergoes processing and finally export from the nucleus in a highly regulated manner. Much of this regulation is performed through the action of RNA-binding proteins (RBPs). Processing involves 5' capping, the addition of a poly-A tail on the 3' end, removal of introns via splicing, and the binding of various proteins to the cap, the 3'-UTR region, and the polyA tail. One of these is the cap binding complex, which once in the cytoplasm is involved in initiation of the pioneering round of translation through exchange with the initiation factor eIF4e, resulting in mRNA circularization and finally the progression to steady state translation. During their entire lifetime, endogenous mRNAs are covered in RBPs forming an RNA-protein complex, also known as ribonucleoproteins (RNPs).

IVT mRNAs do not have a nuclear history, and are instead initially bound only to a delivery vehicle or other delivery formulation components. Instead of entering the cytosol via the nucleus, they typically enter through the endosomal system (1,2), where they may be subject to detection by toll-like receptors (TLRs). Of particular note are TLR3, which detects double stranded mRNA (3-5), and TLRs 7/8, which can detect single stranded RNA (3,6-8). Currently, it is not clear whether exogenous mRNAs interact with the same RNA binding proteins as native mRNAs and if they assemble into RNP complexes in a similar manner.

Innate immune response to exogenous mRNA

Exogenous mRNA has been successfully utilized to generate proteins in both cell culture and *in vivo*. In 1998, human dendritic cells were transfected with carcinoembryonic antigen-encoding mRNA and shown to stimulate a potent cytotoxic T lymphocyte response *in vitro* (9). This methodology was later adapted to generate an immune response to mRNA encoding the HIV Gag protein (10). However, a significant challenge was the induction of strong interferon responses, which hindered efficacy of T cell immunity. Additionally, exogenous mRNAs complexed with cationic lipids were shown to trigger TLR3, TLR7, and TLR8 signaling in cell cultures (4,11). The double-stranded RNA sensors Protein Kinase RNA-activated (PKR) and Retinoic acid-inducible gene I (RIG-I) were also shown to be induced upon lipid-based transfection of exogenous mRNA (12), though signaling by TLR3 was not affected by the PKR-inhibitor, 2-Aminopurine (4).

Appropriate manufacturing is a critical step in enhancing mRNA effectiveness. Efficient enzymatic m7G capping of the 5' triphosphate end reduces or potentially eliminates sensing by RIG-I (12). Incorporation of modified nucleosides into synthesized mRNA can reduce PKR and 2'-5'-oligoadenylate synthetase (OAS) activation in a structure-specific manner in cells as well as improve biological stability (13-15). This was further demonstrated by Kormann et al (3) who used mRNA with the partial incorporation of 2-Thiouridine and 5-methyl cytidine (5meC) to successfully express proteins in mice using intramuscular (IM) injection, tail-vein injection, and intratracheal high-pressure spraying. Finally, high pressure liquid chromatography (HPLC) purification of mRNA has a profound effect in reducing immune activation and increasing translational potential, thus reaction contaminants should be effectively removed during processing (16). For example,

HPLC-purified pseudouridine-incorporated mRNAs were used to successfully increase serum EPO levels in mice with a demonstrable increase compared to unmodified mRNAs (17). Alternatively, unmodified but codon-optimized mRNA and protamine-complexed mRNA has been demonstrated as a self-adjuvating vaccine to modulate immune responses and has progressed through Phase I and II clinical trials in prostate cancer and non-small cell lung carcinoma patients (18-20). How codon-optimized, yet purified, unmodified mRNA can avoid significant TLR activation is currently unknown.

In the field of stem cells, synthetic modified mRNA was successfully used to reprogram human cells to pluripotency (21). Synthetic mRNA encoding vascular endothelial growth factor-A was also used in a mouse myocardial infarction model to induce vascular regeneration (22).

Tools for mRNA characterization

Imaging IVT mRNA at the subcellular level is critical for understanding the mechanisms involved in protein expression as well as studying intracellular mRNA localization. There are currently very few methods for visualizing IVT mRNA. The most common technique is to use an enzymatic linker to covalently bond fluorophores to the mRNA (23,24). However, covalent labeling can adversely affect translatability of the mRNA, as well as altering dynamics of delivery and localization (25). Conversely, incorporation of radioactive nucleotides during synthesis nay allow translatability at the expense of difficult handing and limited matching imaging modalities. Hybridization labeling methods such as Stellaris FISH probes consist of 20-50 nucleic acid oligos containing a single fluorophore each which require several binding sites in order to reach levels adequate for detection (26).

Thesis outline

In order to improve the efficacy of mRNA expression, we first created a labeling assay in order to quantify IVT mRNA at the single cell and single molecule level. The labeling assay had the requirement to not interfere with protein production or delivery in order to become a useful metric. We describe this method in Chapter 2 and apply it in order to understand critical mechanisms regulating IVT mRNA expression. We examined IVT mRNA expression in the context of different delivery routes, and measured levels of innate immune activation in the form of stress granule formation.

In Chapter 3, we focused on modify IVT mRNA in three ways: sequence modification, chemical modifications, and co-delivery with small molecules. We established that certain chemical modification provide higher levels of protein production, but do not achieve maximum potential due to lessened but still detectable levels of innate immune activation. Co-delivery with small molecule inhibitors allows further increases in protein production. Delivery formulation is also important, as it has an effect on the pathway into the cell, the amount of mRNA that reaches the cytosolic compartment, and interactions between mRNA and cellular machinery. Finally, we found that engineering the mRNA sequence can alter interactions with cellular proteins and affect the fate of the mRNA.

In Chapter 4, we applied the mRNA design principles gleaned from earlier chapters in order to design mRNA to contribute to the field of optogenetics. We designed mRNA encoding light-sensitive ion channels, opsins, which allow control over electrical

firing activity in primary neurons and cardiac cells. We successfully expressed opsins and were able to verify their function using multi electrode arrays.

In Chapter 5, we describe future aims regarding effective mRNA delivery and expression in more complex applications. We show preliminary data that shows the capability of co-delivery of multiple mRNA-expressed opsins which allows effective on/off control of cardiac cell beating with different wavelengths of light. We finally show mRNA expression and the distribution *in vivo* following injection into the rat brain. These represent some of the future possibilities achievable through the rational design of mRNA.

CHAPTER 2

METRICS FOR CHARACTERIZATION OF MESSENGER RNA

This work presented here is an excerpt from Kirschman, JL, Bhosle, S, Vanover, D, Blanchard, EL, Loomis, KH, Zurla, C, Murray, K, Lam, BC, Santangelo, PJ (2017). "Characterizing exogenous mRNA delivery, trafficking, cytoplasmic release, and RNA-protein correlations at the level of single cells." Nucleic Acids Res gkx290.

Background

The use of exogenous, *in vitro* synthesized mRNA as an expression vector for therapeutic or antigenic proteins is highly promising. Expression of mRNA-encoded proteins is transient and more direct than DNA-based vectors, which requires intermediate steps such as nuclear localization and transcription. Additionally, mRNA vectors do not pose safety risks such as genomic integration, antibiotic resistance, or strong immunogenic responses due to a replicating vector (27).

Exogenous mRNA has been successfully utilized to generate proteins in both cell culture and *in vivo* (9,10). In order to obtain therapeutic levels of protein expression, strategies for improving *in-vitro* transcribed (IVT) mRNA, such as through the incorporation of modified nucleosides (3,14,28) and purification methods (16), have been the subject of intense study. Despite these improvements, mechanistic studies of mRNA delivery, protein production and innate immune activation at the single cell and single molecule level are needed. The primary reason why these studies have not been performed is the lack of approaches to measure cellular mRNA uptake without compromising

translational potential, interactions with cellular proteins or altering the uptake pathway (29). Current studies are limited to direct-nucleotide labeling methods and the use of mathematical models to approximate mRNA–protein correlations (30,31). Lorenz *et al.* provided evidence that naked mRNA delivered *in vitro* enters cells via receptor-mediated endocytosis and predominantly remains in endosomes (1). Even though this mRNA was not functional, which is a significant drawback of direct labeling, this work highlighted the importance of tracking the subcellular location of delivered mRNA, and, in particular, the number of molecules that reach the cytosolic compartment, the cellular site of translation. In the siRNA community, the inability to measure cytosolic levels of siRNA has greatly limited the optimization of siRNA-based therapeutics, and only recently this barrier was overcome but using low throughput methods such as electron microscopy or single vesicle tracking (32,33); the approach presented here for mRNA, allows for a more rapid, quantitative assessment of cytoplasmic delivery.

Given the enormous potential for mRNA therapeutics and vaccines, we developed a strategy to address these limitations. Here, we present a general methodology for characterizing delivered mRNA at the level of single cells and single RNAs, *in vitro* and *in vivo*. We first constructed fluorescent imaging probes, multiply labeled tetravalent RNA imaging probes (MTRIPs), which bind, via nucleic-acid hybridization, to the 3′ UTR region of synthetic mRNA (34-37). The 3′ UTR of mRNA was used as a binding site in order to preclude any interference with ribosomal loading or progression, and thus prevent interference with translation. Due to the small size of the 3′ UTR of most mRNAs, typically ∼100nt long, a limited number of probes can be bound to the mRNA thus multi-fluorophore probes are necessary to ensure adequate brightness. MTRIPs carry 8–10

fluorophores per probe and when 2–3 probes are bound to an mRNA, allow for 20–30 fluorophores per mRNA, making them easily visible with most fluorescent microscopes and in tissue. In previous publications, we successfully utilized MTRIPs to visualize endogenous mRNAs, viral genomic RNA, as well as plasmid-derived transcripts. Other approaches, such as molecular beacons, etc., only contain one fluorophore per probe, which given the short 3′-UTR, would limit labeled-mRNA brightness and thus the detection of mRNAs. Labeling of mRNA with MTRIPs, in contrast to covalent incorporation of fluorophores, does not significantly affect the behavior or localization of target mRNA and does not illicit cellular immune responses (38-42). Finally, this method does not require large sequence incorporations into the mRNA itself or co-expression with reporters, such as with the MS2 aptamer and MS2-like systems (43).

In order to use MTRIPs to label IVT mRNA, we optimized binding conditions between the mRNA and MTRIP probes through an iterative process where temperature, salt concentration, incubation time and filtration method were varied. Heat was applied to remove secondary structure in the mRNA. Salt concentration allowed stabilization of the hybridization reaction over time. Finally, filtration was used to remove excess probe while minimizing loss of mRNA (see Materials and Methods). We labeled *in vitro* transcribed mRNA consistently with approximately two probes per mRNA and verified that they do not significantly affect translation.

We then applied this labeling strategy to perform a mechanistic characterization of mRNA delivery in cells. Key mechanisms of importance are noted in Figure 2.1A, including mRNA entry pathway, cytoplasmic release, translational efficiency

(RNA/protein correlation), and PKR activation. Here, we demonstrate the ability of our tools to address these mechanisms. Fully addressing each mechanism across all conditions and cell types is beyond the scope of this work, but the measurements presented set the stage for future studies.

We started with entry pathway, followed by whole cell quantification of mRNA uptake, and the quantification of the fraction of mRNA released into the cytosolic compartment. As a model system, we used primary human skeletal muscle cells (HSkMC) in the myoblast stage of development, because IM injection is the most commonly used delivery method for vaccine applications and is relevant for therapeutic delivery due to its practical nature.

The entry pathway is a critical metric for assessing the mechanistic action of different formulations of cationic lipids, lipid nano-particles and other delivery vehicles. The mode of entry can determine downstream interactions with cellular machinery and thus modulate the efficiency of protein expression (44). Traditional methods of colocalization analysis are very useful but can be hindered by imaging limitations. In specific instances, mRNA and an endocytic marker were found to be adjacent with indications of partial encirclement but with little or no overlap. In order to clarify the relationship between the mRNA and pathways of endocytosis, we hypothesized that a proximity-based assay between delivered mRNA and specific endocytic markers would be a more accurate and easily quantifiable method for describing the entry pathway used by the mRNA. Therefore, we performed a proximity ligation assay (PLA), an ideal strategy for the quantitative assessment of the interactions of molecules in the cellular environment (38,45-48). RNA–protein PLA assays

have been pioneered by our lab (34,39-41,49). This method allowed us to differentiate between clathrin-mediated endocytosis, caveolae-mediated endocytosis and clathrin/caveolin-independent pathways in a proximity dependent, and easily quantifiable fashion.

Next, we studied mRNA uptake and expression, which are necessary metrics for generating kinetic models for drug optimization and design (30,31) in the context of both unmodified and modified nucleotides. To date, studies on mRNA therapeutics or vaccines have focused on expression or uptake separately, but were not able to measure these factors simultaneously due to limitations in labeling technologies as described earlier. Using MTRIP-labeled mRNA encoding for a fluorescent reporter, we measured both total mRNA uptake and protein expression per cell using flow cytometry. We extended this measurement to include two delivery methods, cationic lipid complexes and electroporation, and both unmodified and modified mRNA, using 5-methyl-cytidine (5meC) and pseudouridine (Ψ), two commonly used and previously studied modifications. Cationic lipids have been in use for over two decades and are known to deliver nucleic acids into the cell via clathrin and caveolin-mediated endocytosis (42,50). In contrast, electroporation is known to deliver molecules directly to the cytoplasm, where they may interact with various cellular structures, such as microtubules or freely diffuse (51). Delivery via cationic lipids resulted in two populations of mRNA: mRNA trapped in the endocytic compartment, and mRNA released into the cytosol. This allowed us to relate protein production and mRNA localization directly for these two prominent delivery modalities and as a function of mRNA chemistry. Given cationic lipid delivery is complicated by endocytic trapping of mRNA, we next examined the contribution of

cytosolic mRNA. The cytosolic fraction of the mRNA, following release from lipoplexes, represents, at any particular time, the fraction of delivered mRNA which has the potential to interact with translational complexes in order to produce protein (31).

In order to better assess the amount of translatable mRNA per cell, we specifically measured the amount of cytosolic mRNA by using MTRIP-labeled mRNA and performed intracellular antibody staining for the endocytic pathway, using multiple markers, in order to ensure maximum coverage of the entire system. We were able to measure the amount of cytosolic mRNA based on colocalization analysis via high resolution, high dynamic range imaging (33) combined with image processing tools. This approach would not be practical using single labeled probes as they would not be bright enough to detect cytoplasmic mRNA, due to the extremely high dynamic range of signals within the cells.

Cytosolic mRNA can also bind to innate immune sensors which detect exogenous nucleic acids, competing with the translational machinery (52-55). Thus, the copy number of mRNA in the cytosol is dependent on both translation initiation and activation of pattern recognition receptors, such as Protein Kinase R (PKR) (14,21). In order to better understand the contribution to protein production of translation versus innate immune activation, we again used an EGFP mRNA variant modified by the complete incorporation of 5-methyl-cytidine (5meC) and pseudouridine (Ψ), which is known to reduce immune activation (3). Flow cytometry analysis of HSkMCs following lipofection showed an increase of EGFP expression in cells lipofected with mRNA incorporating modified nucleotides, as well as higher transfection efficiencies. This increase was not observed in the case of electroporation. We hypothesized that this was the result of a stress response

due to PKR. Interactions between double stranded sections of delivered mRNA and PKR trigger phosphorylation of the eukaryotic initiation translation factor 2α subunit (eIF2α). This decreases global translation by reducing formation of the ternary complex, stalling translation initiation and causing dissociation of ribosomes (56-58). A direct result of eIF2α phosphorylation is SG formation, which we used via intracellular antibody staining as an indicator for cellular stress upon transfection. We then verified that this was due to PKR using siRNA and a PKR-knockout cell line.

Finally, we verified that this labeling methodology allows for mRNA localization without precluding protein expression *in vivo*. To do so, we utilized the Fluobeam system, an *in-vivo*, near-IR fluorescence imaging system. It consists of a portable and adjustable fluorescence excitation and emission detection system, which allows for real-time intraoperative imaging during surgery. We imaged mRNA in living mice upon intra muscular injection (IM), during post-transfection surgery, and in *ex-vivo* tissue sections. We verified that protein production remained unhindered and that MTRIPs remain on the mRNA after intramuscular injection.

Overall, we demonstrate the ability of our labeled mRNA approach to make critical measurements necessary to optimize mRNA delivery and efficacy. Unfortunately, mRNA delivery, release and translation are complex, and optimization necessitates the ability to make multiple types of measurements, which we demonstrate here.

Labeling of exogenous mRNA with MTRIPs

In order to use MTRIPs (Figure 2.1A) to label IVT mRNA, we designed four MTRIPs complementary to the 3′ untranslated region (UTR) of our *in vitro*transcribed EGFP mRNA, a 93 bp sequence derived from the mouse alpha globin 3′ UTR. We optimized binding conditions through an iterative process where temperature, salt concentration, incubation time and filtration method were varied. We first verified binding of probes to the target mRNA via agarose gel, where labeled mRNA exhibited reduced migration (Figure 2.2) with respect to naked mRNA or denatured mRNA. Labeling efficiency was tested using exclusion chromatography, which resulted in a degree of labeling of approximately two MTRIPs per mRNA, based on the difference in fluorescence signal between MTRIP-labeled mRNA and the same amount of MTRIPs alone prior to filtering (Figure 2.3). We measured the effects of variations in incubation time and temperature, and determined that optimal binding occurs through a short, 10 min heat induced denaturation of mRNA to remove secondary structures, followed by addition of MTRIPs and an incubation overnight at 37°C. We also examined the effect of different buffers, including PBS and SSC at multiple concentrations, and found that PBS provided an adequate salt concentration to stabilize binding of MTRIPs to mRNA. Finally, filtration was necessary to remove unbound MTRIPs. We found that a 200 kD molecular weight cutoff filters provided the highest yield of mRNA while removing unbound MTRIPs.

To demonstrate that MTRIPS remained bound to mRNA upon delivery, HeLa cells were lipofected with Dylight 650-labeled mRNA. Cells were subsequently hybridized post-fixation with Quasar 570 Stellaris RNA FISH probes specific for the coding region

(40). MTRIPs exhibited a high degree of colocalization (Costes overlap coefficient of ~0.6, Manders overlap coefficients m1 and m2 were ~0.6 and ~1 respectively) with FISH probes compared to controls using mRNA with an identical UTR but a different coding region corresponding to Chemokine Ligand 3 (Figure 2.1B, Figure 2.4).

Electroporation and transfection via Lipofectamine 2000 (L2K) of HSkMCs with labeled EGFP mRNA yielded highly distinct distributions of intracellular mRNA. Electroporation resulted in a large number of lower intensity, dispersed mRNA granules while lipofection resulted in a few bright, large granules with a lower number of smaller granules dispersed through the cell (Figure 2.1C).

A strong benefit of using MTRIPs bound to the 3′ UTR region is that they do not significantly inhibit the translation of endogenuous mRNA (34,59). To demonstrate that the labeling of mRNA does not affect translation, we measured differences of protein production following electroporation of HSkMCs cells with labeled and unlabeled mRNA using flow cytometry. Labeled mRNA showed a similar protein expression distribution as unlabeled mRNA. The small decrease in protein production is likely attributable to RNA loss during the purification step following the labeling reaction (Figure 2.1D).

Entry pathway and subcellular localization of L2K transfected and electroporated mRNA

We then investigated the entry pathway of labeled mRNA into the cell. Endocytosis of mRNA can be detected via co-staining with antibodies against clathrin-light chain, caveolin-1 and ARF6 (44,60-62) and subsequent colocalization analysis. These markers

were used to differentiate clathrin-mediated endocytosis, caveolae-mediated endocytosis and clathrin/caveolin-independent pathways, respectively. We initially used 3D images of single cells to determine colocalization between labeled mRNA and relevant pathway markers (Figure 2.5). Based on line profiles (Figure 2.5), mRNA delivered by lipofectamine colocalized with both clathrin and caveolin, but less frequently with ARF6. This was consistent with published transmembrane routes of cationic liposomal delivery (42). In order to confirm and better quantify these results, we verified entry pathway using a RNA–protein proximity ligation assay.

The overall PLA process is summarized in Figure 2.6. Briefly, mRNA was labeled with V5-peptide-tagged MTRIPs (the peptide is covalently attached to neutravidin) and delivered to HSkMCs by lipofection. Cells were fixed 2 h post-transfection. Primary antibodies specific for the V5 tag and different endocytic pathway markers, clathrin light chain, caveolin-1 or ARF6, were then added, followed by PLA proximity probes, oligonucleotide-labeled secondary antibody compatible for PLA. If the mRNA and the protein of interest are close to each other (<40 nm), the oligonucleotides are ligated by the addition of a ligase. Rolling circle amplification then creates a DNA 'ball', which is visualized by fluorescence *in situ* hybridization. This results in very bright (>30 fluorophores), diffraction-limited fluorescent puncta which are easily detected and quantified via microscopy (45). PLA puncta (Figure 2.6B) due to interactions between mRNA and endosomal markers were quantified via 'puncta' detection and counting, and compared to controls including mock transfection and no primary antibody. In the case of clathrin-light chain and caveolin-1, statistically significant differences from controls indicated that lipofectamine-delivered mRNA interacted with clathrin or caveolin-1, but

not with ARF6 (Figure 2.6C). Significantly, this result confirmed observations obtained by colocalization and overlap coefficient measurements.

Whole cell RNA uptake and protein expression measured via flow cytometry

In order to compare efficiencies of delivery methods, electroporation and lipofection, we used flow cytometry, which yields an integration of mRNA signal and protein-reporter fluorescence on a per cell basis. We electroporated HSkMCs with increasing amounts of labeled EGFP mRNA and observed that between 0 and 1000 ng of delivered mRNA, the mean mRNA intensity per cell scaled in a linear fashion (Figure 2.7). In order to maintain similar protein expression between delivery methods, as well as to avoid possible cellular stress response to unfolded protein, in subsequent experiments we delivered 200 ng per 100 000 cells. In order to measure EGFP production and quantify, at the same time, the mean total mRNA delivered per cell, we transfected HSkMCs with 200 ng of labeled mRNA and analyzed cells at 24 h post-transfection via flow cytometry. Cells were categorized into EGFP 'expressing' and 'non-expressing' populations, using a threshold of six standard deviations above the intensity of mock transfected cells. From this experiment, we found that upon electroporation, up to 90% of cells expressed GFP, whereas only 40% of lipofected cells expressed GFP at 24 h post-transfection (Figure 2.8). Importantly, the mean mRNA intensity within expressing cells was 10 times higher upon L2K transfection than electroporation (Figure 2.9A). As previously described in Figure 2.1C, it is clear that much of the mRNA delivered via lipofection localizes in cytoplasmic vesicles, possibly due to compartmentalization in the endosomal system (42,50). Such mRNA likely does not contribute to translation (31).

Additionally, we observed that cell-to-cell heterogeneity in protein expression was much higher with L2K.

We repeated the experiment using an EGFP mRNA variant modified by the complete incorporation of 5-methyl-cytidine (5meC) and pseudouridine (Ψ), which is known to reduce immune activation (3). We determined that the mean mRNA intensity within expressing cells was similar to the one measured for unmodified mRNA. The mean total protein expression per cell was similar between unmodified and modified mRNA upon electroporation, but a significant increase in protein production was observed upon lipofection using modified mRNA (Figure 2.9B).

Cytosolic mRNA correlates with protein production

The flow cytometry data described in Figure 2.9 indicated an order of magnitude increase in total transfected RNA per cell upon L2K transfection compared to electroporation. However, levels of protein production were similar, indicating that L2K delivered mRNA trapped in the endosomal compartments does not contribute to translation. We hypothesized that cytosolic RNA and not total RNA contributed to protein production. In order to discriminate and quantify the cytosolic and endocytic mRNA populations, we lipofected HSkMCs with modified and unmodified labeled EGFP mRNA, and co-stained with endocytic markers at 2, 5, 12, 24 and 48 h post-transfection (Figure 2.10, Figure 2.11). We used multiple endocytic markers including Early endosome antigen 1 (EEA1), CD63 and Lysosomal-associated membrane protein 1 (LAMP1), which provide broad coverage of the endosomal compartments (63,64). Within single cells, we identified labeled mRNA granules, determined their volume and

colocalization with endocytic markers (Figure 2.10B). Large mRNA granules (~>1 μm^3) colocalized with endocytic markers or were typically outside the cell, and therefore were excluded from further analysis. Smaller RNA granules were classified based on their colocalization with endocytic markers. Small granules which did not colocalize with endocytic markers were classified as 'free' cytosolic molecules (see methods section). The quantification of protein expression and cytosolic mRNA per cell over time is shown in Figure 2.12A. It is important to note that detected RNA granules varied in intensity; this intensity difference reflects the diversity in the number of RNAs per granule.

By quantifying the sum of intensity of cytosolic mRNA granules at multiple timepoints, we were able to examine the release kinetics of mRNA. We observed a significant increase of free modified mRNA 5 h post-transfection upon lipofection (Figure 2.12A), suggesting a faster release rate into the cytosol from the endosomal compartment. These are the first experiments, to our knowledge, that permitted the quantification of mRNA cytosolic release upon lipofection.

The amount of free RNA and GFP expression, on a per-cell basis, can serve as a measure of mRNA transfection efficiency. A plot of the sum of GFP intensity versus free RNA for electroporation and lipofection (Figure 2.12B) yielded approximately three times more cytosolic RNA in electroporated cells than in lipofected cells (see Table 2.1 for mean, SEM and statistical comparisons). Consistent with the flow cytometry data described in Figure 3, we observed that similar levels of mRNA yielded different levels of GFP expression. This result was particularly evident comparing the efficiency of lipofection of unmodified versus modified mRNA. During lipofection, the use of

5meC+Ψ modified mRNA resulted in a significantly higher protein–RNA ratio. However, no significant difference was observed using electroporation (see Table 2.1). Statistical analysis of correlations between free mRNA and protein expression showed that they were statistically correlated (Lipofection: unmodified $P = 0.0002$ | modified $P < 0.0001$ and electroporation: unmodified $P = 0.0195$ | modified $P < 0.0001$), though cell-to-cell heterogeneity was still evident. Additionally, levels of cytosolic mRNA were higher upon electroporation but did not result in correspondingly high levels of protein expression (Figure 2.12B, Table 2.1).

Stress granule (SG) formation negatively correlates with protein production

Differences in protein expression for given amounts of cytosolic mRNA, especially between modified and unmodified mRNA upon lipofection, suggested that protein production may be affected by innate immune activation (65). In order to further understand how changes in mRNA chemistry, as well as delivery method, impacted protein production, we used the formation of stress granules as a marker for innate immune activation.

We transfected HSKMCs with unlabeled modified and unmodified mRNA and stained for SG markers Ras GAP-binding protein 1 (G3BP) and T-cell-restricted intracellular antigen 1 related protein (TIAR), in order to characterize the kinetics of SG formation over time (Figure 2.13A). SG formation upon electroporation was readily observable with unmodified mRNA (>80% of cells) 1-h post-transfection, and quickly diminished to become undetectable 5 h post-transfection (Figure 2.13B). Transfection with lipofectamine resulted in ~20% of cells containing SGs, which diminished only

slightly over 24 h. When HeLa cells were transfected with lipofectamine and mRNA, higher levels of SGs were observed (>70%), indicating that SG formation is cell-type dependent (Figure 2.13C). Transfection with modified mRNA significantly reduced, but did not completely eliminate, SGs. Mock transfections did not result in any significant SG formation.

In order to test PKR-dependence of SG formation, we delivered PKR–siRNA into HSKMCs, which were then electroporated with unmodified mRNA. One hour post transfection, only 8% of cells formed SGs, versus >95% treated with control siRNA (data not shown). Then, mRNA transfection by lipofectamine was repeated in mouse embryonic fibroblasts (MEF) and MEF PKR–/– cells (Figure 2.13D). Modified mRNA slightly reduced the number of MEF WT cells containing SGs from 45% to 40%; as expected, MEF PKR–/– transfected cells formed no visible SGs. These cells expressed higher levels of GFP overall, with no differences between modified and unmodified mRNA (Figure 2.14). This strongly suggested a cell type dependence on stress granule formation, and provided further evidence that stress granule formation occurs in a PKR-dependent manner.

Validation of the mRNA labeling protocol for tissue studies in mice

We next examined the applicability of IVT mRNA labeling for *in vivo*experiments in an IM injection mouse model. We utilized MTRIPs labeled with Dylight 680 to visualize the distribution of mRNA upon IM injection in live mice using the Fluobeam 700 live fluorescent imaging system. IM injection of mRNA into the anterior tibialis muscle of mice showed immediate saturation of muscle tissue with

mRNA at the injection site, which remained 16 h post-injection along with fluorescence visible in neighboring lymph nodes (Figure 2.15A). Muscle tissue was then extracted, fixed and sectioned to visualize mRNA distributions in the muscle. We verified that MTRIPs remained bound to mRNA upon injection using FISH, as previously performed *in vitro*, on muscle sections fixed 2 h post-injection. We found that the FISH signal highly colocalized with MTRIP signal in tissue sections (Figure 2.15B).

In order to correlate localization of mRNA with protein expression at the tissue level, we combined Cy3b-labeled EGFP mRNA with a PEI-based delivery vehicle and injected it into the anterior tibialis muscle. Staining for EGFP showed that the majority of protein expression was localized in the perinuclear region of muscle cells and in cells present in the interstitial spaces (Figure 2.15C), where most of the mRNA was found.

Last, we examined Cy3b-labeled mRNA localization in relation with markers for cell structure and cell type. Following injection of Cy3b-labeled mRNA, we stained fixed sections of muscle with antibodies against CD11b, a marker for leukocytes, as well as for vimentin, an intermediate filament marker, which enabled the visualization of striated muscle (Figure 2.16). Skeletal muscle cells are the intended target during IM injection, while uptake by leukocytes is critical for vaccine applications. Labeled RNA was visibly located in the perinuclear region of muscle cells, and also colocalized with CD11b-marked leukocytes. Red blood cells were visible and indicative of blood vessels, though they did not contain labeled mRNA. Overall, these experiments serve as a proof of concept that RNA uptake and expression can be assessed for specific cell populations and localization within tissues.

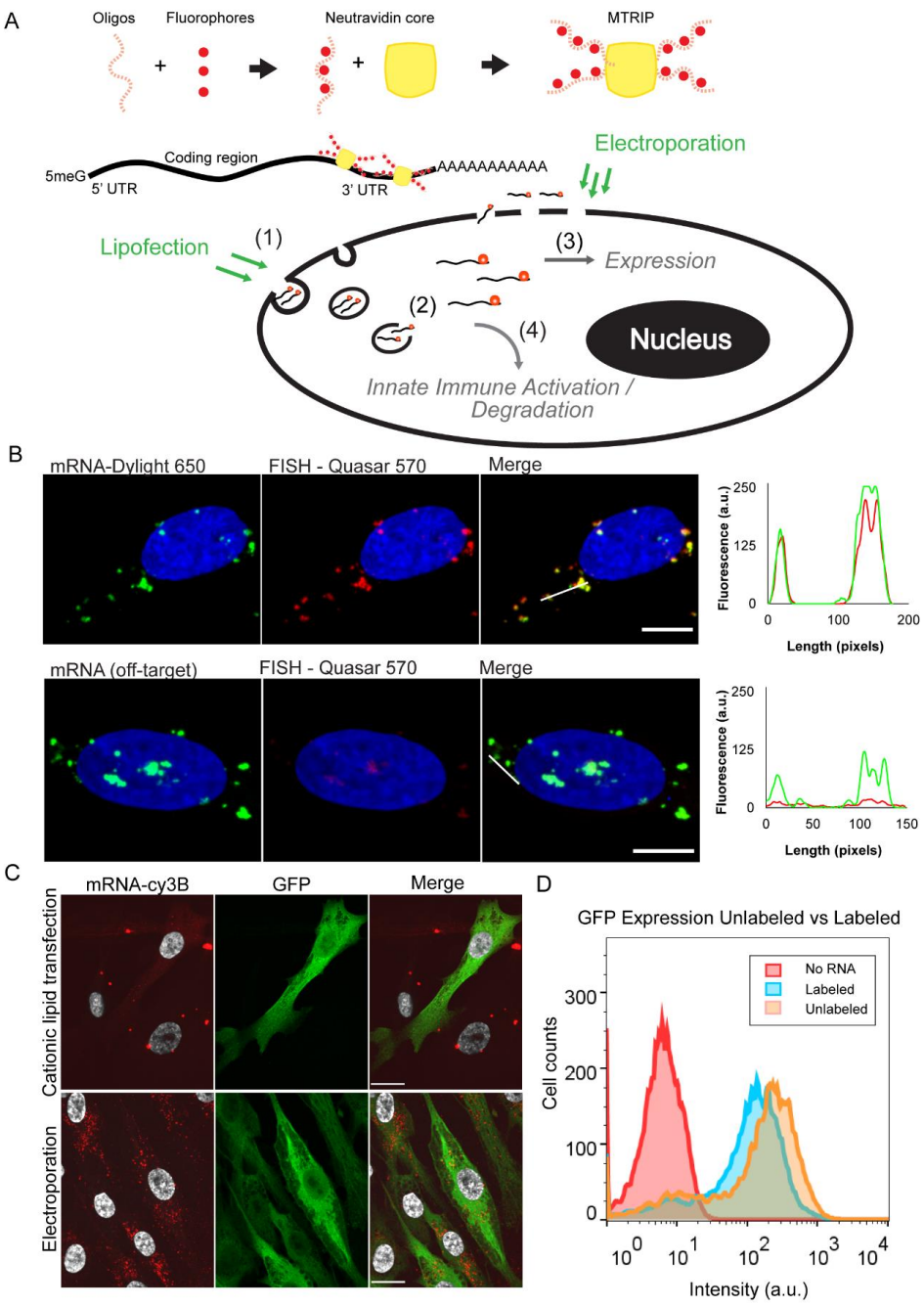

Figure 2.1: mRNA labeling, validation, and transfection into cells using cationic lipids or electroporation. (A) Illustrative diagram of mRNA labeling and delivery. MTRIPS are composed of four biotinylated and fluorescently labeled oligonucleotides assembled on a Neutravidin core. They bind to IVT mRNA in the 3´ UTR region. Fluorescently labeled mRNA is electroporated or lipofected into cells. Electroporated mRNA is immediately available in the cytosol, while lipofected mRNA must first travel through endosomes until released. Degradation and sequestration of mRNA

reduces final expression of the target protein. Highlighted mechanisms of importance include (i) mRNA entry pathway, (ii) cytoplasmic release, (iii) translational efficiency (RNA/protein correlation) and (iv) innate immune (PKR) activation. (B) Labeled mRNA (green) delivered via lipofection colocalized with Stellaris FISH probe signal (red). Line profiles are indicated by white lines. No FISH signal was visible in cells transfected with an mRNA containing a different coding region. (scale bar = 10 μm). (C) Cationic lipid transfection and electroporation with labeled mRNA encoding EGFP resulted in similar levels of protein production (green) but distinct subcellular distributions of mRNA (red) at 2 h post-transfection. Upon electroporation, small mRNA granules were observed throughout the cell cytoplasm, while cationic lipid transfection resulted in few large mRNA granules (scale bar = 20 μm). (D) Flow cytometry of EGFP expression using labeled versus unlabeled EGFP mRNA showed only a slight reduction in protein expression.

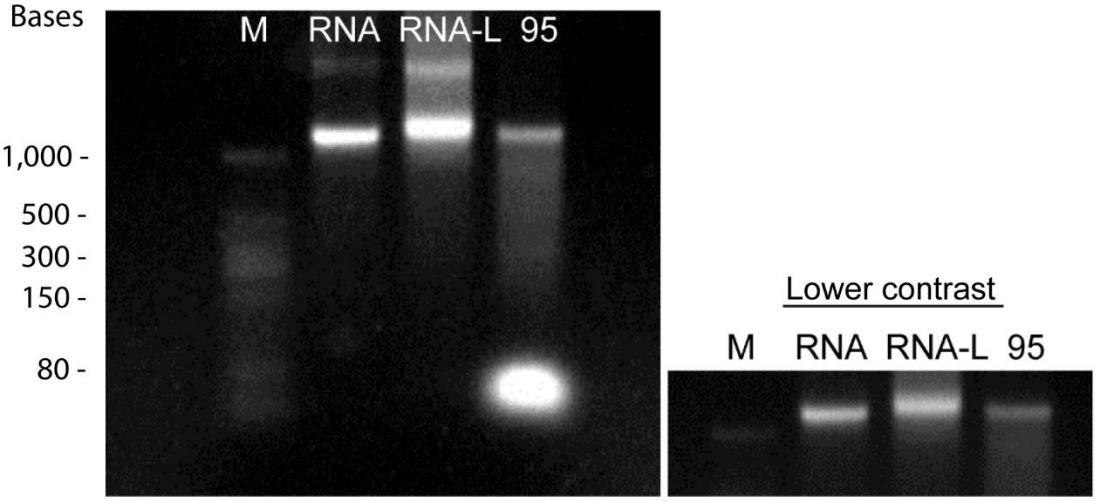

Figure 2.2: Agarose gel comparing unlabeled mRNA (RNA) and labeled mRNA (RNA-L). Labeled mRNA visibly migrated slower than unlabeled mRNA. Labeled mRNA was heated to 95°C in order to denature MTRIPs resulting in recovery of the band for unlabeled mRNA as well as an additional band at the bottom of the gel for denatured MTRIPs. M indicates Low Range ssRNA Ladder (NEB).

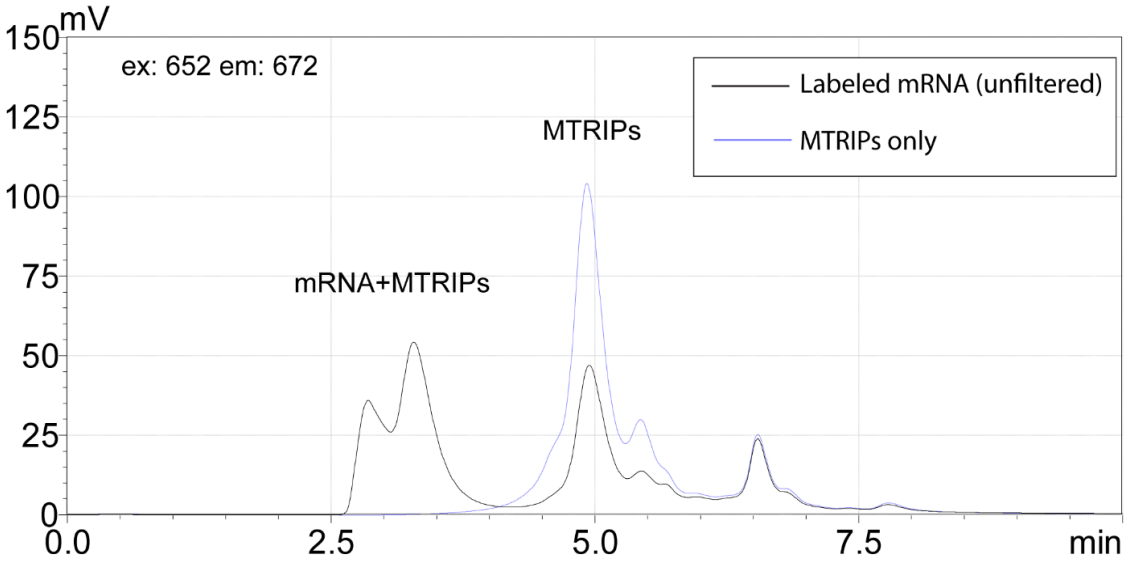

Figure 2.3: Quantification of degree of labeling of mRNA with MTRIPs by size exclusion chromatography. Dylight-650 labeled mRNA fluorescence was compared to the same molar amount of MTRIPs without mRNA. The degree of labeling is calculated based on the difference in peak fluorescence of the MTRIPs (~5 min) corresponding to the amount of MTRIPs which are bound to the mRNA (~3 min). This corresponds to a degree of labeling of approximately 2 MTRIPs per mRNA.

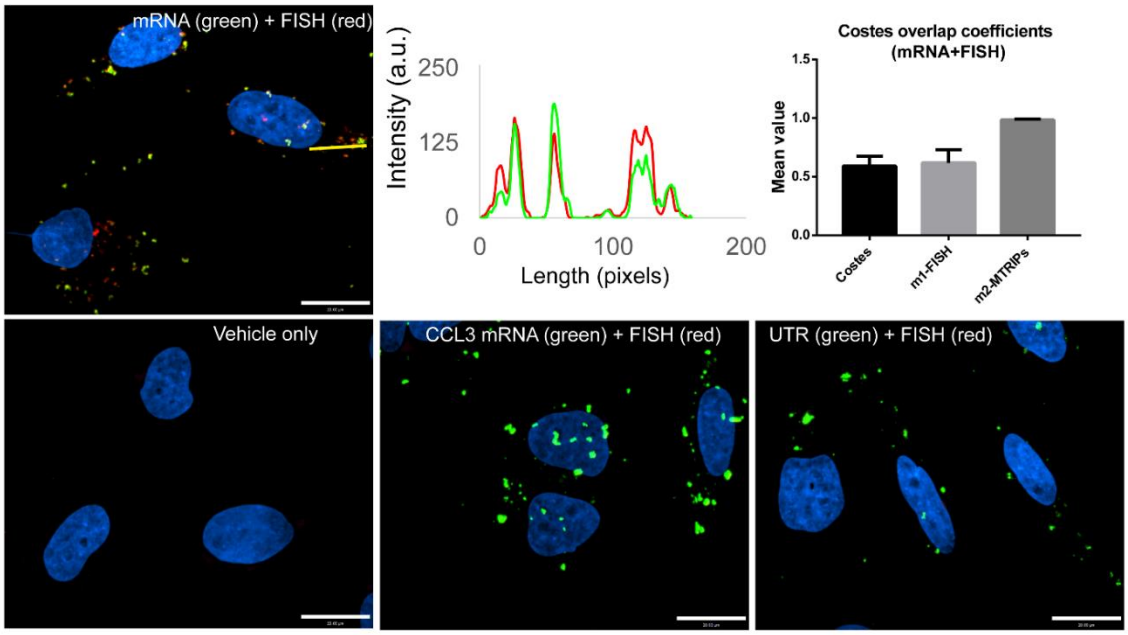

Figure 2.4: mRNA labeled with Dylight-650 MTRIPs colocalizes with Quasar 570 labeled FISH probes targeted to the coding region of the mRNA in Hela cells. A representative image, line profile (yellow), and Mander's overlap coefficients are plotted (overall Costes, where m1-refers to FISH signal containing MTRIP signal, and m2 refers to MTRIP signal containing FISH signal). There was no detectable FISH signal above background in controls including vehicle only, an mRNA encoding CCL3 containing the same 3'UTR probe binding sites, and a DNA containing the 3' UTR probe binding site only (lower panels). Images were analyzed in Volocity software with at least 15 cells per condition.

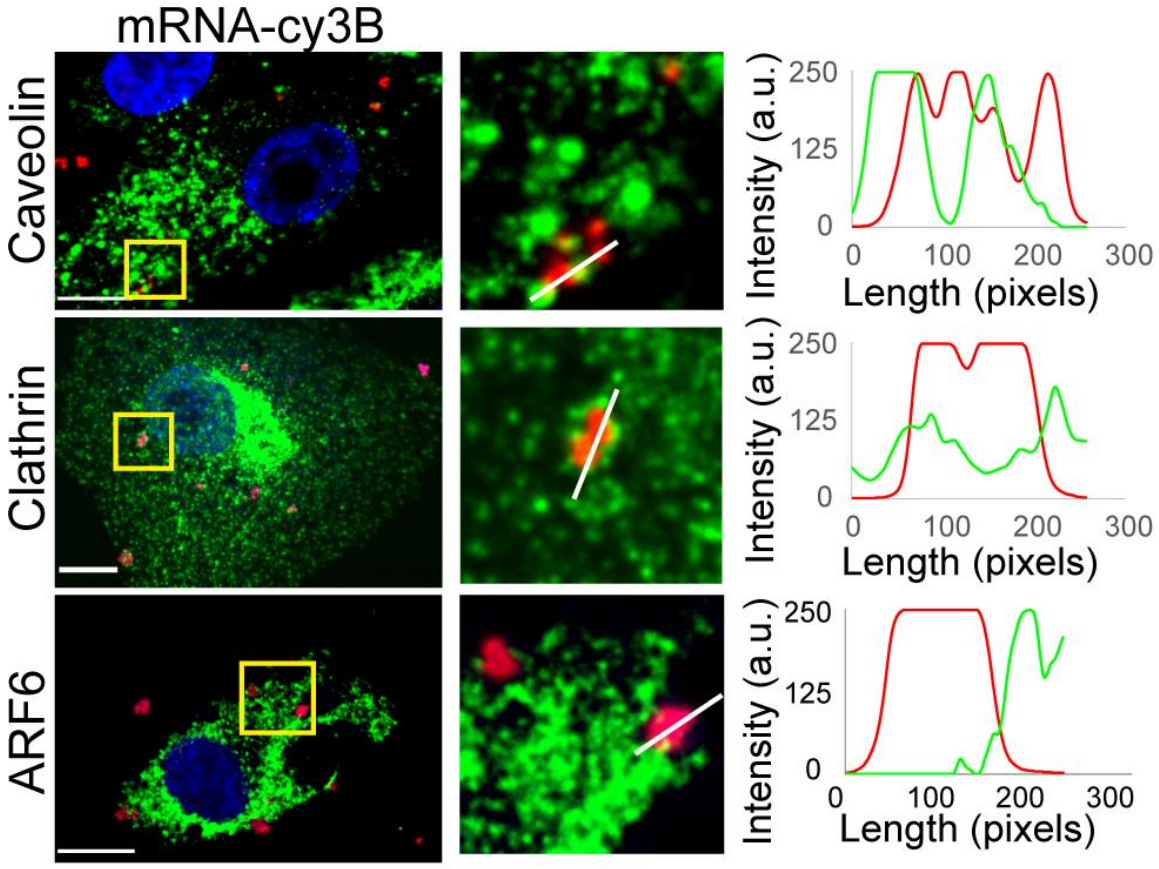

Figure 2.5: mRNA labeled with MTRIPs and delivered by lipofection allowed characterization of delivery route by costaining with Clathrin light chain, Caveolin, or ARF6. mRNA appeared associated with Clathrin Light Chain and Caveolin containing vesicles, but not with ARF6 (scale bar =11µm). Line profiles as indicated by white lines.

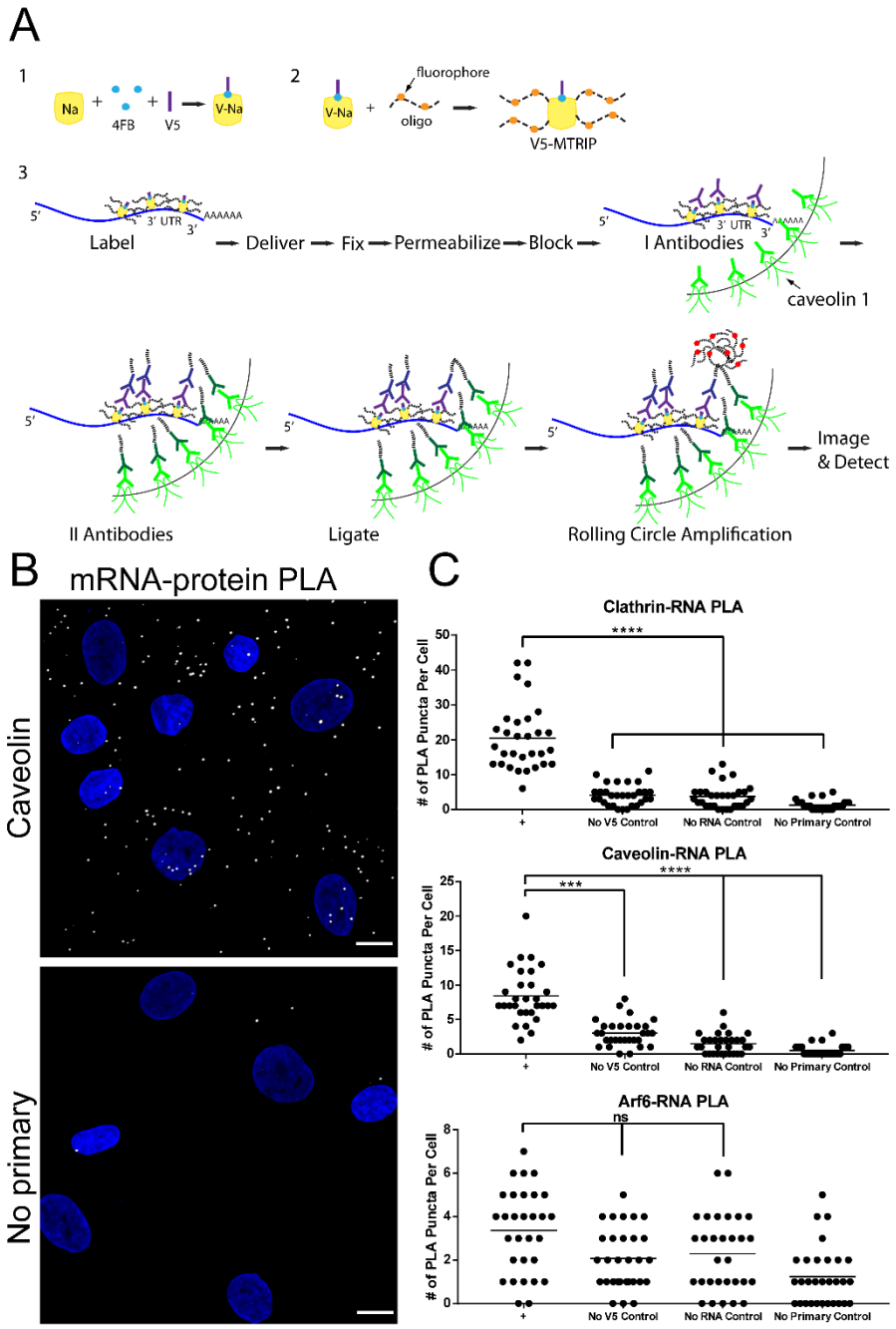

Figure 2.6: Analysis of lipofection-mediated mRNA uptake pathway via PLA. (A**) Overall schematic of PLA experiments to quantify interactions between mRNA and endocytic markers. A V5 tag is covalently bound to the MTRIPs prior to mRNA labeling. Following mRNA delivery by lipofectamine, primary antibodies target the V5 tag and either clathrin light chain, caveolin-1, or ARF6. PLA proximity probes recognize the primary antibodies and provide the substrate for ligation and rolling circle amplification. mRNA–protein interactions result in PLA puncta of homogeneous size and brightness. Standard controls include experiments performed**

without primary antibodies, without mRNA or using MTRIPS without the V5 tag. (B) PLA between V5-tagged MTRIPs and caveolin-1 in HSkMCs two hours post-lipofection resulted in significantly higher numbers of PLA puncta when compared to no primary control. (scale bar = 10 µm). (C) The number of PLA puncta per cell was quantified for 30 cells per condition for each endocytic marker. Significant proximity with endocytic markers and mRNA was detected for clathrin and caveolin but not ARF6 when compared to controls. (*****P* < 0.0001, ******P*= 0.0005).**

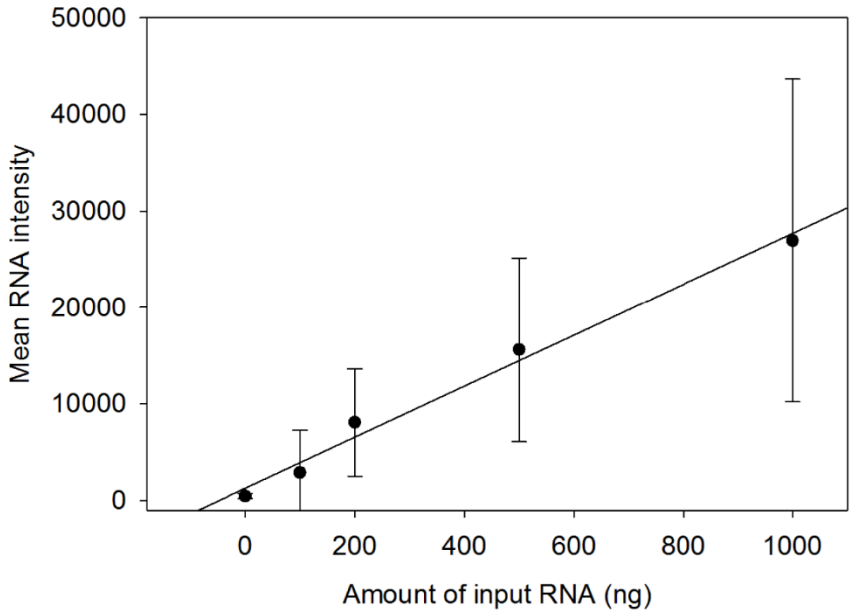

Figure 2.7: Upon electroporation, mean mRNA intensity scales linearly with increasing amounts of transfected cy3b-labeled mRNA. This ranged up to 1000ng per 1000000. HSkMCs were electroporated with cy3b labeled mRNA, fixed 30 minutes post transfection, and analyzed by flow cytometry.

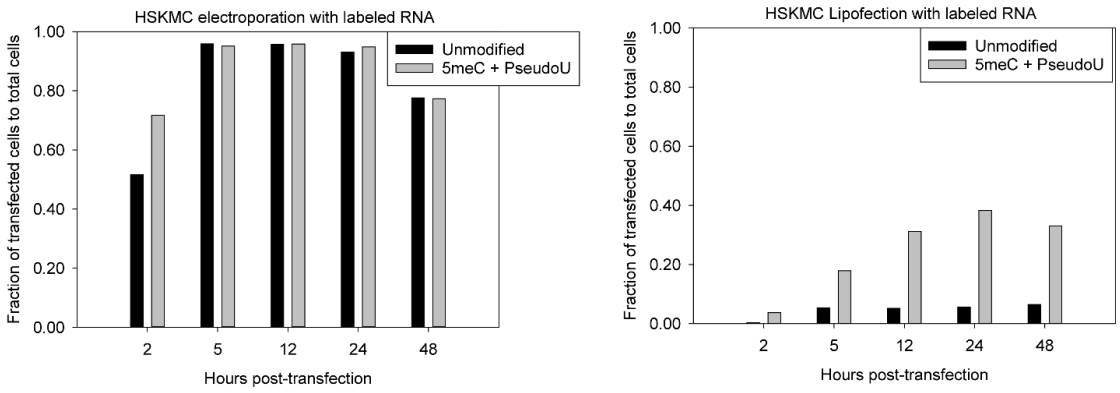

Figure 2.8: Transfection efficiency of HSkMC cells upon electroporation or lipofection with labeled modified or unmodified EGFP mRNA. "Expressing cells" are characterized by the sum of EGFP intensity greater than 6 times the standard deviation of non-transfected cells. Note that this cutoff results in lower detected fractions of lipofected cells transfected due to higher cell-to-cell variation of protein expression. The percent of GFP expressing cells in HeLa and MEF cells upon electroporation or lipofection (data not shown) were typically higher than 90% of cells transfected.

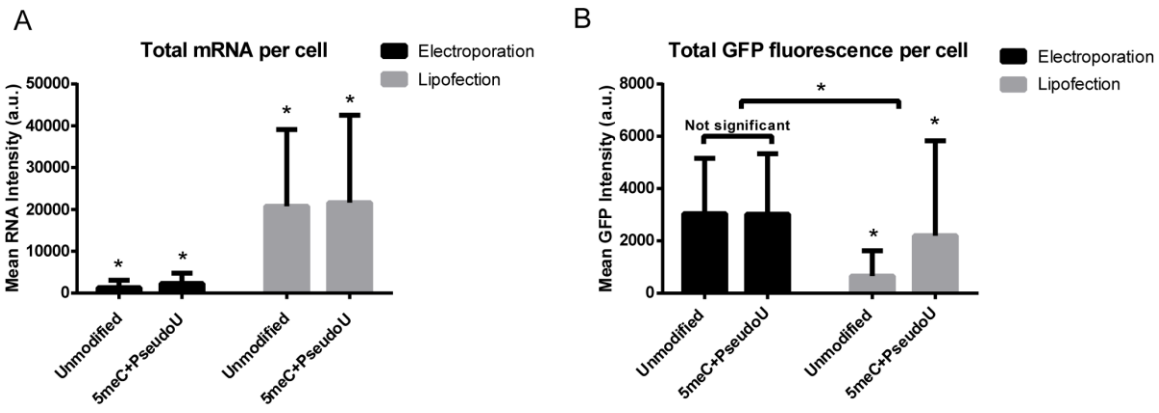

Figure 2.9: Flow cytometry analysis of HSkMCs following electroporation or lipofection with labeled 5meC + Pseudouridine or unmodified EGFP mRNA showed differences in mRNA uptake and protein expression. (A**) The mean total labeled mRNA intensity per cell was evaluated at 24 h post-transfection. Lipofection resulted in ~10 times higher mRNA per cell than electroporation. All comparisons are statistically significant based on two-way ANOVA (*P* < 0.0001) (bars = S.D. of population). (**B**) The mean total EGFP intensity per cell was measured at 24 hours post-transfection. A significant drop in intensity was observed upon lipofection of unmodified mRNA. Also, protein expression upon lipofection did not correlate with the amount of mRNA per cell. Statistical comparisons performed by two-way ANOVA with *a* = 0.05, *P* < 0.0001 for all conditions except as indicated. Experiment was performed in duplicate (bars = S.D. of population).**

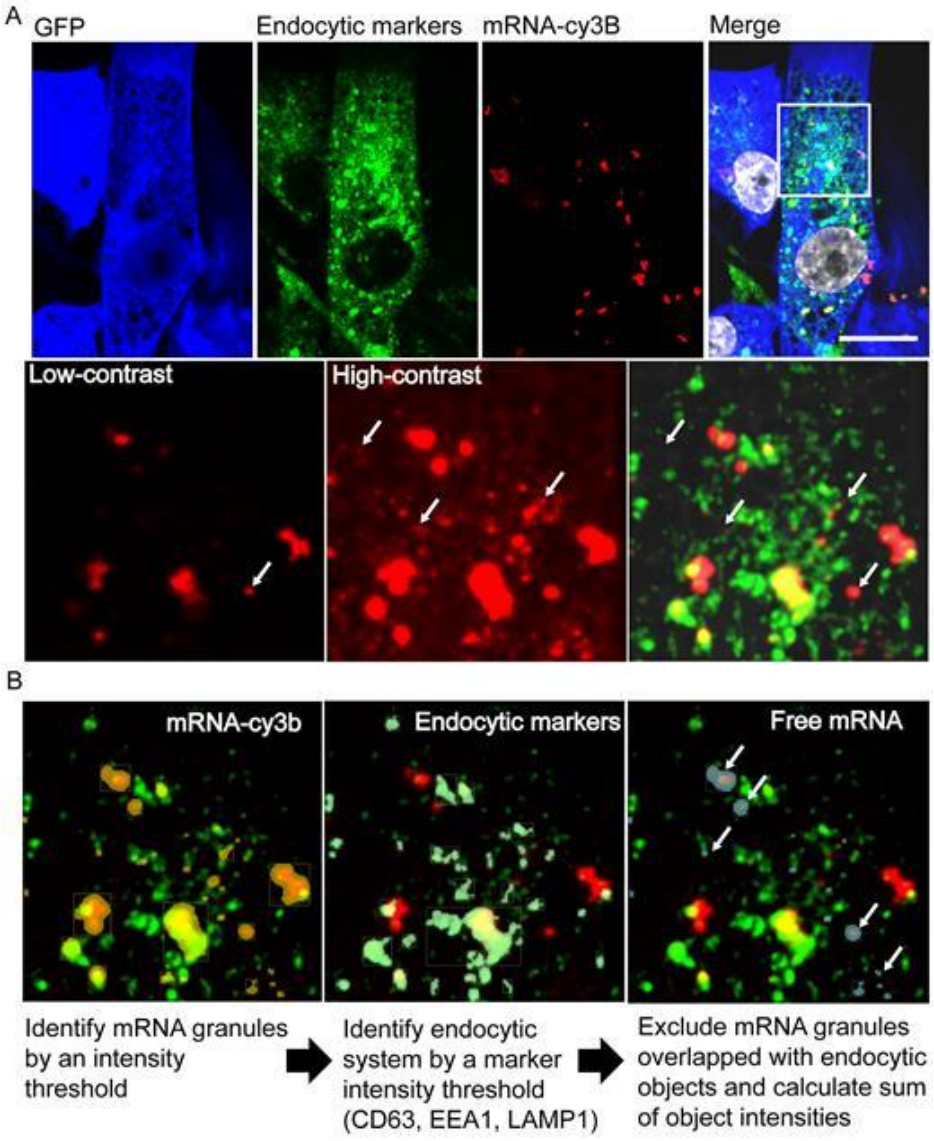

Figure 2.10: Imaging and analysis of transfected cells fixed and stained with endocytic markers EEA1, CD63 and LAMP1 allows quantification and correlation of cytosolic mRNA and EGFP synthesis. (A**) Representative images of 5meC + PseudoU modified EGFP mRNA lipofected into HSkMCs and fixed at 24 h post-transfection. Due to high dynamic range, the contrast enhancement necessary to visualize small mRNAs resulted in large mRNA granules to appear larger. White arrows indicate mRNA granules (red) that did not colocalize with endocytic markers (green), indicating cytosolic mRNA. (scale bar = 20 µm). (**B**) Representative images describing the protocol for the identification of mRNA granules and endocytic vesicles based on voxel intensity in each channel using Volocity software. mRNA granules not overlapping with endocytic objects were considered free, cytosolic mRNA (white arrows). Here, the number of identified objects shown was simplified for clarity.**

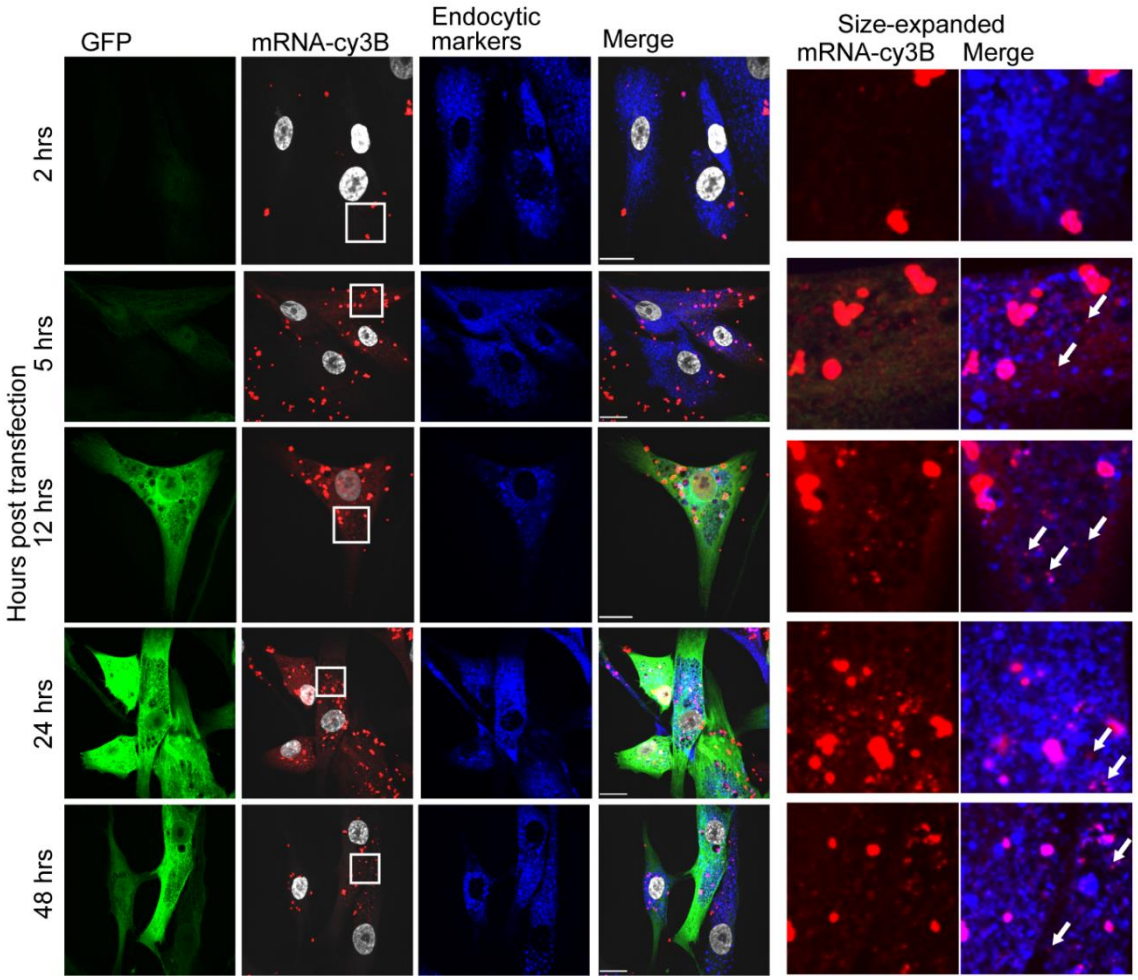

Figure 2.11: Imaging of lipofected cells fixed and stained with endocytic markers EEA1, CD63, and LAMP1. Representative images of 5meC+PseudoU modified EGFP mRNA lipofected into HSkMCs and fixed at 2, 5, 12, 24 and 48 hours post-transfection. White boxes indicate magnified regions. Due to high dynamic range, contrast enhancement was necessary to visualize small mRNAs and resulted in mRNA granules to appear larger. White arrows indicate single mRNAs (single point spread functions) in red which do not overlap with endocytic markers (blue), indicating that the fraction of cytosolic mRNA increases over time. (scale bar = 20µm).

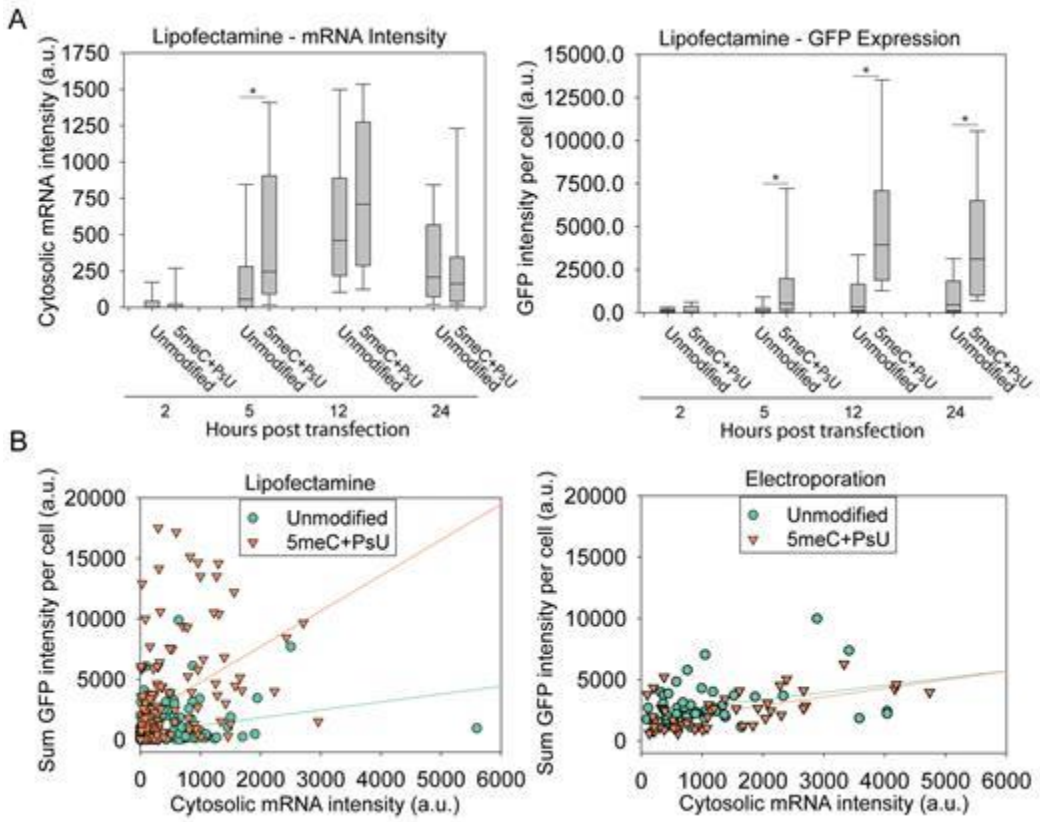

Figure 2.12: Cytosolic mRNA intensity and protein levels indicated differences in release rate as well as differential expression for given amounts of mRNA. (A**) Cytosolic mRNA and GFP intensity per cell at different time points post-lipofection. Data were collected from 30 cells per sample (box = median, upper and lower quartile, and min/max). (**B**) Cytosolic mRNA and protein expression correlation per cell based on microscopy imaging combining all timepoints. Lines are provided as a qualitative measure to show differences in distribution. The distributions between modified and unmodified mRNA upon lipofection were significantly different (*P* < 0.0001) but not electroporation distributions (*P* = 0.6677). All comparisons between mRNA and GFP in each distribution were statistically correlated (Lipofection: unmodified *P* = 0.0002 | Modified correlated *P* < 0.0001 and Electroporation: unmodified *P* = 0.0195 | Modified, *P* < 0.0001).**

Table 2.1: RNA intensity Mean, SEM, and P values for treatments in Fig 2.12:

RNA values	Lipofectamine (mean+-SEM)	Electroporation (mean+-SEM)	Significantly different? (Mann-Whitney test)
Unmodified mRNA	*346488 ± 43126*	*1073724 ± 96611*	Yes, P<.0001
Modified mRNA	*398804 ± 44168*	*1316282 ± 113595*	Yes, P<.0001
Significantly different? (Mann-Whitney test)	No, P=.4453	No, P=.2346	

Table 2.2: GFP intensity Mean, SEM, and P values for treatments in Fig 2.12:

EGFP values	Lipofectamine (mean+-SEM) x 10^6	Electroporation (mean+-SEM) x 10^6	Significantly different? (Mann-Whitney test)
Unmodified mRNA	*759 ± 102*	*2826 ± 172*	Yes, P<.0001
Modified mRNA	*2977± 313*	*2402 ± 139*	Yes, P=.0046
Significantly different? (Mann-Whitney test)	Yes, P<0.0001	No, P=0.0699	

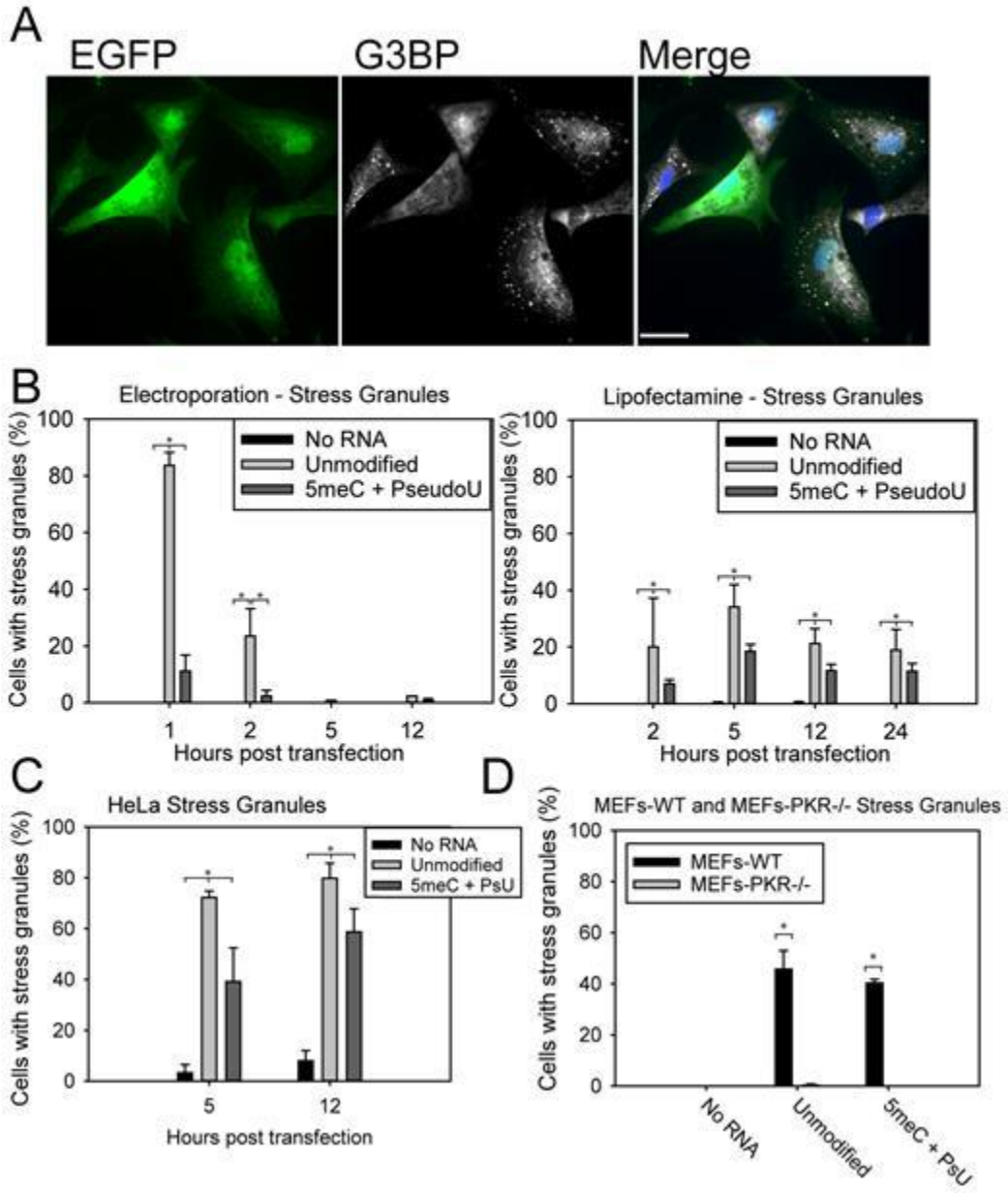

Figure 2.13: PKR-dependent stress granule formation correlates with decreased protein production and is cell type-dependent. (A) HSkMCs were fixed 1 h post-electroporation with EGFP mRNA and stained for stress granules (G3BP, white). Cells with stress granules produced less GFP (green) (scale bar = 20 µm). (B) Kinetics measurements in HSkMCs show a brief but strong increase in the number of cells with SGs 1 h after electroporation, which rapidly diminishes. The extended SG response upon lipofectamine transfection is still detectable 24 h post-transfection. 5meC + PseudoU reduced but did not completely eliminate SGs. (C) SG formation was found to be cell type-dependent. HeLa cells more readily formed SGs upon lipofection regardless of mRNA modification. (D) SGs formed readily 5 h post-lipofection in MEF cells but not in MEF PKR–/– cells, indicating that mRNA sensing

by PKR resulted in SG formation. MEF cells 5 h post-lipofection produced extensive SGs regardless of mRNA modification. MEF PKR-/- cells produced no detectable SGs (bars in B, C, and D = S.D. of triplicate measurements of 100 cells each).

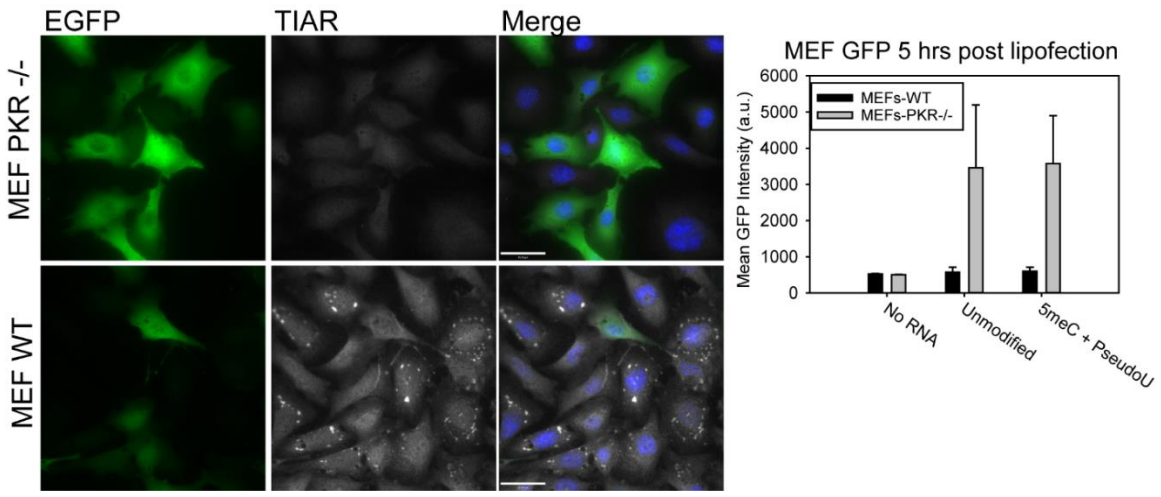

Figure 2.14: Wild-type MEF cells lipofected with EGFP mRNA produced very little protein 5 hours post transfection due to extensive SG formation with both modified and unmodified mRNA. MEF PKR-/- cells produced similar levels of protein regardless of modification. These cells did not form stress granules. The SG marker TIAR is used for staining of SGs (white) and the mean GFP intensity was quantified for at least 30 cells per sample in 40x widefield images using Volocity software. (bars = S.D of population, scale bar = 20µm)

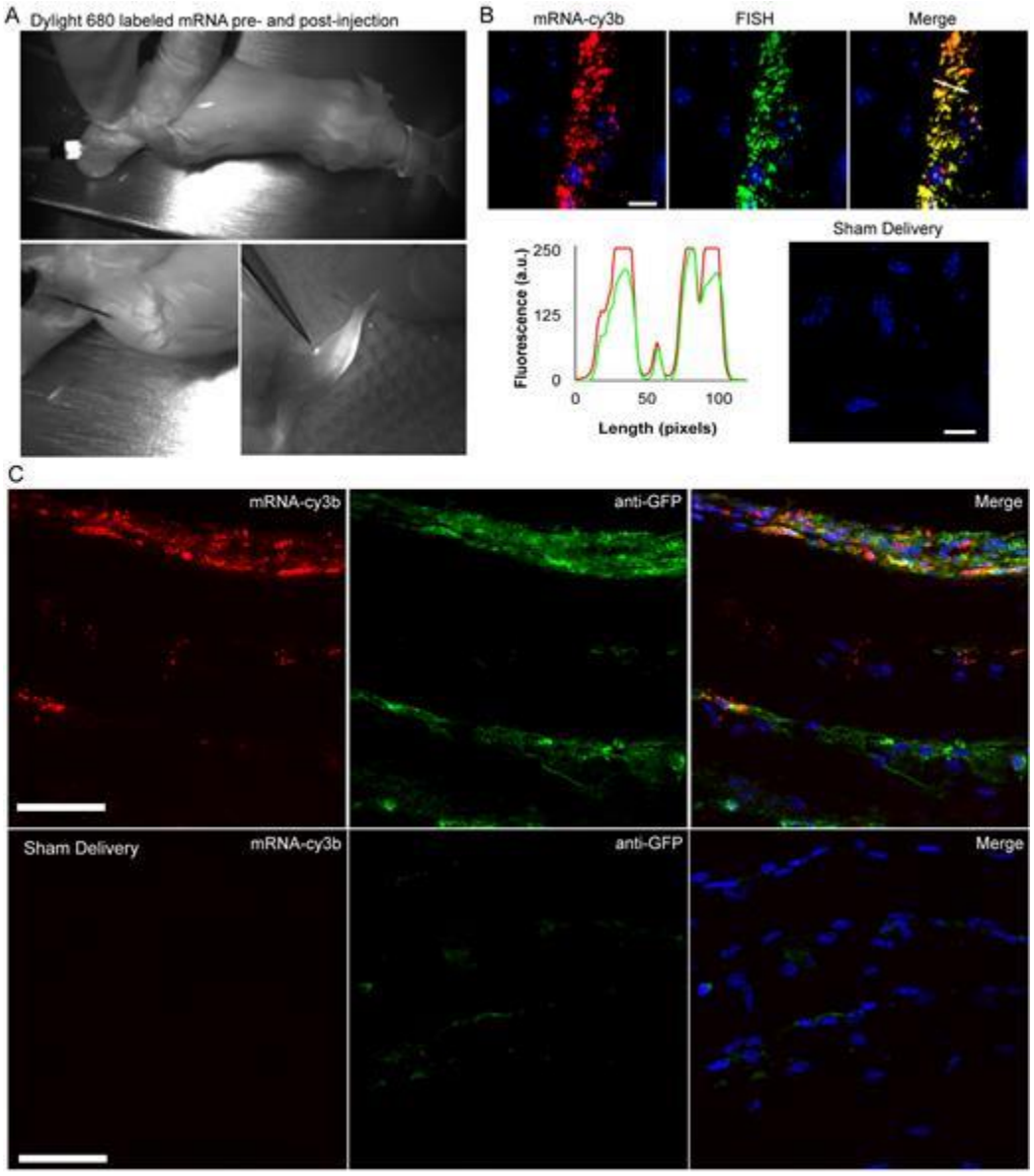

Figure 2.15: Visualization of labeled mRNA during IM injection and in extracted tissue sections. (A**) Dylight-680 labeled mRNA (white) was imaged during surgery prior to and immediately following IM injection into the anterior tibialis of a live mouse using the Fluobeam near-IR fluorescence imaging system. The third panel obtained 16 h post-injection shows localization of mRNA to a lymph node. (**B**) Labeled mRNA (red) colocalized with Stellaris FISH probe signal (green), as indicated by the intensity line profile (white line). No FISH signal was visible in mock transfected tissue (scale bar = 10 µm). (**C**) Cy3b-labeled mRNA (red) and antibody staining for GFP expression (green) imaged in anterior tibialis muscle sections removed from a mouse 16 h post-IM injection. Sham delivery (without mRNA) shows comparatively low levels of background signal in the GFP channel due to non-specific binding of antibodies.**

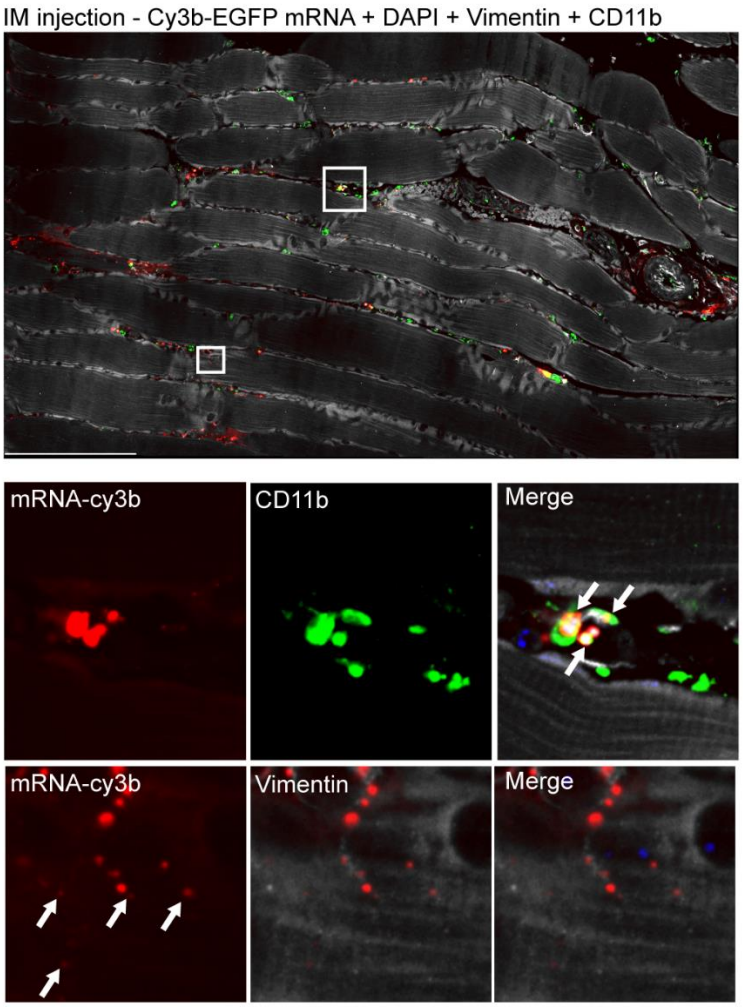

Figure 2.16: Visualization of labeled mRNA following IM injection in mouse muscle tissue sections. Cy3b-labeled mRNA (red) was imaged in anterior tibialis muscle sections removed 16 hours post-IM injection. Immunofluorescence staining for anti-cd11b (green) and anti-vimentin (white) is shown. Expanded views of white boxed areas are single-xy planes and have been contrast enhanced differently for visualization. Cells that are CD11b-positive are indicated by arrows, as well as RNA located near the perinuclear region of muscle cells. (scale bar =150µm)

Conclusion

A serious concern for the future of mRNA therapeutics is the efficiency of protein production in a given organ for a single dose. Delivery vehicles must be designed and optimized to ensure efficient delivery of mRNA to target cells and their cytosol, as well as to encourage translation. Likewise, the design of the mRNA sequences along with delivery formulations must be carefully considered. It is important to modulate the negative immune effects of mRNA, based on pathogen sensing mechanisms within various cell types. All three of these factors require new tools and methodologies to study mRNA uptake and kinetics of protein expression.

We have developed a labeling strategy for exogenous mRNA, which allows single RNA-sensitive detection (∼2 probes and 16–20 fluors per mRNA), without significant reductions in the translational potential of therapeutic molecules. Probes were hybridized to *in vitro* transcribed mRNA in controlled conditions, and were purified and characterized using syringe filters and size exclusion chromatography. Encoding secondary proteins for visualization or co-expression with reporter molecules is not required. These probes can potentially be designed against any 3′ untranslated region. UTR regions can also be extended with specific binding sequences for MTRIP binding, without affecting the coding region or reading frame of the mRNA. The resulting labeled mRNAs are functional in both cells in culture and after *in vivo* delivery in animal models. Labeling of therapeutic RNA allowed fast and accurate screening of RNA formulations through compatibility with high-throughput tools such as flow cytometers and plate readers. Combining MTRIPs with a proximity ligation assay provided a novel method for

defining uptake pathway by discrete quantification of interactions between mRNA and specific endocytic markers. For *in vivo* studies, this methodology enabled the imaging of RNA localization in tissue slices co-stained with markers for cell type or target proteins. Future mechanistic studies will be performed in order to evaluate the effectiveness of different formulations.

Translation of mRNA occurs in the cytosol, and thus delivery vehicles have the two-fold requirement of first reaching the target cells within tissues, and then either escaping from an endocytic compartment or entering the cytosol directly. Our results indicated that while both lipofectamine-mediated delivery and electroporation of mRNA resulted in protein expression, the amount of protein expression was based upon the amount of mRNA that reached the cytosol as well as a complex interplay between mRNA translation and innate immune activation. Lipofectamine delivery resulted in large amounts of mRNA trapped in intracellular vesicles. Measures of protein–RNA correlation indicated a higher efficiency of protein production per cytosolic mRNA using lipofection. This implied that mRNA were released from the endosome slowly over time, and can more readily interact with the translational machinery. In addition, L2K delivered mRNA may be protected from degradation during the mRNA assembly process with proteins (forming a messenger ribonucleoprotein (mRNP)). Therefore, controlling the kinetics of mRNA release may be critical to the optimization of protein production with cationic lipids. In contrast, electroporation removed the endosomal escape aspect entirely and resulted in a large amount of mRNA entering the cytosol directly.

It is also important to note that MTRIPs remain bound to the mRNA *in vivo*. This allows subsequent studies for biodistribution and mRNA trafficking on a whole-animal level as well as cell-type specific uptake and expression. MTRIPs can be labelled with different fluorophores depending on the imaging application. They can also be labeled with radionuclides, such as ^{64}Cu, which would enable the use of position emission tomography detection of the mRNA in the deep tissue of live animals. This can be a critical aspect of testing mRNA therapeutics prior to translation into humans.

The presence of stress granules is indicative of PKR activation and translational repression via eIF2α phosphorylation, and is linked to abrogating apoptosis (57,58,66). Not only does SG formation negatively correlate with the expression of the therapeutic protein of interest, but they also influence host gene expression regulation, an undesirable side-effect for most therapies. Incorporation of modified nucleotides into mRNA substantially reduced this effect, but in a cell-type and delivery-dependent manner. Decreased SG levels in HSKMCs compared to HeLa and MEF cells might be due to lower overall PKR levels in human skeletal muscle. Electroporation resulted in a strong but short-lasting stress response, and thus SGs had a partial effect on the RNA–protein correlation. The longer-lasting, SG response observed using lipofectamine is likely due to slow release of mRNA from endosomes over time, and, thus, continuous activation of PKR and eIF2α phosphorylation. It is also possible that ‘priming’ of the stress response occurs through activation of toll-like receptors (TLRs) in the endosomal compartment, which does not happen during electroporation (21,66). Results with MEF PKR–/– cells indicate that the benefits of mRNA modification primarily stem from reduction in the

stress response. Overall, SG formation should be avoided in order not to perturb cell state and produce the maximum amount of desired protein.

The biggest challenge to the development of mRNA therapeutics is efficiency. Reduction of eIF2α phosphorylation and efficient delivery of mRNA and subsequent release into the cytosolic compartment are instrumental to overcoming this barrier. mRNP formation kinetics may also limit protein production but this will be addressed in future work using the MTRIP-PLA approach. Overall, this methodology allows for the measurements of critical metrics to not only compare prospective mRNAs and their formulations, but also in probing the biological mechanisms limiting expression. Overcoming barriers of efficiency will enable new mRNA-based therapeutics which are safer and more effective.

Methods

IVT mRNA and multiply labeled tetravalent imaging probes (MTRIP) labeling

All IVT mRNAs were synthesized by Moderna Therapeutics (Boston, MA, USA) containing identical sequences and included 5′ capping and polyadenylation. EGFP-encoding mRNAs either were synthesized without modified nucleosides or with total incorporation of 5meC and Pseudouridine. RNA was stored frozen in –80°C and subjected to minimal freeze-thaw cycles. MTRIPs were constructed as previously described (35,37). A detailed protocol for MTRIPs assembly and characterization was described in Santangelo *et al.* (67). Four oligos complementary to four adjacent sequences spanning the mouse alpha globin 3′ UTR (NM_001083955.1) of the IVT mRNA were generated.

Sequences were adjacent due to the small length of the UTR region. Probe sequences were as follows:

- Biotin-T(C6-Amino)-TTTTT-T(C6-Amino)-G-C-A-A-G-C-C-C-C-G-C-A-G-A-A-G-G-T(C6-Amino)
- Biotin-T(C6-Amino)-TTATT-T(C6-Amino)-A-G-A-G-A-A-G-A-A-G-G-G-C-A-T(C6-Amino)-G-G
- Biotin-T(C6-Amino)-TTTT-T(C6-Amino)-A-C-C-A-A-G-A-G-G-T(C6-Amino)-A-C-A-G-G-T(C6-Amino)-G-C
- Biotin-T(C6-Amino)-TTTTTT-C-T(C6-Amino)-A-C-U-C-A-G-G-C-T(C6-Amino)-U-U-A-U-T(C6-Amino)-C

Each sequence was analyzed via nucleotide BLAST to ensure minimal off-target binding. Sequences were purchased as 2′-*O*-methyl RNA-DNA chimeric oligonucleotides 17–18 bases long with a short 5–7 poly(T) linker and 4 C6-amino-modified thymidines. The oligos included a 5′ biotin modification and were purchased from Biosearch Technologies (Petaluma, CA, USA). The oligonucleotides were labeled with Cy3b-NHS ester (GE Healthcare) or Dylight 650/680-NHS esters (Pierce) using manufacturer protocols. MTRIPs were assembled by incubation with Neutravidin (Pierce) for 1 h at RT followed by filtration using 30 kD MWCO centrifugal filters (Millipore). mRNA was buffer exchanged into 1× PBS, heated to 70°C for 10 min and immediately placed on ice, combined with MTRIPs in a 1:1 mRNA:MTRIP ratio and then incubated overnight at 37°C. The next day, the labeled mRNA was filtered using a 200 kD MWCO ultrafiltration unit (Advantec MFS Inc.) and concentrated by 50 kD MWCO centrifugal filters

(Millipore). Alternative filters tested during protocol optimization included 100 and 300 kD MWCO, but either did not filter unbound MTRIPs successfully or failed to successfully retain mRNA.

Microscopy

Stress granule (SG) imaging was performed using a Nikon Plan-Apo 40 × 0.95 NA air objective on a Nikon Eclipse TE2000 widefield microscope equipped with a Hamamatsu C9000-02 EM-CCD camera. All other samples, including tissue slides, were imaged using a Zeiss Plan-Apo 63 × 1.4 NA oil objective on an UltraVIEW Spinning Disk Confocal Microscope equipped with a Hamamatsu Flash 4.0v2 CMOS camera. The full dynamic range of the camera was necessary to capture intensities of large and small granules without undersampling or saturating images. All microscopes were controlled by the Volocity acquisition software (PerkinElmer).

Quantification of cytosolic mRNA

mRNA quantification was performed using Volocity software in images obtained on the spinning disk confocal microscope described above and a 63× objective. Briefly, thresholds were set to detect the dimmest mRNA granules (Cy3b), which were near the detectable limit of the camera (~500/65536). All mRNA were identified as objects and sorted based on size (greater than or less than 1 μm^3) and overlap with endocytic markers. Large granules either overlapped with endocytic markers or were found to be outside the cell, which was verified by visual inspection. Such mRNAs were discarded from subsequent analysis. Smaller granules (<1 μm^3) were considered to be cytosolic if they did

not overlap endosomal markers. For each cell, the sum of cytosolic mRNA and GFP expression was recorded and plotted using Sigmaplot. At least 30 cells were used per condition. In detail, in Volocity software, the 'Find Objects' function was used to automatically select RNA granules using intensity set above background levels. The objects found by the 'find objects' tool, for a given intensity setting, were verified by visual inspection (see Figure 4). A manual threshold was applied to sort objects into populations ('Filter Population' function) based on size (~1 μm^3). 'Find Objects' was applied again to generate an object population representing endosomal markers (CD63/EEA1/LAMP1) with manual intensity threshold set above background values. All populations were clipped and compartmentalized to ROIs which were manually drawn around individual cells. Populations were subdivided using the 'Exclude touching' and 'Exclude non-touching' functions between RNA granules of every size and endosome objects. Large and small RNA granules touching endosome objects were considered 'trapped' RNA granules. Large granules in contact with endosome objects, which were extremely rare, were individually inspected and removed from analysis as all appeared to be located above the cell. Small RNA granules not touching endosome objects were considered 'free' mRNA granules. The sum of all free mRNA per cell was calculated using the 'Analysis' tab in Volocity. Protein expression was calculated in Volocity for each ROI as well. At least 30 cells were counted in this manner per condition per timepoint.

Colocalization between pre-labeled mRNAs and Stellaris FISH

100 ng of unmodified mRNA was pre-labeled with Dylight-650 labeled MTRIPs, as previously described. After filtration to remove the unbound MTRIPS, the mRNA was

transfected to HeLa cells using Lipofectamine 2000 according to manufacturer's instructions. The cells were fixed 5 h post-transfection in 4% PFA and permeabilized in 70% ethanol at 4°C overnight. The following day we performed FISH using Stellaris FISH RNA probes labeled with Quasar 570 (Biosearch) designed against the codon optimized coding region. FISH was performed according to the Stellaris protocol. Briefly, cells were washed 5 min in wash buffer (10% formamide, 2% SSC). Cells were then incubated at 37°C in the presence of 200 nM 570-labeled Stellaris probes in hybridization buffer (10% formamide, 2% SSC, 10% dextran sulfate, .5% tRNA, 0.5% ssDNA, 0.2% bovine serum albumin—BSA) in a humid chamber. After 4 h, cells were washed in wash buffer for 30 min at 37°C, nuclei were stained with DAPI and coverslips were mounted on glass slides using Prolong gold (Life Technologies). Mander's coefficients were measured using Costes threshold calculation in >15 cells using Volocity software. Controls consisted of FISH on vehicle only-transfected cells, cells transfected with an mRNA containing a different coding region (Chemokine ligand 3), and DNA oligos with the same sequence as the mRNA 3′ UTR region.

For experiments performed in tissue sections, 10 μg of unmodified mRNA was pre-labeled with Cy3b labeled MTRIPs. After filtration to remove the unbound MTRIPS, the mRNA was complexed with a PEI polymer (Viromer Red, Lipocalyx) and injected intramuscularly in a Ringer's Lactate (RiLa) buffer into the anterior tibialis muscle of BALB/C mice. Controls consisted of an intramuscular sham injection of RiLa buffer. The mice were sacrificed and the muscle harvested 2 h post-injection. The harvested tissue was fixed in 4% PFA overnight at 4°C, soaked in PBS containing 30% sucrose overnight at 4°C, and then embedded in optimal cutting temperature solution. The tissue blocks were

then snap frozen in isopentane and dry ice. Finally, the frozen tissue blocks were cut into ~10 um thick sections with a cryostat and put onto slides to be used for FISH. The tissue was fixed and permeabilized in 50:50 methanol:acetone at -20°C for 10 min. Stellaris FISH probes labeled with Quasar 670 (Biosearch) were designed matching the probes used for the *in vitro* experiment. FISH was then performed according to the Stellaris protocol. Briefly, after methanol:acetone fixation, the tissue was equilibrated in wash buffer (10% formamide, 2% SSC). Tissue was then incubated at 37°C in the presence of 20 nM of 670-labeled Stellaris probes in hybridization buffer (10% formamide, 2% SSC, 10% dextran sulfate, 0.5% tRNA, 0.5% ssDNA, 0.2% BSA) in a humid chamber overnight. The next morning, tissue was washed in wash buffer for 30 min at 37°C. Finally, the nuclei were stained with DAPI and coverslips were mounted on top the tissue using Prolong gold (Life Technologies).

Proximity ligation assays

Protein/mRNA PLA has been previously described (28,29) and a detailed protocol can be found in Zurla *et al.* (39). Briefly, neutravidin was tagged with a V5 epitope through Solulink conjugation technology. A maleimide hynic linker (Solulink) was conjugated to the V5 tag, while an S-4FB linker (Solulink) was conjugated to the neutravidin, following manufacturer's instructions. After conjugation, the two reagents were mixed with the Turbolink catalyst (Solulink) to covalently bind the V5 tag to neutravidin. MTRIPs were then assembled as previously described using V5 labeled neutravidin (Na-V5), mRNA was labeled as above, and then used for transfection. Two hours post-transfection, cells were fixed with 1% paraformaldehyde and permeabilized with 0.2% Triton X in 1× PBS. Cells

were then blocked for nonspecific interactions for 30 min at 37°C with PLA blocking buffer (0.1% gelatin, 2% donkey serum and 1% BSA in 1× PBS). Primary antibodies consisted of rabbit anti-V5 (Abcam), mouse anti-V5 (abcam), mouse anti-caveolin-1 (Sigma), mouse anti-clathrin light chain (Sigma) and rabbit anti-ARF6 (Pierce). Primary antibodies were then delivered (1:1000 V5 Ab and 1:250 ARF6 Ab, 1:500 clathrin light chain Ab or 1:10 000 caveolin Ab in PLA primary diluent (1% BSA, 1% donkey serum and 0.2% Triton-X in 1× PBS) for 30 min at 37°C. Cells were washed in wash buffer A (Sigma) at RT for 10 min. Secondary antibodies for rabbit and mouse antibodies (Sigma) were delivered at a concentration indicated by the manufacturer in PLA secondary diluent (0.05% tween 20 in 1× PBS) for 30 min at 37°C. This was followed by another 10 min wash in wash buffer A (Sigma) at RT. PLA ligation and rolling circle amplification were performed as specified by the manufacturer. Finally, cells were washed and mounted on a slide with DAPI mounting medium (Sigma). PLA interactions were quantified using a 63× (oil) objective on a spinning disk confocal microscope. Thiry cells were measured per experimental condition and analyzed by Volocity software.

Cell culture and transfection

HeLa cells and Mouse Embryonic Fibroblasts were obtained from ATCC and maintained in DMEM or EMEM (Lonza) and supplemented with 10% FBS (Hyclone), 100 U/ml penicillin and 100 μg/ml streptomycin (Life Technologies). Primary human skeletal muscle cells (Promocell) were grown in HSkMC growth media (Promocell) supplemented without FBS and only with penicillin and streptomycin as above. Cells were plated the day before an experiment in preparation for lipofectamine transfection. Lipofectamine was

combined with labeled mRNA in Optimem (Life Technologies) using manufacturer protocols. Lipofectamine solutions were replaced by fresh media 5 h post-transfection. For electroporation, cells were placed into suspension using trypsin which was subsequently deactivated by the addition of media containing serum. Cells were counted, pelleted, and re-suspended at a final concentration of 5 million cells/ml in electroporation buffer R (Life Technologies) containing 200 ng/10 ul of mRNA. All electroporations were performed using the Neon Transfection System (Life Technologies) using a 10 μl reaction size per well in a 24-well plate and following manufacturer protocols. Pulse voltage was set to 1100 V with a pulse width of 30 ms and a pulse number of 2. Media was replaced after 5 h. Knockdown experiments for PKR were performed by Neon electroporation with anti-PKR siRNA (Smartpool, Dharmacon) 48 h prior to mRNA transfection and knockdown efficiency was quantified to be >80% using PCR.

Immunofluorescence

Cells were fixed in 4% PFA for 10 min, blocked in 25% BSA and immunostained as previously described (47) using appropriate antibodies. Endosomal route markers used were caveolin, clathrin light chain and ARF6 (Santa Cruz Biotechnology). General endocytic markers used for evaluating cytosolic mRNA were CD63 (mouse anti-CD63, Developmental Studies Hybridoma Bank- DSHB), EEA1 (mouse anti-EEA1, BD Biosciences) and LAMP1 (mouse anti-LAMP1, DSHB). Stress granule markers included G3BP (mouse anti-G3BP, BD Biosciences) and TIAR (goat anti-TIAR, Santa Cruz). EGFP was stained using a rabbit anti-GFP polyclonal antibody (Life Technologies). Secondary antibodies were purchased pre-conjugated to either Alexa Fluor 488 (Life Technologies),

Cy3 (Jackson Immuno) or Alexa Fluor 647 (Life Technologies). Cells were finally stained with DAPI for 5 min and mounted on glass slides with Prolong gold. Tissue immunofluorescence staining was performed following 4% PFA fixation, paraffinization and antigen retrieval with standard protocols using antibodies as above or anti-cd11b (Abcam) and anti-Vimentin (Santa Cruz Biotechnology). Tissues were imaged with a 40× objective on the Ultraview Spinning Disk microscope using stitching algorithms in Volocity.

Flow cytometry

Cells were prepared for flow cytometry using warm Versene-EDTA (Lonza) for 5 min for detachment followed by 10 min fixation in 4% paraformaldehyde at 4°C, multiple washing steps and resuspension using FACS buffer (Dulbecco's phosphate buffered saline–Ca^{2+}–Mg^{2+} supplemented with 1% FBS and 5 mM EDTA). Dylight-650 labeled mRNA was used for flow cytometry experiments, performed using a BD FACS-Canto II flow cytometer and analyzed using FlowJo software. Experiments were performed in duplicate with >5000 cells per condition.

Gel shift to demonstrate MTRIPS binding to mRNA

100 ng of unmodified EGFP mRNA was pre-labeled with Dylight-650 using the above protocol. After filtration to remove unbound MTRIPS, the labeled mRNA was loaded on a 2% agarose gel and run with constant voltage (50 V for 2 h). As a control, we ran naked mRNA (incubated over night at 37°C without MTRIPS) or labeled mRNA boiled at 95°C for 10 min.

Size exclusion chromatography to assess degree of labeling

In order to assess labeling efficiency, mRNA and MTRIPs labeled with Dylight-650 or the same amount of MTRIPs without mRNA was analyzed by size exclusion chromatography using an SEC-4000 Yarra column (Phenomenex). Samples were flowed using 1× phosphate buffer and analyzed by fluorescence reading in real-time on a Shimadzu Prominence HPLC system.

Mouse experiments

Mice were injected in the anterior tibialis muscle using 10 μg of Dylight680 or Cy3b-labeled mRNA in 40 μl of Ringer's Lactate (RiLa) or with RiLa alone. For *in vivo* EGFP production, 2 ul of Viromer Red (Lipocalyx) delivery vehicle was mixed with mRNA. Imaging during surgery was performed using the Fluobeam 700 Near-IR Imaging System (Fluoptics). The anterior tibialis muscle was removed 16 h post-delivery, fixed in 4% PFA and cryopreserved in optimum cutting temperature solution. Staining was performed on slices and imaged as described above. All animal handling and experiments were performed in accordance with protocols approved by the IACUC at Georgia Institute of Technology.

Statistics

Significance in proximity ligation assays was determined by running a one-way ANOVA on the data, using the Kruskal–Wallis test and Dunn's multiple comparisons test. Correlation statistics (Pearson, two-tailed *P* values), and Mann–Whitney *t*-tests were calculated in Graphpad Prism software. All other data was tested with two-way ANOVA

at a = 0.05 followed by Holm–Sidak method for multiple comparison testing. All measurements were analyzed with Microsoft Excel, Graphpad Prism, and/or Sigmaplot 13.

CHAPTER 3

ENGINEERING MESSENGER RNA FOR INREASED STABILITY AND PROTEIN EXPRESSION

Background

This chapter examines making alterations to mRNA in order to effect greater protein production or reduced immune responses in cells transfected with IVT mRNA. These changes are classified into two categories – sequence and chemical modification. Chemical modification occurs through the substitution of modified ribonucleosides during the manufacturing process of IVT mRNA, and the subsequent purification of the mRNA to remove impurities during production. Sequence modification can take the form of codon optimization in the coding region, and the addition of sequences in the 3' UTR region which are intended to interact with trans-acting factors within a transfected cell.

IVT mRNAs, unlike native mRNAs, will not possess a nuclear history. Native, cellular mRNAs are transcribed in the nucleus and undergo post-transcription processing such as splicing as well as forming an RNP complex with accessory proteins prior to nuclear export. An important example of proteins associated with mRNA during processing include the cap-binding complex (CBP80/20), which is exchanged for the translation initiation factory eukaryotic initiation factor 4E (EIF4E) within the cytosol (68,69). Following export from the nucleus, mRNA is subject to post-transcriptional regulation by a large number of proteins and RNP complexes (70). Native mRNAs may also possess advantages for rapid translation through intracellular localization. One

example is localization to the endoplasmic reticulum, where ribosomal profiling has shown higher levels of translation occurring (71,72).

Chemical modification of mRNA nucleotides occurs naturally through mechanisms such as the addition of a methyl or thiol group to bases (73). Chemical modification of IVT mRNA requires the substitution of modified bases during production. An example of a common modification is a methylation reaction. Complete substitution is helpful for ensuring homogeneity of the final product. In early research on mRNA therapeutics, Kormann et al pointed out that pseuoduridine combined with 5-methyl cytodine resulted in diminished immune response and higher levels of protein production. Later work by Kariko et al showed that HPLC purification of mRNA removed impurities which would otherwise result in immune activation. More recently, 1-methyl pseudouridine has produced the highest level of protein production (74). Codon optimization was also shown to drastically improve protein production, even without the inclusion of any modified nucleotides (75). However, it is important to note that these studies were limited to usually a single coding region, typically a reporter protein such as luciferase, and some of these improvements may not

IVT mRNA does not follow the same cellular routing and processing as endogenous mRNAs. It does not contain a nuclear history, and aside from any conjugated delivery vehicle, does not enter the cell with accessory proteins. In comparison, native mRNAs exit the nucleus as an RNP complex, with elements which can preserve or bring them to a translational complex for subsequent translation. In this chapter, we show that IVT mRNAs do interact with trans-acting factors, particularly with the cellular protein HuR, which is

involved in mRNA longevity (76,77), and thus can be engineered through sequence changes to take advantage of cellular systems of mRNA regulation.

One method of regulation is to use RNA interference by taking advantage of cellular mechanisms to control mRNA copy number through cellular miRNAs and the endogenous RNA Silencing Complex (RISC). Through the inclusion of specific miRNA binding sites in the 3' UTR of IVT mRNA, protein production can be decreased in cell types with a high copy number of matching miRNAs, but remain the same in cell types with diminished miRNA expression. This allows the introduction of cell-type specificity, adding another element of control to mRNA expression.

Incorporation of modified nucleotides into mRNA attenuates protein expression primarily due to stress granule formation.

Following the results in chapter 2 showing decreased stress granule formation and thus overall higher protein production following incorporation of modified nucleotides, we tested a larger number of chemical modifications. Complete substitution of a modified nucleotide with the corresponding nucleotide during the manufacturing process assured a homogenous population of mRNAs. These mRNAs were transfected into HeLa cells using Lipofectamine 2000 (L2K) which resulted in GFP expression as detected by flow cytometry (Figure 3.1). The presence of stress granules (SG) was evaluating using intracellular staining and is presented as the percentage of cells containing SGs (Figure 3.2). In all cases where protein expression is reduced compared to the best performing modified nucleotide, 1-methyl pseudouridine (1mY), formation of stress granules is apparent. This clearly indicated a primary mechanism of action for modified nucleotides

to have improved protein expression due to reduction in immune sensing, likely by protein kinase R (PKR) as shown in chapter 2.

Protein expression using modified mRNA is dependent on the nucleotide sequence

Schlake et al (75,78) demonstrated that codon optimization of luciferase encoding mRNA remarkably increase protein expression compared to incorporation of modified nucleotides in luciferase. Common algorithms for codon optimization choose optimal amino acid codes based upon species occurrence rates, as well as checking for secondary structure and increasing GC content (79-86). However, it cannot be inferred from the data presented that this approach universally applies to all sequence and modification combinations. We repeated the previous GFP expression and SG testing using luciferase-encoding mRNA (Figure 3.3). Notably, the incorporation of 5meC or pseudouridine produced strong improvements in GFP expression but not luciferase, even in some cases resulting in a decrease in expression compared to wild type mRNA. As this work was performed in the same Hela cell type, the results indicate that there is likely an interplay between factors such as the incorporation of differing amounts of modified nucleotides, the spatial locations of modified nucleotides within a sequence, the spatial location relative to structures in the mRNA which may be potential binding sites for pattern recognition receptors, and possible effects on overall secondary structure in the mRNA. However, 1mY-modified mRNA continued to show increased expression in both mRNA sequences as well as a nearly complete reduction in stress granules.

Reduction of cellular innate immune response is possible through co-delivery of mRNA with small molecule inhibitors of PKR.

For subsequent work, 1mY was incorporated into mRNAs because of increased protein expression and reduced immune sensing. However, to test whether protein expression could be reduced further through reduction in immune response, we co-delivered unmodified and 1mY modified mRNA with 2-aminopurine (2AP) and C16, both known as inhibitors of PKR (87,88). Protein expression as evaluated by flow cytometry showed increased with both 2AP and C16, even in the case of 1mY modified mRNA (Figure 3.4). This strongly implies that even incorporation of 1mY does not fully suppress immune sensing. When performing a similar test in another cell type and using luciferase mRNA (Hek293 cells – Figure 3.5), it is notable that the trends of protein expression increase remained the same but the relative differences changed, which may be due to differential expression of immune sensing factors and signaling proteins.

We performed RT-PCR on hek293 cells transfected with GFP mRNA 1mY and unmodified. Levels of IFNB and IL6 showed higher levels with unmodified mRNA compared to modified mRNA. For IL6, significant reductions were shown with both unmodified and modified mRNA when co-delivered with C16 (Figure 3.6).

Optimization of mRNA-delivery vehicle N/P ratio

We also searched for alternatives to l2k delivery in order to find a delivery vehicle with transfection capability for *in vivo* applications. Specifically, polyethylamine derivatives are known to be effective *in vivo*, though effectiveness is largely dependent on the ratio of delivery vehicle to mRNA, or nitrogen to phosphate content respectively (N/P) (89,90). We performed a protein expression screen for different modified PEI formulations in primary rat cortical neurons, A549 cells, Hela cells, and RAW cells using multiple N/P

ratios of delivery vehicle and GFP mRNA. Flow cytometry screening showed that certain delivery vehicle combinations resulted in higher at expression, though only at specific N/P ratios in a cell type dependent manner. These results are shown in Figure 3.7, 3.8, and 3.9 for HepG2 cells, A549 cells, and primary rat neuronal cells respectively. Notably, protein expression differed greatly between different cell types and N/P ratios. Due to its commercial availability and overall high levels of protein expression in multiple cell types at medium to high N/P ratios, Viromer Red (Lipocalyx, GMBH) was chosen for subsequent transfection experiments.

To better understand why one N/P ratio might perform better than another, we labeled mRNA with cy3b and measured the cytosolic sum intensity of mRNA for each N/P ratio in mod PEI 4 (Figure 3.10), comparing to our highest overall performing formulation in A549s (Viromer Red at medium N/P ratio). Viromer Red showed a higher cytosolic concentration which matches with previously measured protein expression, indicating that N/P ratio may result in higher cytosolic mRNA levels.

Interactions between delivered mRNA and cellular RNA-binding proteins

While it has been shown that IVT mRNA delivered to a cell interacts with pattern recognition receptors, it is unknown whether these mRNAs, lacking a nuclear history, can interact with regulatory proteins. One cellular system of importance in mRNA regulation is the miRNA system and the associated RISC complex. If delivered IVT mRNAs can interact with the RISC complex in a sequence specific-manner, it would be possible to design mRNAs such that they would be expressed differentially in cell types with different levels of miRNA expression. We designed mRNAs with miRNA sites in the 3’ UTR

region. In order to pursue a future goal of neuron-specific expression, miRNA sites were chosen using a miRNA known to be low copy number in rat cortical neurons compared to other neuronal cell types, miR146a, as well as a miRNA known to be upregulated in neurons but not in other neural cell types, miR376a (91).

To test that miRNA sites were capable of binding to cellular machinery in a sequence specific manner in IVT mRNA delivered to cells, we co-delivered them with miRNA mimics corresponding to miR146a and miR376a respectively, as well as delivering the opposite miRNA sequence as a control. Delivery of matching mimics showed a decrease in protein expression but not with mimics of a different miRNA sequence – showing that miRNA sites function in a sequence specific manner (Figure 3.11). This showed a promising technique for inducing cell-type specificity through careful engineering of miRNA sites in the UTR of IVT mRNA; however, it is not known whether cellular copy numbers of miRNAs will be sufficient to completely suppress mRNA expression.

Next, we tested if the incorporation of UTR sites from long lived mRNAs could yield increased protein production or mRNA longevity. We added the polyprotein UTR from the Sindbis virus or the human beta globin gene UTR into the UTR region of GFP encoding mRNA already containing the previously used mouse alphaglobin UTR sequence. We examined GFP expression in Hela cells for over 120 hours in order to determine if the new UTR sequences resulted in greater stability or initial protein production. In addition, we tested the miR146a-incorporating RNA sequence. Interestingly, the miR146a mRNA performed with higher initial expression compared to the others, followed closely by the mRNA with the human beta globin UTR (Figure 3.12).

Hela cells do not contain particularly high levels of either miRNA tested, though their presence would only decrease expression. Based on comparison of calculated half-lives and corresponding confidence intervals, GFP miR146 had a slightly higher half-life than the others mRNAs. While the decay rates of GFP expression overall remain similar, the increased protein expression in GFP miR146 should not have resulted as compared to wild-type GFP mRNA. We hypothesized that this was the result of RNA binding proteins related to stability binding to the additional sequences in the UTR. Considering that miR146a and miR376a are relatively AU rich, we tested for interaction with the RNA binding protein HuR, involved in mRNA stability. We performed a proximity ligation assay between HuR protein and V5-tagged MTRIP probes bound to the UTR of the mRNA. This resulted in notably high interaction between HuR and the mRNA, which was not present in the controls (Figure 3.14). However, while no significant statistical differences was found between the GFP-miR constructs and GFP alone, it was clear that cellular RBPs interact with IVT mRNA.

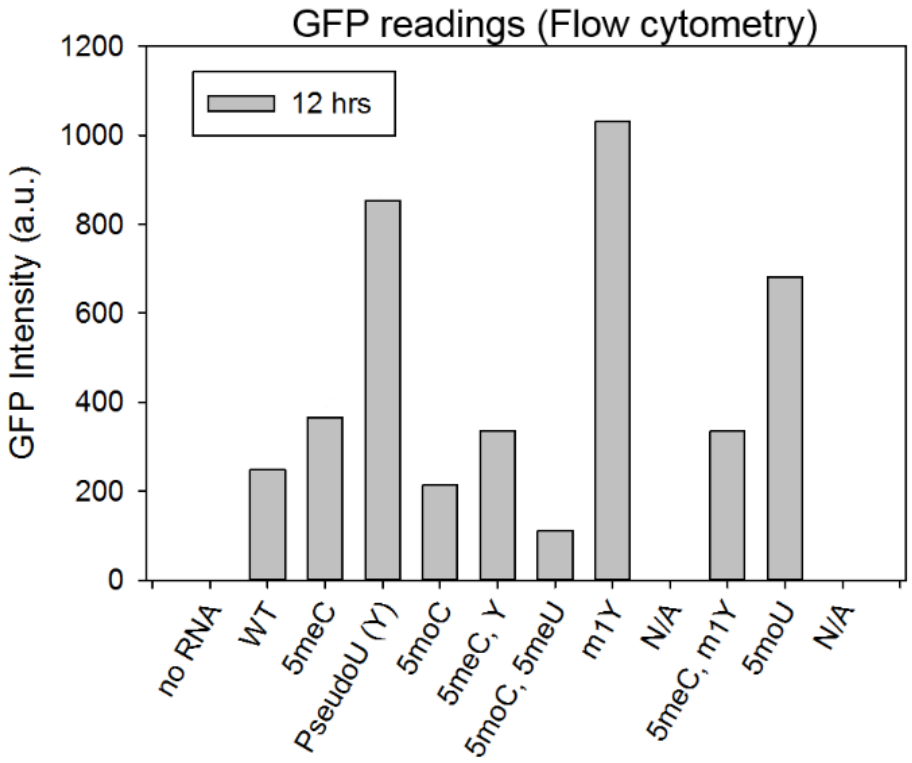

Figure 3.1: Incorporation of modified nucleotides into GFP mRNA results in differential levels of GFP expression. Hela cells were transfected with GFP mRNA and lipofectamine and analyzed by flow cytometry 12 hours post-transfection. 1-methyl-pseudouridine (m1Y) presents the highest level of protein compared to wild type (unmodified) mRNA. PseudoU, m1Y, and 5moU are significant compared to WT ($P<0.05$).

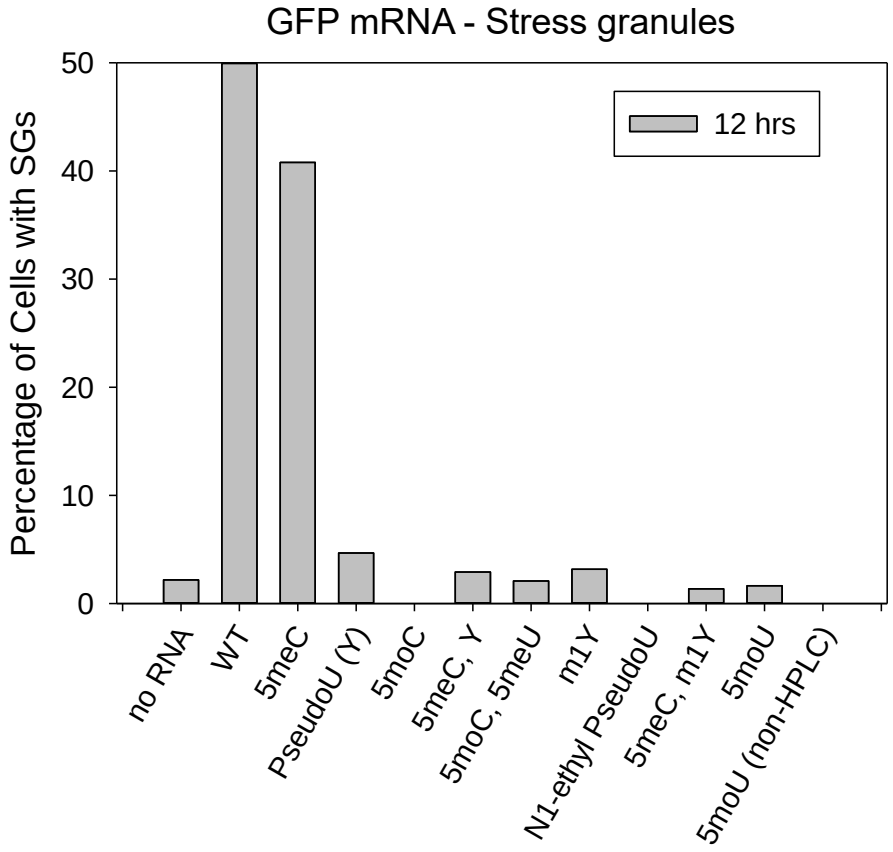

Figure 3.2: Differences in stress activation between different modified chemistries in GFP mRNA. Hela cells were transfected with GFP mRNA and lipofectamine and analyzed by flow cytometry 12 hours post-transfection. Lower stress granule formation from modifications including pseudouridine (PseudoU) or m1Y corresponds to higher levels of GFP expression as shown in the previous figure.

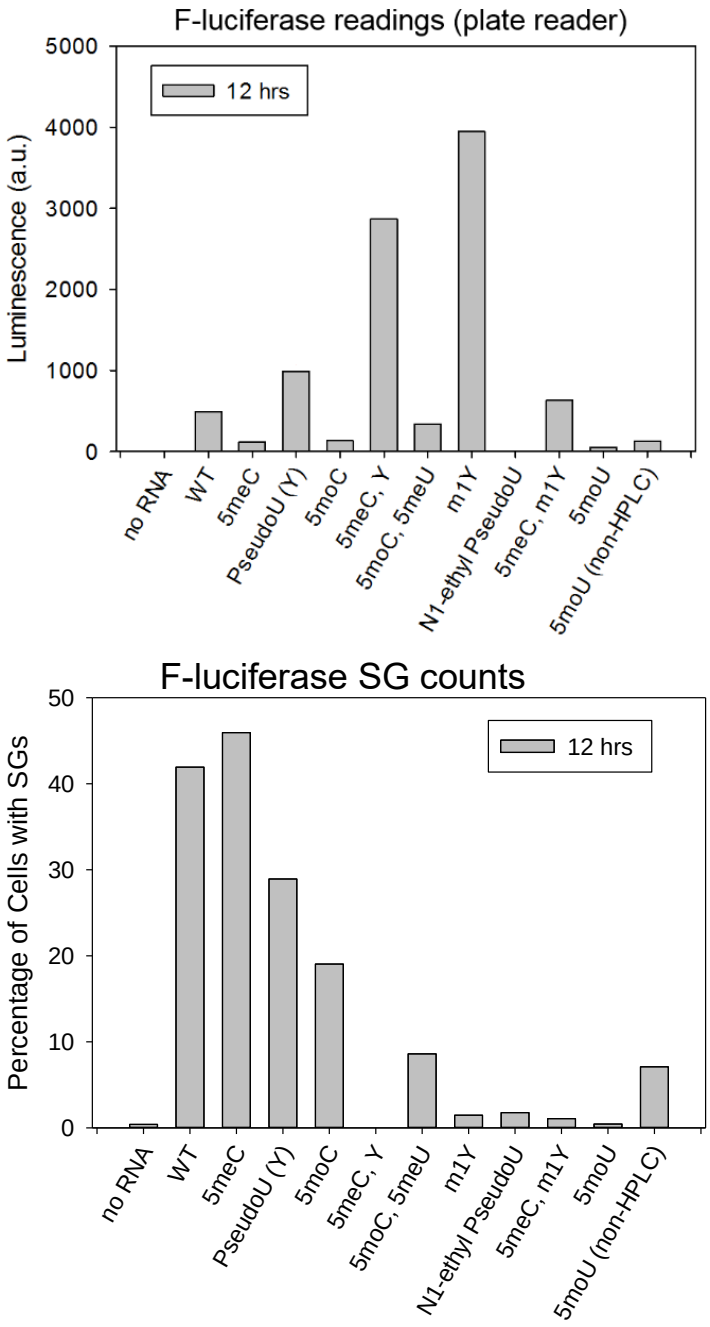

Figure 3.3: Protein expression and SG formation using modified nucleotides in luciferase encoding mRNA. Hela cells were transfected with firefly luciferase mRNA and lipofectamine and analyzed by flow cytometry 12 hours post-transfection. 1-methyl-pseudouridine (1mY) presents the highest level of protein compared to wild type (unmodified) mRNA, but pseudouridine alone produces lower protein expression due to stress granule formation.

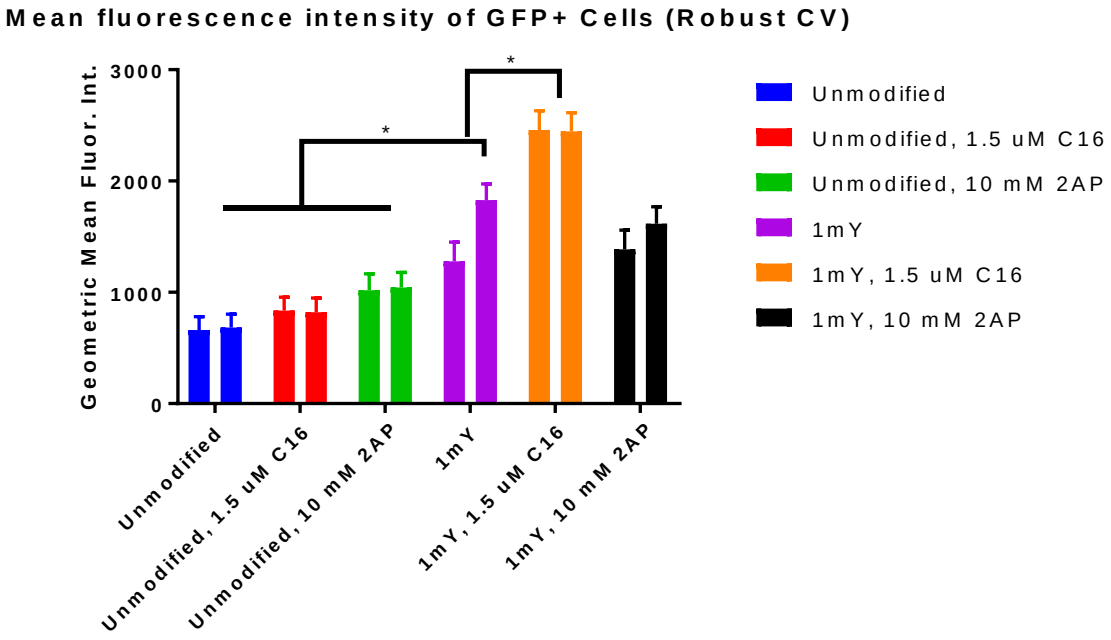

Figure 3.4: Effect of codelivery of GFP mRNA and small molecule inhibitors on protein expression in Hela cells. Unmodified and 1mY modified GFP mRNA was delivered using lipofectamine and analyzed by flow cytometry at 5 hours post-transfection. While no significant difference was shown between unmodified mRNA cases, a significant increase ($P<0.05$) was detected by one-way ANOVA with multiple comparisons between 1mY GFP mRNA delivered with and without C16 inhibitor.

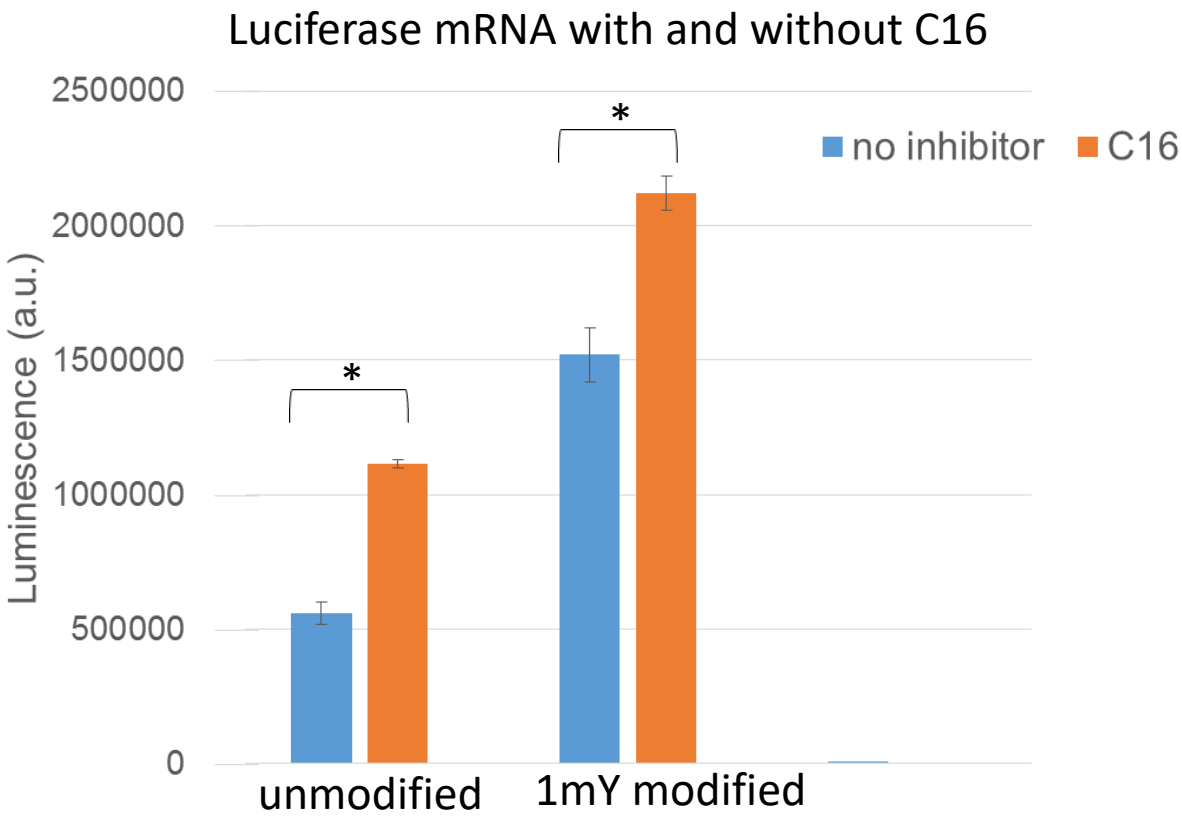

Figure 3.5: Effect of codelivery of luciferase mRNA and C16 on protein expression in hek293 cells. Unmodified and 1mY modified GFP mRNA was delivered using lipofectamine and analyzed by flow cytometry at 16 hours post-transfection. Higher levels of protein expression are achieved with C16 in both modified and unmodified cases.

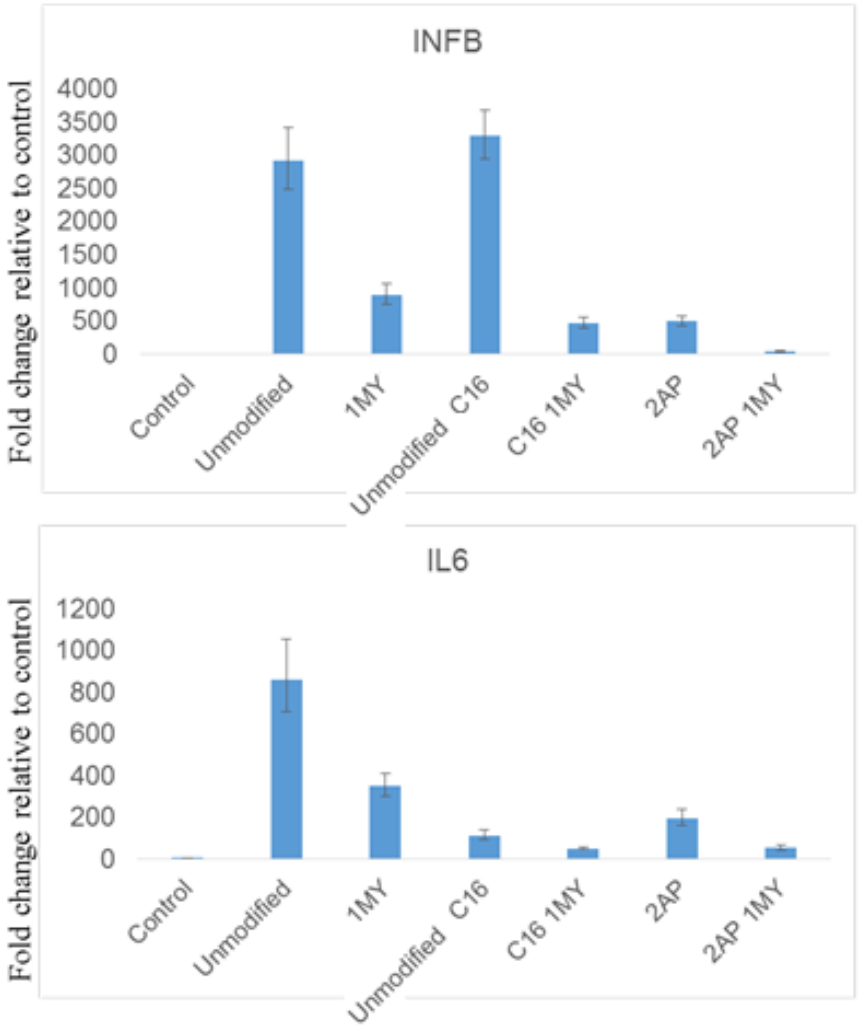

Figure 3.6: Cytokine analysis of hek293 cells 5 hours post transfection with GFP mRNA. Unmodified GFP mRNA results in significantly higher levels of INFB and IL6. 1mY mRNA shows reduced cytokine response. C16 has a noticeable effect on Il6 level reduction but not significant in INFB. Bars indicate SD.

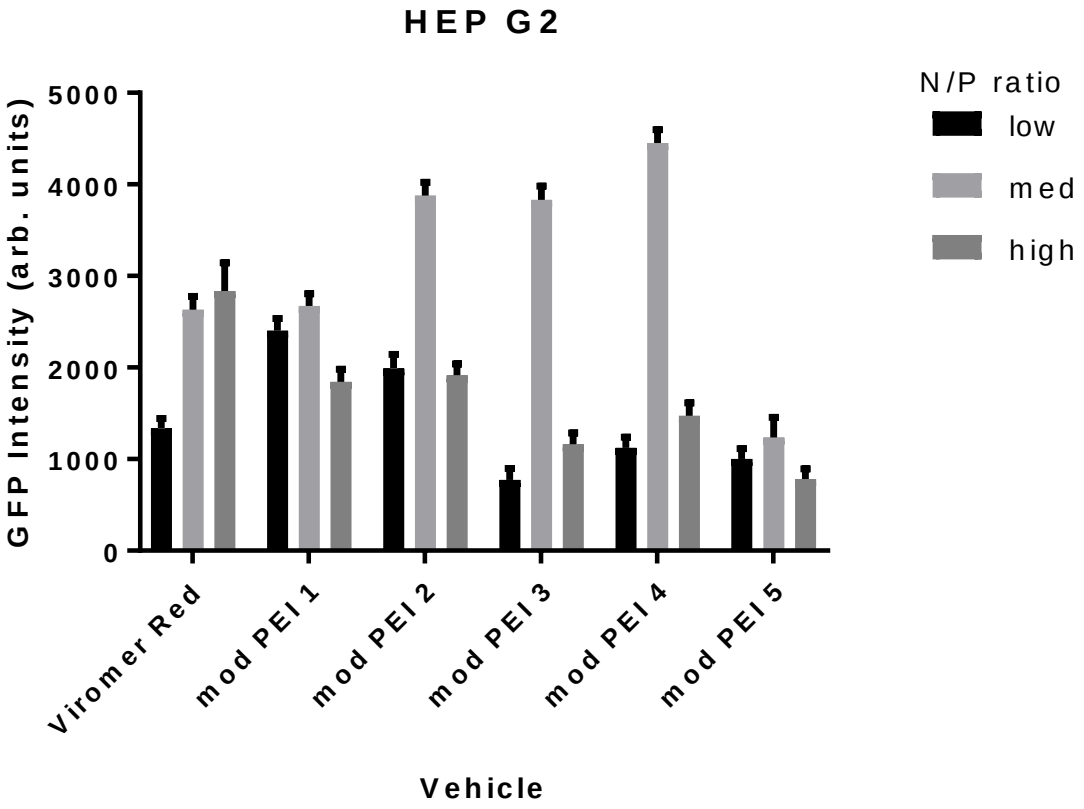

Figure 3.7: Protein expression 24 hours post-transfection of hepG2 cells with 1mY GFP mRNA formulated at different N/P ratios and PEI derivatives. Viromer Red, the only commercially available formulation here, shows significantly higher levels of GFP intensity at medium and high N/P ratios compared to low N/P ratio. Mod PEI 1 shows similar levels of GFP, while mod PEI 2/3/4 show significantly higher protein expression than all other formulations but only at a medium N/P ratio. These comparisons were made by one-way ANOVA with $P<0.05$. Bars indicate CV.

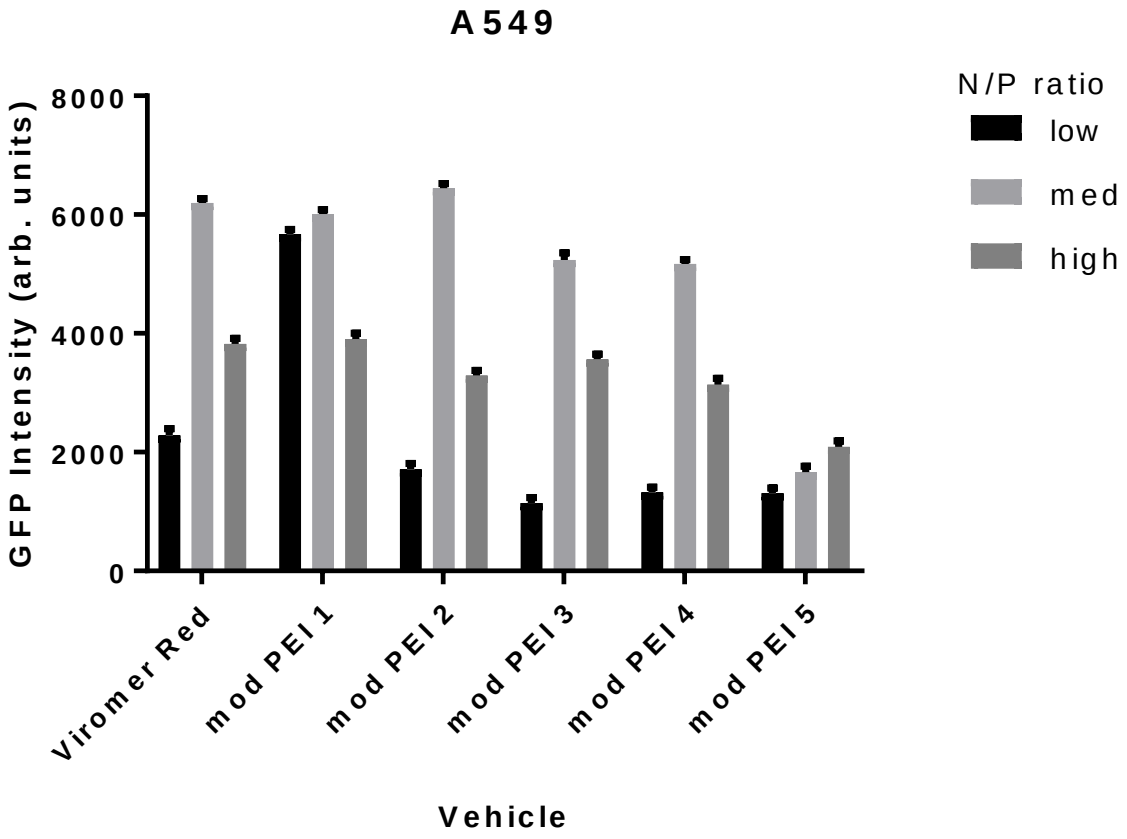

Figure 3.8: Protein expression 24 hours post-transfection of A549 cells with 1mY GFP mRNA formulated at different N/P ratios and PEI derivatives. Medium N/P ratios perform statistically better than low or high N/P. Exceptions include mod PEI 5, which performed poorly at all ratios, and mod PEI 1, which produced similar protein levels between low and medium N/P ratios. These comparisons were made by one-way ANOVA with $P<0.05$. Bars indicate CV.

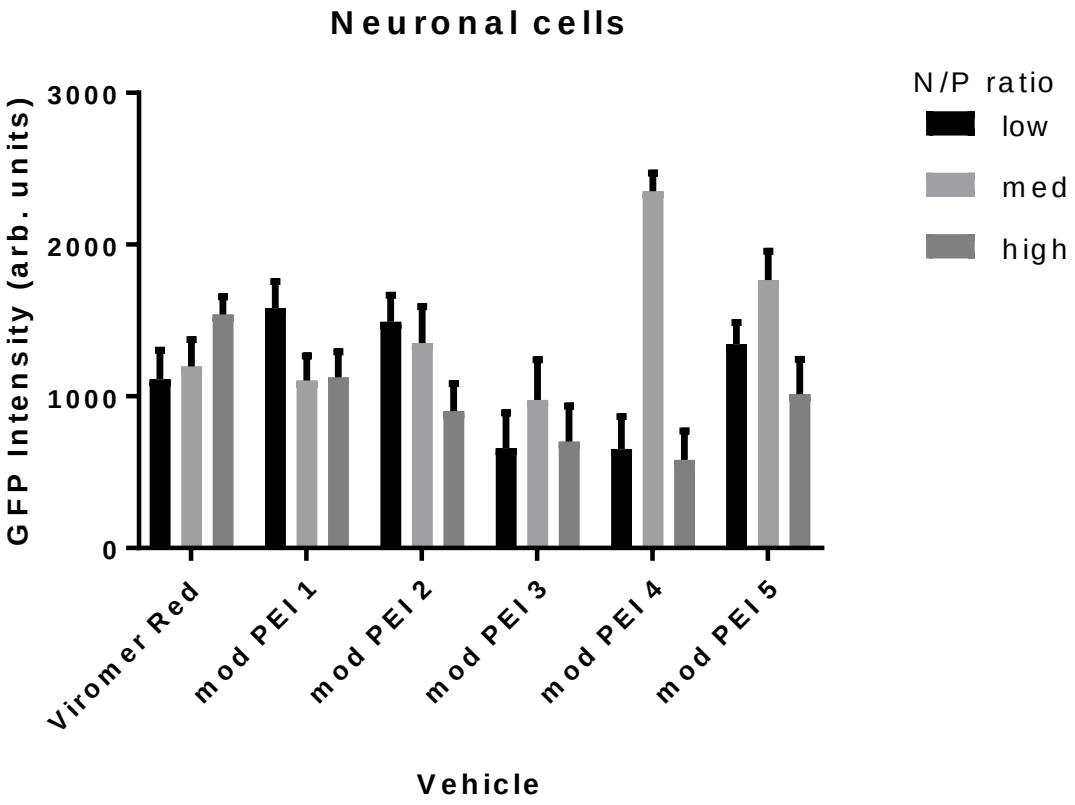

Figure 3.9: Protein expression 24 hours post-transfection of primary rat cortical neuronal cells with 1mY GFP mRNA formulated at different N/P ratios and PEI derivatives. Viromer Red performs significantly better than other delivery vehicles at high N/P ratios, though mod PEI 4 at medium N/P performs best overall followed by mod PEI 5. These comparisons were made by one-way ANOVA with $P<0.05$. Bars indicate CV.

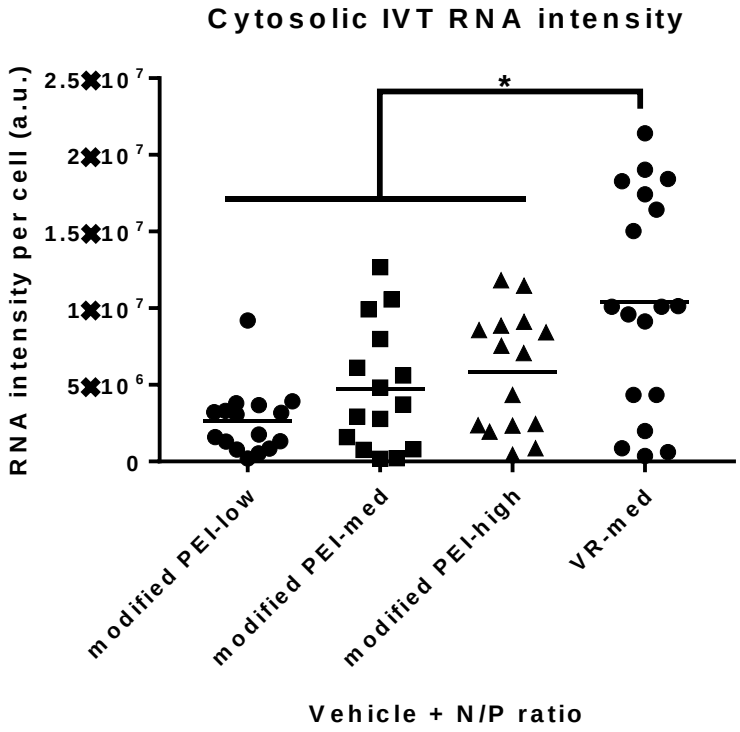

Figure 3.10: Cytosolic mRNA intensity 5 hours post transfection of A549 cells with 1mY mRNA and Viromer Red at medium N/P ratio or modified PEI (mod PEI 4). Viromer Red at medium N/P ratio shows a higher level of cytosolic mRNA, compared to the other modified PEI. Each dot represents a single cell and flat bars indicate mean RNA intensity. Statistical significance evaluated by one-way ANOVA with $P<0.05$.

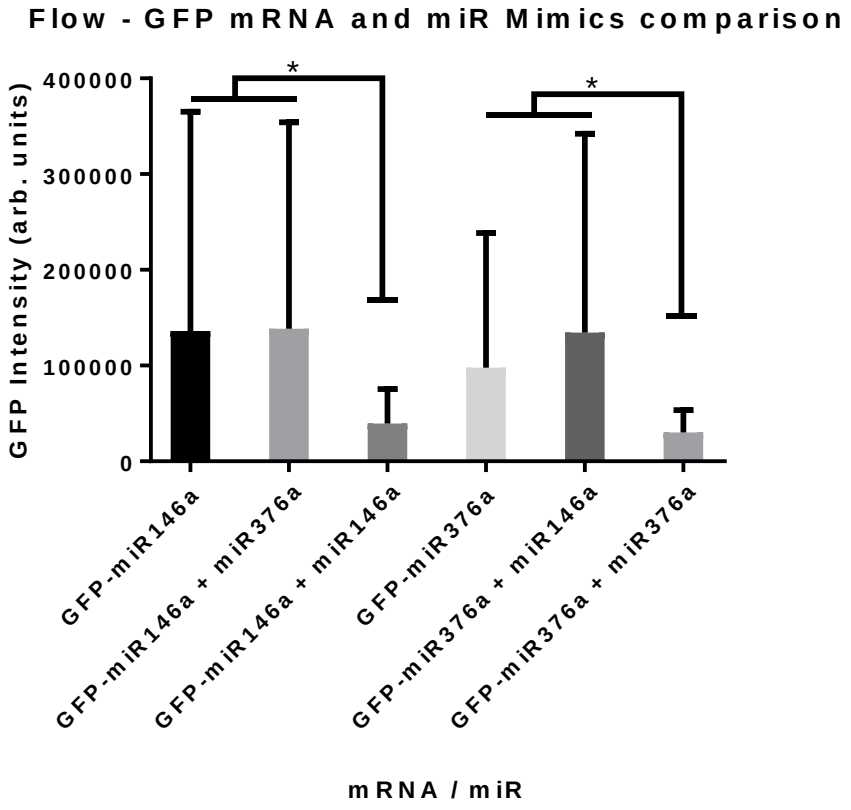

Figure 3.11: GFP expression following transfection of Hela cells with GFP mRNA containing miR sites in the 3' UTR co-delivered with miRNA mimic constructs. Co-delivery with a miRNA mimic corresponding to embedded miRNA sites results in significant reduction in GFP expression, but not when co-delivered with a different sequence mimic. Experiment was performed in duplicate. Statistical significance evaluated by one-way ANOVA with $P<0.05$. Bars indicate SD.

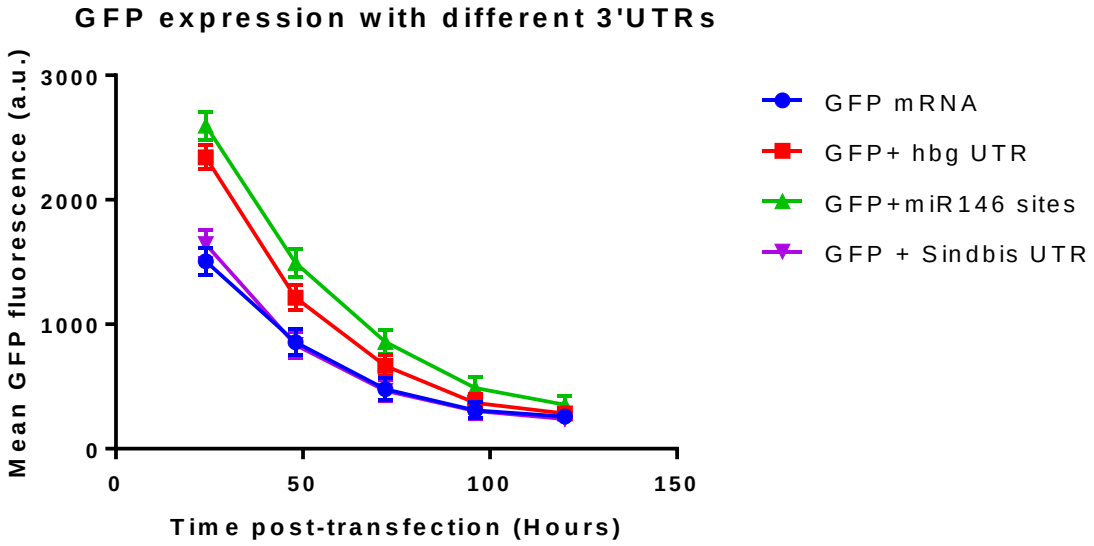

Figure 3.12: GFP expression following transfection of Hela cells with GFP mRNA with various 3' UTR regions. The UTR region corresponding to the Sindbis viral polyprotein UTR, the human betaglobin UTR, or 6x repeats of miR146 binding sites was inserted into the existing 3' UTR of GFP mRNA in addition to the existing mouse alphaglobin UTR sequence. Initial protein levels were higher with either the human beta globin UTR or the UTR containing miRNA sites. Note that the miRNA site 146 is not highly expressed in Hela cells. Bars indicate CV.

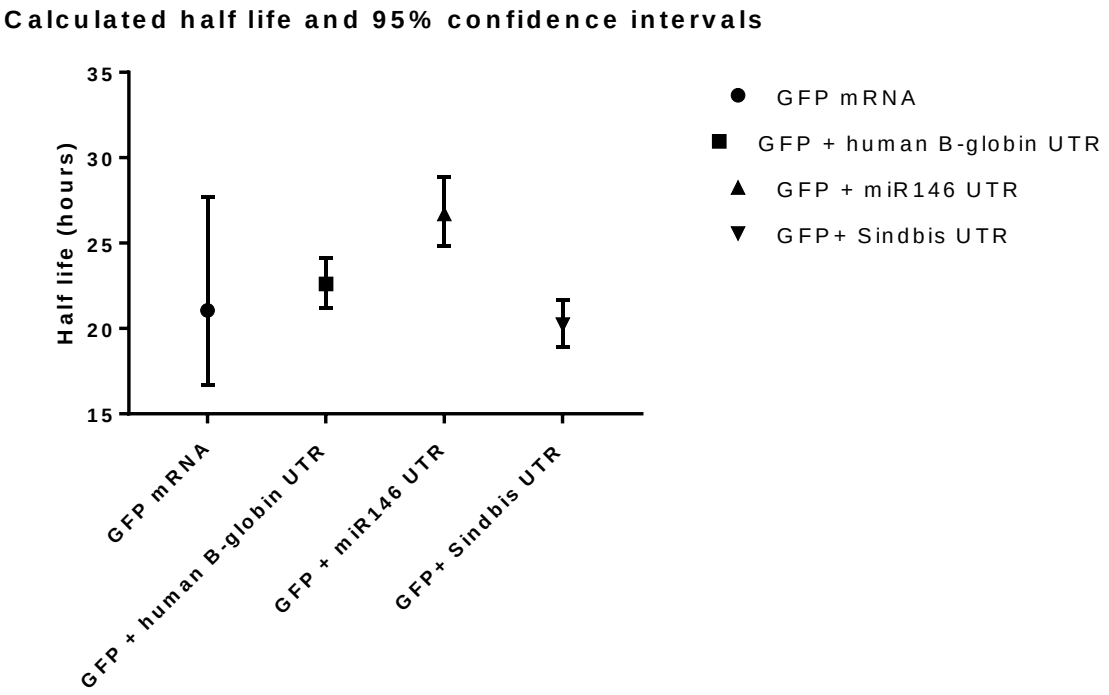

Figure 3.13: Half-lives of GFP expression following transfection of Hela cells with GFP mRNA with various 3' UTR regions. Bars indicate 95% confidence intervals.

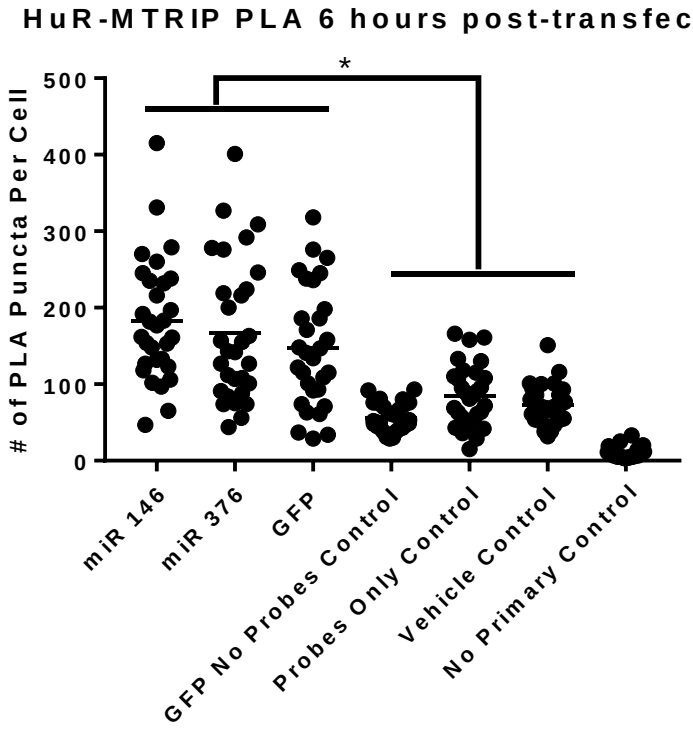

Figure 3.14: Proximity ligation assay between mRNA and HuR shows interaction between IVT mRNA and native HuR protein. GFP encoding mRNA was labeled with V5-tagged MTRIP probes and delivered to Hela cells using lipofectamine. Cells were fixed and PLA performed 6 hours post-transfection. GFP constructs showed significant HuR binding versus delivery of RNA without probes, probes only, vehicle only, and no primary antibody controls. No significant difference was found between controls or between GFP mRNA and GFP with miRNA sites incorporated in the UTR region.

Conclusion

This study has shown that there is a strong interplay of multiple factors between a transfected cell and IVT mRNA. This interplay can be effected by the synthesis of the mRNA, where incorporation of modified nucleotides can result in increased protein production through the reduction of stress response and other cellular factors related to innate immune sensing. However, while 1mY produced the highest levels of protein expression for both GFP and luciferase mRNA, observations of protein expression and stress granule formation with other chemistries show differential expression between sequences. This could be due to differences in availability of modified nucleotides to be detected by PRRs, as determined by the number of incorporated nucleotides (i.e. the amount of uridines), the location of these nucleotides, and effects on secondary structure of the RNA molecule.

Even with the stress granule-abrogating effects of 1mY incorporation in IVT mRNAs, there still exists a degree of immune activation in a PKR-dependent manner as shown when 1mY GFP mRNA is combined with PKR inhibitors. We have shown increased protein production and decreased cytokines when mRNA is co-delivered with C16 imidazolo-oxindole. Importantly, this opens room for further improvement of the mRNA, though it is uncertain whether nucleotide modification alone can achieve this.

Another factor greatly impacting mRNA performance is the delivery vehicle. As shown in Chapter 2, endosomal versus cytosolic delivery of mRNA results in different kinetics of protein production as well as stress response. Furthermore, different

formulations of mRNA and delivery vehicle can lead to higher or lower expression. This is partially due to the amount of mRNA released to the cytosol, due to the amount of mRNA that enters the cell and escapes from the endosome. Delivery vehicles may also alter interactions between the mRNA and cellular machinery, such as shielding mRNA from detection by PRRs, or by providing spatial localization advantages for forming translational RNP complexes. Even within the same class of vehicle, such as PEI derivatives, varying the ratio of delivery vehicle to mRNA results in significantly different protein expression levels in a cell-type dependent manner. Once again, the themes of one size fits all do not apply here, and that mRNA design and delivery must be specifically tested for effectiveness in target cells and tissues.

It is evident that IVT mRNAs can form translational complexes, activate PRRs, and degrade over time; however, it has not been previously shown that IVT mRNA interacts with regulatory RBPs in a controllable manner. This study has shown that engineering miRNA sites into the 3' UTR results in reduction of protein expression in a sequence dependent manner. This would allow the incorporation of cell type specificity by choosing miRNA sites which are diminished in target cells but upregulated in off-target cells. Incorporation of these sites into therapeutic mRNAs could reduce off-target effects and/or allow for higher doses. Furthermore, it shows that IVT mRNAs are subject to control by the RNA silencing complex (RISC). Incorporation of other UTRs such as those from long-lived mRNAs may impact protein production over time, though this is subject of further study.

Using the proximity ligation assay, we showed that the regulatory protein HuR interacts with IVT mRNA. This is additional evidence that mRNA is subject to regulation

by RBPs in a similar manner to native mRNAs, though the extent is unknown due to the differences between the native mRNA RNP and the relatively less protected IVT mRNA. This also opens possibilities for co-expression or codelivery of mRNAs encoding cellular host factors, such as protein involved in mRNA stability or that promote translation initiation. This may lead to an increase in the upper limit of protein expression for transfected cells.

In summary, when confronted with the problem of designing mRNA for a given task, mRNA needs to be designed based on available knowledge of target cell type, levels of innate immune sensing, and possible off-target effects. A formulation must be designed through in-depth testing with different mRNA-vehicle ratios as well as inclusion of small molecules or other protein-encoding mRNAs. Rational design of mRNA therapeutics will be key to achieving therapeutic levels of protein necessary for success in clinical applications.

Methods

IVT mRNA and multiply labeled tetravalent imaging probes (MTRIP) labeling

All IVT mRNAs were synthesized in lab from plasmids purchased from Life Technologies. Plasmids contained a T7 promoter followed by the mRNA sequence including a Kozak consensus sequence, gene sequence of interest, and the mouse alpha globin 3' UTR in addition to other UTR sequences (miRNA sites x6, Sindbis polyprotein UTR, human beta globin UTR, etc. A NOTI restriction site was inserted following the mRNA sequence in order to allow overnight digestion to linearize plasmids creating a 5' overhang for transcription. The digested DNA template was then purified using the

QIAquick PCR purification spin column (Qiagen). The T7 mScript Standard mRNA production system was used to generate mRNA (Cellscript). A cap-1 structure as well as an enzymatic poly(A) tail was added using manufacturer's instructions. mRNAs either were synthesized without modified nucleosides or with total incorporation of modified nucleotides. All nucleotides were purchased from Trilink. Purification steps were carried out using the RNeasy midi kit (Qiagen). Following transcription, mRNA was treated with Antartic phosphatase (New England Biolabs) for 30 minutes to remove residual triphosphates, and quantified on a Nanodrop 2000 (Thermo Scientific). RNA was stored frozen in –80°C and subjected to minimal freeze-thaw cycles.

For cytosolic mRNA quantification, mRNA was labeled with MTRIPs. MTRIPs were constructed as previously described (17,19). A detailed protocol for MTRIPs assembly and characterization was described in Santangelo *et al.* (38). Four oligos complementary to four adjacent sequences spanning the mouse alpha globin 3′ UTR (NM_001083955.1) of the IVT mRNA were generated. Sequences were adjacent due to the small length of the UTR region. Probe sequences can be found in Chapter 2 methods.

Each sequence was analyzed via nucleotide BLAST to ensure minimal off-target binding. Sequences were purchased as 2′-*O*-methyl RNA-DNA chimeric oligonucleotides 17–18 bases long with a short 5–7 poly(T) linker and 4 C6-amino-modified thymidines. The oligos included a 5′ biotin modification and were purchased from Biosearch Technologies (Petaluma, CA, USA). The oligonucleotides were labeled with Cy3b-NHS ester (GE Healthcare) or Dylight 650/680-NHS esters (Pierce) using manufacturer protocols. MTRIPs were assembled by incubation with Neutravidin (Pierce) for 1 h at RT followed

by filtration using 30 kD MWCO centrifugal filters (Millipore). mRNA was buffer exchanged into 1× PBS, heated to 70°C for 10 min and immediately placed on ice, combined with MTRIPs in a 1:1 mRNA:MTRIP ratio and then incubated overnight at 37°C. The next day, the labeled mRNA was filtered using a 200 kD MWCO ultrafiltration unit (Advantec MFS Inc.) and concentrated by 50 kD MWCO centrifugal filters (Millipore). Alternative filters tested during protocol optimization included 100 and 300 kD MWCO, but either did not filter unbound MTRIPs successfully or failed to successfully retain mRNA.

Microscopy

Stress granule (SG) imaging was performed using a Nikon Plan-Apo 40 × 0.95 NA air objective on a Nikon Eclipse TE2000 widefield microscope equipped with a Hamamatsu C9000-02 EM-CCD camera. All other samples, including tissue slides, were imaged using a Zeiss Plan-Apo 63 × 1.4 NA oil objective on an UltraVIEW Spinning Disk Confocal Microscope equipped with a Hamamatsu Flash 4.0v2 CMOS camera. The full dynamic range of the camera was necessary to capture intensities of large and small granules without undersampling or saturating images. All microscopes were controlled by the Volocity acquisition software (PerkinElmer).

Quantification of cytosolic mRNA

mRNA quantification was performed using Volocity software in images obtained on the spinning disk confocal microscope described above and a 63× objective. Briefly, thresholds were set to detect the dimmest mRNA granules (Cy3b), which were near the

detectable limit of the camera (~500/65536). All mRNA were identified as objects and sorted based on size (greater than or less than 1 μm^3) and overlap with endocytic markers. Large granules either overlapped with endocytic markers or were found to be outside the cell, which was verified by visual inspection. Such mRNAs were discarded from subsequent analysis. Smaller granules (<1 μm^3) were considered to be cytosolic if they did not overlap endosomal markers. For each cell, the sum of cytosolic mRNA and GFP expression was recorded and plotted using Sigmaplot. At least 30 cells were used per condition. In detail, in Volocity software, the 'Find Objects' function was used to automatically select RNA granules using intensity set above background levels. The objects found by the 'find objects' tool, for a given intensity setting, were verified by visual inspection (see Figure 4). A manual threshold was applied to sort objects into populations ('Filter Population' function) based on size (~1 μm^3). 'Find Objects' was applied again to generate an object population representing endosomal markers (CD63/EEA1/LAMP1) with manual intensity threshold set above background values. All populations were clipped and compartmentalized to ROIs which were manually drawn around individual cells. Populations were subdivided using the 'Exclude touching' and 'Exclude non-touching' functions between RNA granules of every size and endosome objects. Large and small RNA granules touching endosome objects were considered 'trapped' RNA granules. Large granules in contact with endosome objects, which were extremely rare, were individually inspected and removed from analysis as all appeared to be located above the cell. Small RNA granules not touching endosome objects were considered 'free' mRNA granules. The sum of all free mRNA per cell was calculated using the 'Analysis' tab in Volocity. Protein

expression was calculated in Volocity for each ROI as well. At least 15 cells were counted in this manner per condition per timepoint.

Proximity ligation assays

Protein/mRNA PLA has been previously described (28,29) and a detailed protocol can be found in Zurla *et al.* (39). Briefly, neutravidin was tagged with a V5 epitope through Solulink conjugation technology. A maleimide hynic linker (Solulink) was conjugated to the V5 tag, while an S-4FB linker (Solulink) was conjugated to the neutravidin, following manufacturer's instructions. After conjugation, the two reagents were mixed with the Turbolink catalyst (Solulink) to covalently bind the V5 tag to neutravidin. MTRIPs were then assembled as previously described using V5 labeled neutravidin (Na-V5), mRNA was labeled as above, and then used for transfection. Two hours post-transfection, cells were fixed with 1% paraformaldehyde and permeabilized with 0.2% Triton X in 1× PBS. Cells were then blocked for nonspecific interactions for 30 min at 37°C with PLA blocking buffer (0.1% gelatin, 2% donkey serum and 1% BSA in 1× PBS). Primary antibodies consisted of rabbit anti-HuR. Primary antibody was delivered (1:1000 V5 Ab and 1:5000 HuR Ab in PLA primary diluent (1% BSA, 1% donkey serum and 0.2% Triton-X in 1× PBS) for 30 min at 37°C. Cells were washed in wash buffer A (Sigma) at RT for 10 min. Secondary antibodies for rabbit and mouse antibodies (Sigma) were delivered at a concentration indicated by the manufacturer in PLA secondary diluent (0.05% tween 20 in 1× PBS) for 30 min at 37°C. This was followed by another 10 min wash in wash buffer A (Sigma) at RT. PLA ligation and rolling circle amplification were performed as specified by the manufacturer. Finally, cells were washed and mounted on a slide with DAPI

mounting medium (Sigma). PLA interactions were quantified using a 63× (oil) objective on a spinning disk confocal microscope. Thirty cells were measured per experimental condition and analyzed by Volocity software.

Cell culture and transfection

HeLa cells, A549s, and Hek293s were obtained from ATCC and maintained in DMEM or EMEM (Lonza) and supplemented with 10% FBS (Hyclone), 100 U/ml penicillin and 100 μg/ml streptomycin (Life Technologies). Cells were plated the day before an experiment in preparation for lipofectamine or PEI transfection. Lipofectamine was combined with labeled mRNA in Optimem (Life Technologies) using manufacturer protocols. For Viromer Red and other PEI derivates, transfections were carried out using manufacturer protocols in a similar manner to lipofectamine transfections, except using provided buffers in place of Optimem.

Immunofluorescence

Cells were fixed in 4% PFA for 10 min, blocked in 10% Donkey Serum and 5% BSA and immunostained as previously described (47) using appropriate antibodies. General endocytic markers used for evaluating cytosolic mRNA were CD63 (mouse anti-CD63, Developmental Studies Hybridoma Bank- DSHB), EEA1 (mouse anti-EEA1, BD Biosciences) and LAMP1 (mouse anti-LAMP1, DSHB). Stress granule markers included G3BP (mouse anti-G3BP, BD Biosciences) and TIAR (goat anti-TIAR, Santa Cruz). Secondary antibodies were purchased pre-conjugated to either Alexa Fluor 488 (Life

Technologies), Cy3 (Jackson Immuno) or Alexa Fluor 647 (Life Technologies). Cells were finally stained with DAPI for 5 min and mounted on glass slides with Prolong gold.

Flow cytometry

Cells were prepared for flow cytometry using warm Versene-EDTA (Lonza) for 5 min for detachment and resuspension using FACS buffer (Dulbecco's phosphate buffered saline–Ca^{2+}–Mg^{2+} supplemented with 1% FBS and 5 mM EDTA. Flow cytometry experiments, were performed using a BD Fortessa flow cytometer and analyzed using FlowJo software. Experiments were performed in duplicate with >5000 cells per condition.

Statistics

Significance in proximity ligation assays was determined by running a one-way ANOVA on the data, using the Kruskal–Wallis test and Dunn's multiple comparisons test. All other data was tested with two-way ANOVA at $a = 0.05$ in Graphpad Prism software.

CHAPTER 4

RNA-BASED EXPRESSION OF OPSINS IN CARDIOMYOCYTES AND NEURONAL CELLS

Background

This chapter presents an application of mRNA design for the expression of opsins, or optogenetic proteins, using mRNA in neurons and cardiomyocytes. Opsins are light-responsive ion channels which can be used for the control of action potentials in cells that exhibit electrical activity. They are currently in use for the scientific study of brain and cardiac electrical function (92-94). Other uses may include the generation of model systems for testing of new drugs and therapeutics.

The current use of opsins is limited by the vectors of expression. The primary expression vector for opsins includes viral vectors such as Adeno-associated Virus (AAV) (95,96). This results in limitations inherent to the individual virus used – this can include permanence of expression, the induction of a strong innate and adaptive immune response, possible integration into the genome, and difficulty in controlling localization .

An mRNA expression vector allows transient expression of an opsin with fewer safety risks. This enables a new set of optogenetic studies which can include repeated, alternating, or combined dosing with one or multiple opsins. Since opsins can be excitatory or inhibitory, transfection with both allows new combinations of opsin expression leading to the ability to form control networks.

Examples of opsins commonly used in neuron experiments include the excitatory opsin, Channel-rhodopsin II (ChR2), activated with pulsed blue light, and the inhibitory opsin JAWS (97), activated by constant orange or red light . For proper characterization of cells transfected with opsins, in addition to protein expression, another metric, function, is required to properly optimize the use of mRNA as an expression vector.

Functional characterization was performed with the use of a multi-electrode array (MEA). An MEA device uses electrodes to measure the field potential of nearby cells. Changes in field potential, such as spiking activity in neurons and cardiomyocytes, can be detected in an amplitude and location-specific manner depending on the pickup electrode. The MEA device used, a Maestro from Axion Biosystems, allows the simultaneous measurement and light excitation of 16 electrodes per well in a 48 well plate. While spontaneous activity occurs in both rat cortical primary cells and neonatal rat ventricular myocytes (NRVMs), functional expression of an opsin such as ChR2 can be measured as a synchronization event between electrical activity and pulsed light excitation from the LEDs embedded in the Axion Lumos device.

After verification with primary rat cortical cells and primary rat cardiomyocytes using an MEA device, it was necessary to measure function and expression in an *in vivo* system, injection of mRNA directly into the rat cortex. Injection can be performed by the use of a neurosyringe, but must be performed using small volumes to avoid damage. Additionally, while expression can be evaluated using immunohistochemistry in brain slices fixed post-transfection, function must be evaluated in the live animal via an electrode coupled to a fiber optic used for excitation.

As a future aim of this work, various delivery methods for therapeutic mRNA as alternatives to direct injection will be tested, with the goal of reducing invasiveness and thus translatability. These methods can include intranasal inhalation, ultrasound-guided transfection, intrathecal injection, and release from implanted devices. Alternatively, there are pathological states, such as traumatic brain injury, which can lead to permeability of the blood brain barrier to more traditional delivery methods such as IV or intramuscular injection.

Development and verification of mRNA expressing opsins

In order to develop a platform for opsin expression using IVT mRNA, we first generated mRNA corresponding to the sequence for Channel Rhodopsin II (ChR2), a blue light excitable ion channel which allows the controlled firing of action potentials in cells which exhibit electrical activity. ChR2 was initially chosen due to its widespread use in optogenetics studies. We codon optimized the coding region and embedded it in the same 5' and 3' UTR cassette including the mouse alpha globin 3' UTR as used in studies in chapters 2 and 3. mRNA was formulated with the PEI-derivative Viromer Red based on results in chapter 3. Following the IVT process, we transfected Hek293 cells to ensure that the protein expressed and was localized to the cellular membrane (Figure 4.1) in a similar manner to that shown using pDNA transfection by Lin *et al (95)*.

Functional validation of expressed opsins

Though we confirmed protein expression of ChR2 in cells, it was necessary to perform functional validation of the expressed protein. We first transfected HEK293 cells with ChR2 mRNA and 24 hours later used intracellular patch clamping performed by the

Forrest Lab at Georgia Tech to read changes in membrane potential. Patch clamping results showed response in membrane polarization to blue light excitation (Figure 4.2). The response amplitude (~200pA) and waveform was consistent with published results using a DNA-based ChR2 expression vector in Hek293 cells (95).

Expression of ChR2 in primary rat cortical neuronal cultures

Channel Rhodopsin 2 is the most commonly used opsin for optogenetic studies in the field of neuroscience. In order to show that mRNA-based expression was possible in neurons, we transfected primary rat cortical neural cells obtained from E18 Embryonic rat cortex using GFP-mRNA and Viromer Red. Using antibody staining with a nuclear marker which is neuron specific, NeuN, we observed that some cells contained both GFP fluorescence and NeuN nuclear staining, indicating that rat cortical neurons were being transfected (Figure 4.3).

We then performed a more robust functional assay using a multi-electode array (MEA) on an Axion Maestro-Lumos system. This system consisted of 16 electrode readouts per well multiplexed to a 48 well simultaneous measurement format, with fully controllable and synchronized 4-color LED excitation per well. The MEA approach is particularly suited to testing opsin function because although it is single-cell sensitive, it has the capability of broad spatial detection using multiple electrodes as well as excellent throughput.

An example of an MEA reading of neurons expressing ChR2 and responding to blue pulsed excitation light is depicted in Figure 4.4. We transfected rat cortical neurons three weeks post-plating on an MEA plate with ChR2 mRNA using 2000ng, 4000ng, and

6000ng of mRNA while maintaining the same delivery vehicle to mRNA ratio. In order to issues of excitation absorption by the YFP tag, we used mRNA encoding ChR2 with a V5 epitope tag sequence included. We measured electrical response to LED stimulation from 24 to 144 hours post-transfection. At 24 hours post-transfection, wells in all replicates showed action potential stimulation synchronized with blue light excitation pulses (Figure 4.4). 2 out of 3 wells responded to excitation at 48 and 72 hours post-transfection, with complete lack of response at 144 hours. This indicated that the opsin has a relatively long half-life. We also calculated the synchronization of excitation and neuronal firing. We found that the response rate, the percent of excitation signals which resulted in a synchronized neuronal network firing event, was best with 4000ng of mRNA (Figure 4.5). Complete synchronization was not achieved which is indicative of the need to increase levels of ChR2 expression, which was possibly affected by the presence of multiple cell layers and cell types thus reducing the ability of the mRNA formulation to reach neurons. The percent of wells which responded to light at each time point is shown in Figure 4.6, showing a decrease over time.

CatCH outperforms ChR2 in NRVMs

Opsins are also used for research in cardiac cell types. Pacing cardiac cells allows the screening of new drugs in a simulated pacing environment, where the effect on beat frequency and waveforms can be measured. While neurons continued to be a primary focus, the higher transfection efficiency in cardiomyocytes (90% vs 50%, data not shown) allowed better screening for opsin improvement. We transfected neonatal rat ventricular myocytes (NRVMs) with ChR2 and a modified ChR2 with a single amino acid substitution, CatCH (98). NRVMs were plated on MEA plates and the next day were transfected with

ChR2 or CatCH mRNA at difference concentrations in triplicate wells using Viromer Red. CatCH-transfected cells exhibited electrical response to 15 times less light than ChR2 at 24 hours post-transfection (Figure 4.7). Furthermore, when interrogated with excitation rates of 1hz, 2hz, and 3hz, CatCH transfected cells were able to be driven at higher beat rates (3hz) up to 72 hours post-transfection (Figure 4.8) compared to ChR2 transfected cells. As the amount of mRNA and structure of the opsin are very similar, this can be inferred as due to enhance sensitivity – fewer opsins per cell were necessary to drive cardiac action potentials. When opsin expression is low, such as at timepoints several days following transfection, cardiac cells could only be driven at the slower rate of 1hz successfully.

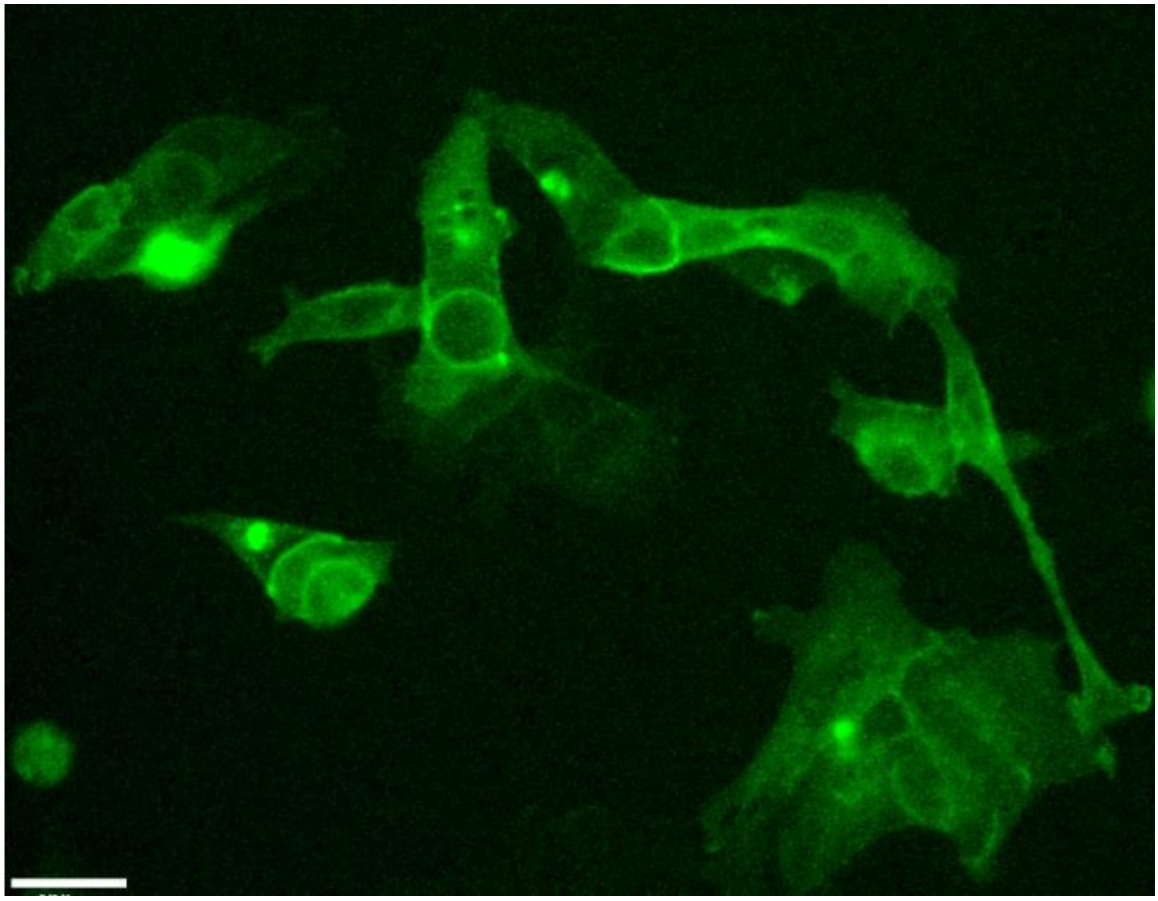

Figure 4.1: Opsin expression in Hek293 cells 16 hours post-transfection with ChR2-YFP mRNA. Live cells were imaged on a widefield microscope using a YFP filter set and 10x / NA 0.25 objective.

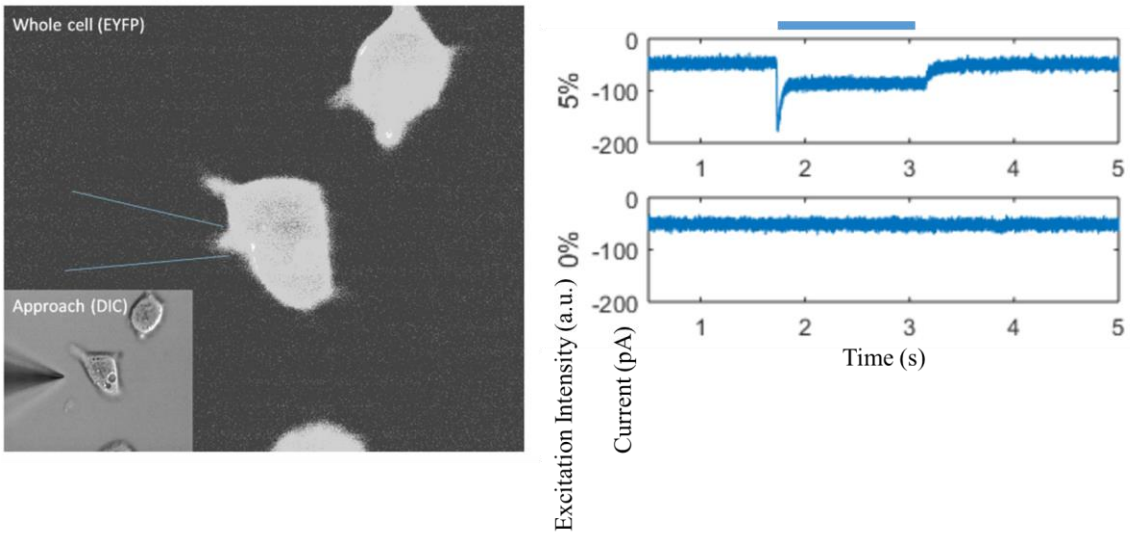

Figure 4.2: Functional validation by patch clamping of Hek293 cells 16 hours post-transfection with ChR2-YFP mRNA. Live cells were imaged in both fluorescence and DIC and patch clamped to obtain membrane potential measurements. Excitation with blue light at 5% intensity on from 1.8 to 3 seconds, as shown as a blue bar, indicates a distinct change in membrane potential. This work was conducted with Corey Landry from the Forest Lab at Georgia Tech.

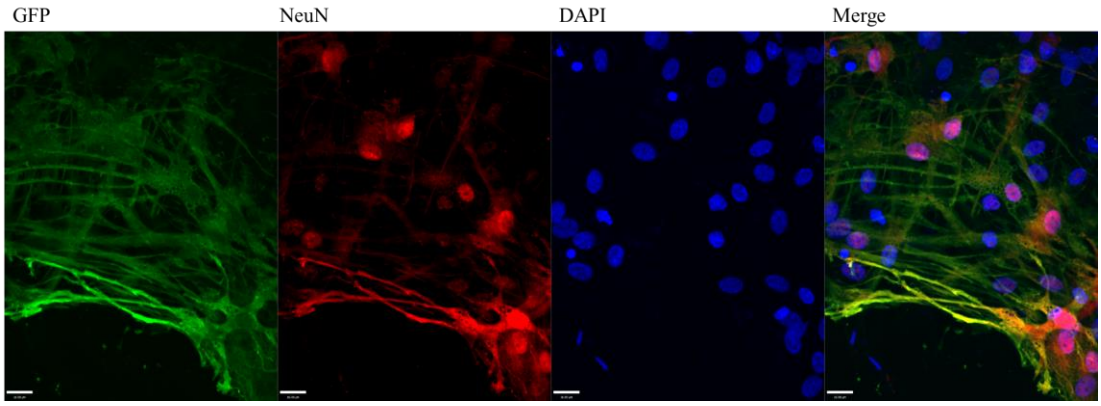

Figure 4.3: GFP expression colocalizes with the neuron-specific nuclear marker NeuN in mixed rat cortical neuronal cultures transfected with GFP mRNA. NeuN (red) marks the nuclei of neurons. GFP is visibly expressed in neurons, though other cell types are visible and may or may not express GFP. Cells were fixed and stained at 24 hours post-transfection and imaged with a 40x 1.2NA objective on an Ultraview Spinning Disk microscope.

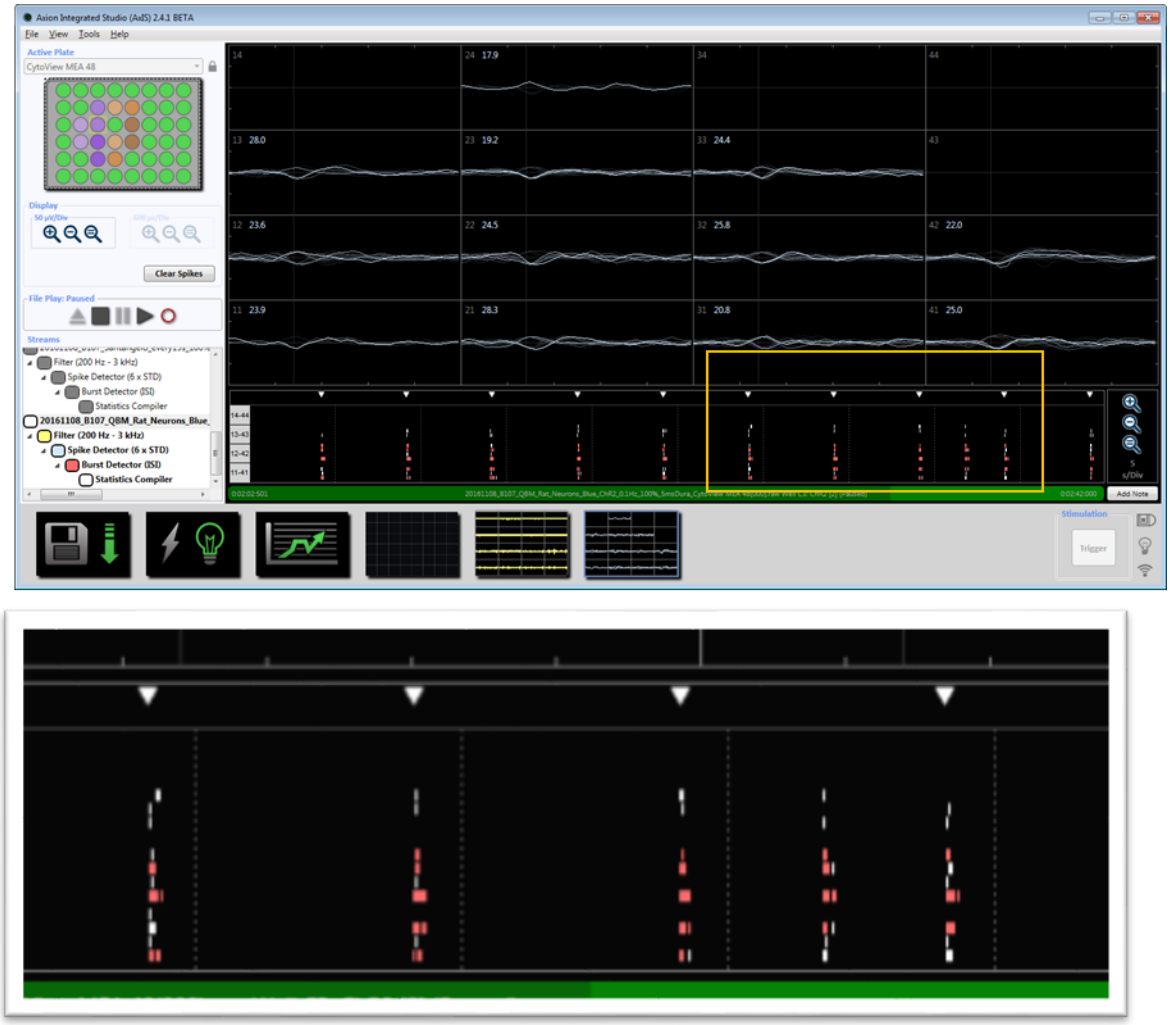

Figure 4.4: Example of ChR2 functional testing in rat cortical neuronal cultures. The screen displays waveforms detected in 16 electrodes in a single well of a 48 well plate. The blowup shows arrows which represent pulsed blue light. White and red dots indicate detected action potentials synchronized with the expression. Red dots in particular indicate neuron burst activity. Note that spontaneous firing activity also occurs without stimulus.

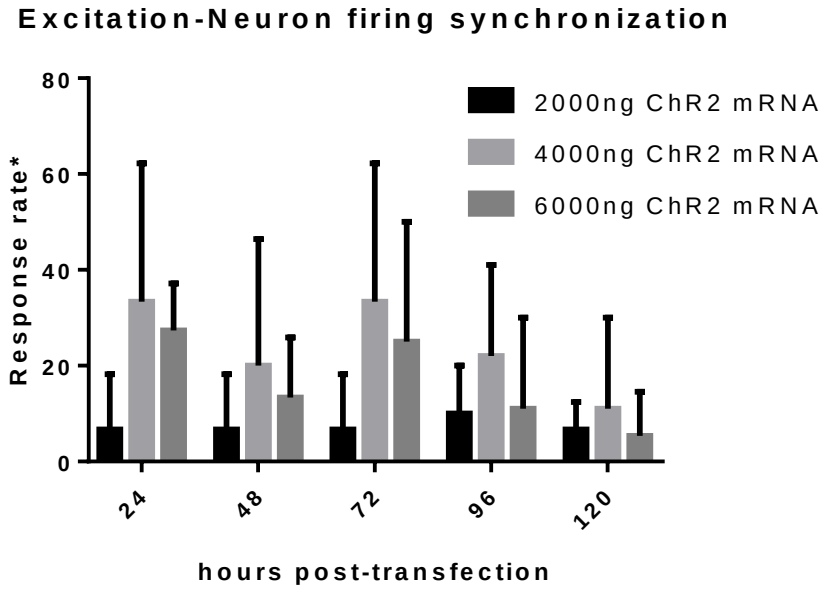

Figure 4.5: Synchronization of ChR-2 transfected neuron action potentials and excitation. The response rate is calculated by the number of time-synchronized action potentials corresponding to an excitation pulse. An excitation of 100% light pulsed for 5ms was used to stimulate action potentials, with a 3 second delay between pulses. Response rates are shown along with SD for 3 wells per condition. Three amounts of mRNA were used in order to find an optimal delivery amount.

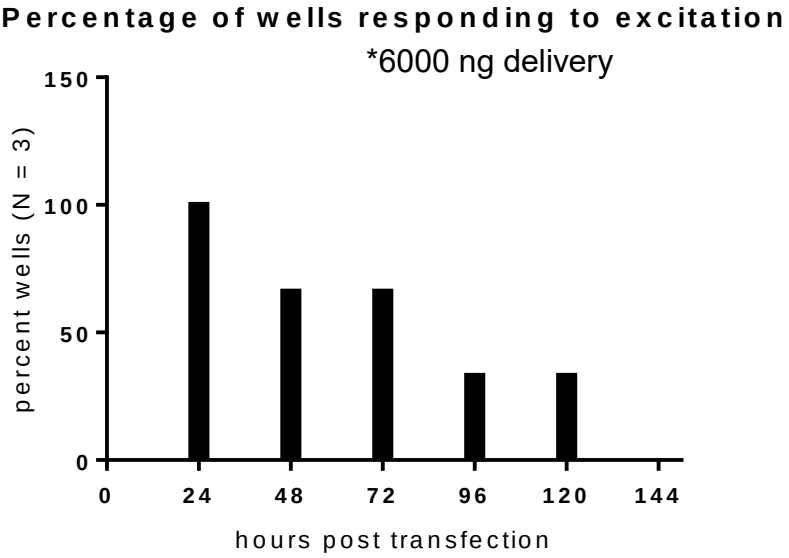

Figure 4.6: Response of ChR2-transfected neurons up to 144 hours post-transfection with ChR2 mRNA. Rat cortical neuronal cells were transfected with 6000ng of ChR2 mRNA and assayed via MEA daily until no response was detected from excitation light at 6 days post transfection. Percent of 3 transfected wells responding are plotted at each time point.

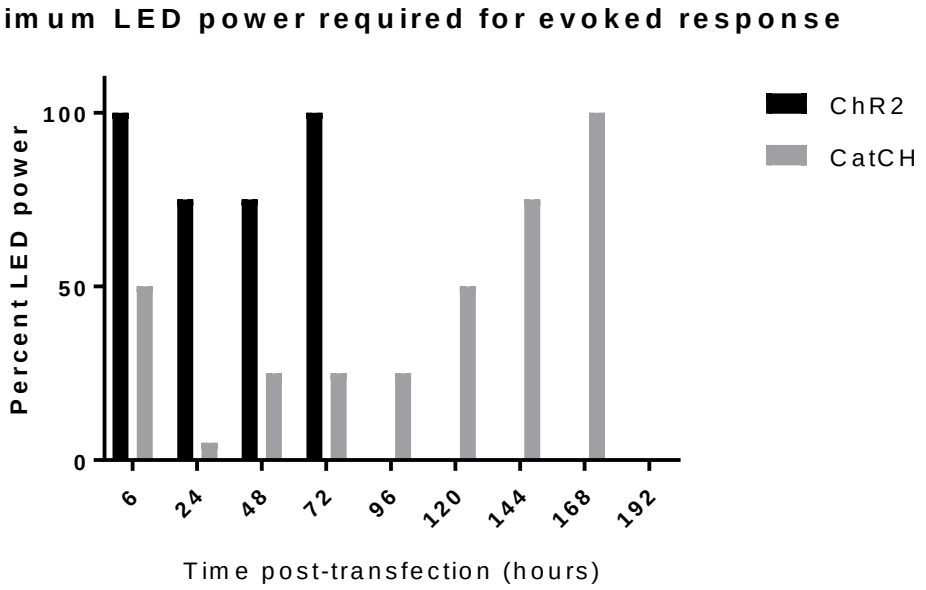

Figure 4.7: Excitation intensity comparison between ChR2 and CatCH mRNA-transfected NRVMs. NRVMs were transfected one day after plating on MEA plates with either ChR2 or CatCH mRNA. The sensitivity of the opsin to excitation light is inversely proportional to the percent LED power required to evoke a response. CatCH shows the highest sensitivity at 24 hours post transfection, where it responds to 5% intensity LED light. This is 15 times the LED power required for ChR2.

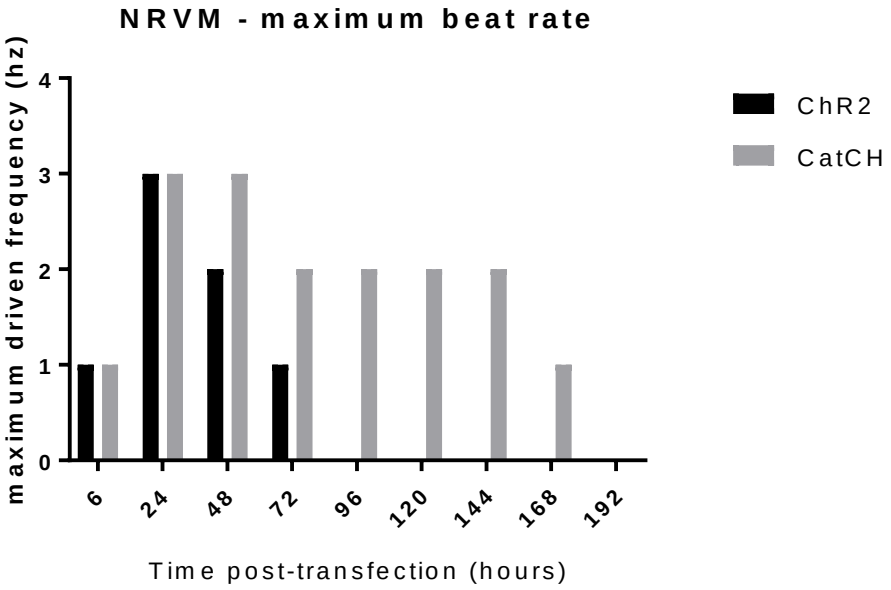

Figure 4.8: Maximum beat rate comparison between ChR2 and CatCH mRNA-transfected NRVMs. NRVMs were transfected one day after plating on MEA plates with either ChR2 or CatCH mRNA. They were driven at 1hz, 2hz, and 3hz via LED pulsing. Responses were recorded here if all 3 replicate wells were able to beat at the indicated rates using maximum intensity excitation light. CatCH is able to sustain higher frequencies throughout the time course.

Conclusion

The expression of opsins using mRNA provides an alternative to viral vectors for use in optogenetic studies involving neurons, as well as drug testing with cardiomyocytes. We successfully expressed functional ChR2 in primary rat cortical cells, and verified by immunostaining that neurons were transfected. Using patch clamping and an MEA, we verified function by using light stimulation to trigger action potentials. However, one difficulty is in the transfection efficiency even when using Viromer Red which showed positive expression in our screening in Chapter 3. One difficulty is the multiple cell types present in neuronal ex vivo cultures. Delivery is not as efficient due to multiple layers of cells as well as a large amount cells present 3 weeks after plating. This increases the proportion of non-dividing cells to neurons with time. However, following digestion and plating, neurons require substantial time to form networks capable of signaling, thus cannot be transfected immediately post-plating. These difficulties mimic some of the challenges for in vivo delivery. Further optimization will be required to realize higher transfection efficiencies and the future goals of expression in vivo.

Compared to neurons, cardiac cells transfect efficiently with mRNA, with longer expression times up to 144 hours post-transfection and higher light sensitivity based on MEA measurements. CatCH performs which much higher sensitivity than ChR2, though the literature reveals that there is a tradeoff in terms of higher reset times. This was not an issue for the time scales used in our experiments. Also, compared to neurons, a lower amount of mRNA was necessary for light response (500ng versus 4000ng), which again is attributable to the difficulty in access to the cultures as well as transfecting neurons in general. With the success of the opsin transfections in cardiomyocytes, though requiring

further validation, it is possible to express multiple opsins, or perform repeated dosing, due to the controllable and temporary nature of using mRNA as an expression vector.

Methods

In vitro transcription of opsin-encoding mRNAs

All IVT mRNAs were synthesized in lab from plasmids purchased from Life Technologies. Plasmids contained a T7 promoter followed by the mRNA sequence including a Kozak consensus sequence, gene sequence of interest, and the mouse alpha globin 3' UTR. Gene sequences used were sequences for opsins ChR2, CatCH, and JAWS. ChR2 sequence was obtained from Genbank AF461397. CatCH was generated from the same sequence with the single amino acid substitute as outlined by (Kleinlogel 2011). JAWS sequence was obtained from Genbank KM000925.1. All sequences were codon optimized using the Life Technologies Geneart website. A NOTI restriction site was inserted following the mRNA sequence in order to allow overnight digestion to linearize plasmids creating a 5' overhang for transcription. The digested DNA template was then purified using the QIAquick PCR purification spin column (Qiagen). The T7 mScript Standard mRNA production system was used to generate mRNA (Cellscript). A cap-1 structure as well as an enzymatic poly(A) tail was added using manufacturer's instructions. mRNAs either were synthesized without modified nucleosides or with total incorporation of modified nucleotides. All nucleotides were purchased from Trilink. Purification steps were carried out using the RNeasy midi kit (Qiagen). Following transcription, mRNA was treated with Antartic phosphatase (New England Biolabs) for 30 minutes to remove

residual triphosphates, and quantified on a Nanodrop 2000 (Thermo Scientific). RNA was stored frozen in –80°C and subjected to minimal freeze-thaw cycles.

Rat cortical neurons and NRVM cells

Cryopreserved rat cortical cells from rat E18/E19 embryonic neuronal cells were purchased from Lonza (R-CX-500) and immediately stored in the gas phase of liquid nitrogen. 1 day prior to plating on 48 well Lumos MEA plates (Axion Biosystems), plates were coated with sterile filtered 0.1% PEI solution in borate buffer using 5ul per well. Plates were incubated for 1 hour at 37C then washed 4 times with deionized water and left to dry overnight. The next day, plates were again coated with 5ul of laminin solution (Sigma), comprised of Neuron media and laminin at 20ug/ml. Neuron media consisted of Neurobasal medium (Life Technologies) supplemented with 5% fetal bovine serum, 1% penicillin-streptomycin, 2% B-27 supplement (Life Technologies), and 2mM l-glutamine (Life technologies). Following the addition of laminin, water was added to the space between wells to reduce evaporation. Plates were incubated for 2 hours at 37C. At the same time, rat cortical cells were removed from liquid nitrogen and thawed at 37 degree for 2.5 minutes. Media was added gently followed by mixing by swirling. Cells were pelleted at 400g for 5 minutes and resuspended at approximately 200,000 cells per 5ul. Laminin coating was aspirated and immediately replaced with 5ul media containing cells. Plate was then incubated in 37C for 1 hour prior to gentle addition of 300ul media per well. Media was exchanged every other day.

NRVM cells were a generous gift from the Cho Lab in the biomedical engineering department at Emory University. Provided media was exchanged every two days. Measurements could begin immediately the day after plating.

Immunofluorescence

Cells were fixed in 4% PFA for 10 min, blocked in 10% Donkey Serum and 5% BSA and immunostained as previously described (47) using appropriate antibodies. Primary antibodies included rabbit anti-GFP (Life Technologies) and mouse anti-NeuN (1B7, Abcam). Secondary antibodies were purchased pre-conjugated to either Alexa Fluor 488 (Life Technologies), Cy3 (Jackson Immuno) or Alexa Fluor 647 (Life Technologies). Cells were stained with DAPI for 5 min and mounted on glass slides with Prolong gold.

Transfections with Viromer Red and opsin encoding mRNA

All cells were transfected with Viromer Red (Lipocalyx) and mRNA using an adaptation of manufacturer protocols. For each well to be transfected, 500ng of mRNA was added to 25ul of buffer red. Simultaneously, 25ul of buffer red was added to 0.2ul of Viromer Red reagent. Each tube was mixed by pipetting then combined, mixed again, and incubated for 15 minutes at room temperature. The mixture with total volume ~50ul was then added to wells already containing normal media and cells. For increased amounts of mRNA, the ratio of delivery vehicle and mRNA remained constant. A total volume of 50ul of transfection formulation per well was maintained regardless of mRNA amount.

Electrophysiology by MEA

Electrophysiology measurements were performed using a Maestro MEA system (Axion Biosystems) with the capability of simultaneous readout from 48 wells, with 16 electrodes per well. This was coupled with the Lumos device (Axion Biosystems), which possesses 4 fully programmable LEDs per well and sits on top of the Maestro system. Lumos MEA 48 well plates were used for all experiments. The system was set to 37 degrees prior to recordings, and was supplemented with gas containing 5% CO2 with regulated flow. Baseline measurements were taken prior to each recording, which consisted of 5 minutes recording from electrodes without any light excitation. Light excitation and recording control were performed with Axis software (Axion Biosystems). Recordings were taken for a total of 30 minutes per time point from all wells. The neuron or cardiac cell real-time optical stimulation modes were used for each respective cell type. Recordings were analyzed through visual counting during playback. For excitation pulses, neurons were excited at 100% blue LED intensity using a 5ms pulse and 3 second duration between pulses for at least 50 pulses. For NRVMs, a range of intensities was used including 1%, 5%, 10%, 25%, 50%, 75%, and 100% with pulse width 10ms and periods corresponding to 1hz, 2hz, and 3hz.

CHAPTER 5

PERSPECTIVES AND FUTURE DIRECTIONS

This work investigated factors which affect the expression of therapeutic proteins and highlights areas where mRNA can be improved in order to facilitate translation to the clinic. Chapter 2 outlined an imaging metric for the identification of the cytosolic fraction of delivered mRNA which provides superior resolution compared to whole-cell methods of mRNA-protein correlation. This method of labeling mRNA without affecting translation allowed the comparison of delivery methods between a cationic lipid delivery vehicle using the endocytic pathway to enter cells compared to electroporation, which is a direct-to-cytosol route. We highlighted the importance of balancing the correct delivery vehicle with considerations for kinetics of mRNA transport via the respective pathway, sensing by innate immune sensors, and the subsequent formation of stress granules. By reducing stress granule formation through the use of modified nucleotides, we showed that significant improvement in protein production could be made, though this functioned in a delivery and cell type dependent manner.

Chapter 3 built upon the previous chapter on mRNA characterization by examining methods to improve the function of mRNA through improvement of protein production, reduction of innate immunity, and by testing the ability for IVT mRNA to interact with cellular machinery involved in RNA regulation. A number of chemical modifications were compared for both GFP- and luciferase-encoding mRNA. The result was that chemical modifications to a large degree performed by abrogating the formation of stress granules due to reduced sensing by PKR in a sequence dependent manner. The best performing

chemistry, 1mY, showed the highest level of protein expression for both genes as well as no detectable stress granules. However, we found via co-delivery with a small molecule PKR inhibitor that protein expression was increased even with 1mY incorporation into GFP mRNA, indicating that there were still levels of innate immune sensing and thus room for improvement. We also found that N/P ratio is highly important for protein production which was likely related to the amount of mRNA reaching the cytosol. However, the best formulations varied between delivery vehicle and cell type.

We then tested the effects of sequence modifications in the 3' UTR region of the mRNA. We incorporated miRNA sites and found that these sites resulted in significantly reduced protein expression in cells containing matching sequence miRNAs. A future goal of this work is to examine the relation of the copy number of miRNA sites on the mRNA and host miRNAs present in target knockdown cells. These mRNAs can then be tested in a mixed-cell culture to determine if the cell-type specificity is able to achieve adequate knockdown.

We also tested incorporation of different UTR regions from long lived mRNAs including the Sindbis virus polyprotein (99) and human beta globin gene . Unexpectedly, changing the UTR showed differences in initial protein production, which was increased for GFP mRNA containing the human beta globin UTR or miRNA sites. One possible reason for this was the increase in binding sites for the regulatory protein HuR. We performed PLA to examine the association between delivered IVT mRNA and HuR and found that IVT mRNA interacted with HuR. Though differences between mRNAs with modified UTR regions were not apparent, this was the first direct data showing interaction between IVT mRNA and proteins involved in mRNA stability.

In Chapter 4, we applied knowledge from the previous chapters on mRNA design, using 1mY as a modified chemistry as well as formulation with a delivery vehicle at an optimized N/P ratio. We expressed ChR2, an important opsin commonly used in optogenetic research, and subsequently the improved version CatCH, in both primary rat cortical neuronal cultures and primary rat cardiomyocytes. As an alternative to viral vectors, mRNA-based expression of opsins can be used to express opsins in a fast and temporary manner, which expands the range of optogenetic experiments possible. One future aim is to expand the optogenetic toolbox through dual expression of multiple mRNAs for both excitation and inhibition, thus building a control system. As a pilot experiment, we tested the cruxhalorhodopsin JAWS in conjunction with ChR2 in iPS-derived cardiomyocytes, showing that cardiac cell activity could be turned on and off in the same cells (Figure 5.1).

A future goal of this work is to achieve functional expression of these opsins in vivo. However, delivery is a major challenge. As a preliminary experiment, we delivered ChR2 encoding mRNA to the rat cortex via stereotaxic injection with a neurosyringe. Antibody staining for the V5 tag on the protein showed positive expression of the protein near the injection site (Figure 5.2). However, this will require further refinement to achieve functional expression. One issue is damage due to the injection. In vivo experiments using viral vectors to express opsins typically allow up to a month for expression before an experiment can be performed, allowing the brain to heal damage from the injection. Another issue is delivery, as volume limitations result in difficulties in getting enough mRNA-delivery vehicle to the target area, and keeping it there long enough for adequate

transfection to occur. A future goal of this work is to test different delivery vehicles as well as targeting methods such as ultrasound to achieve appropriate transfection as well as reduce off-target effects. Overall, we demonstrate the ability to study fundamental mechanisms necessary to optimize delivery and therapeutic strategies, in order to design the next generation of novel mRNA therapeutics and vaccines.

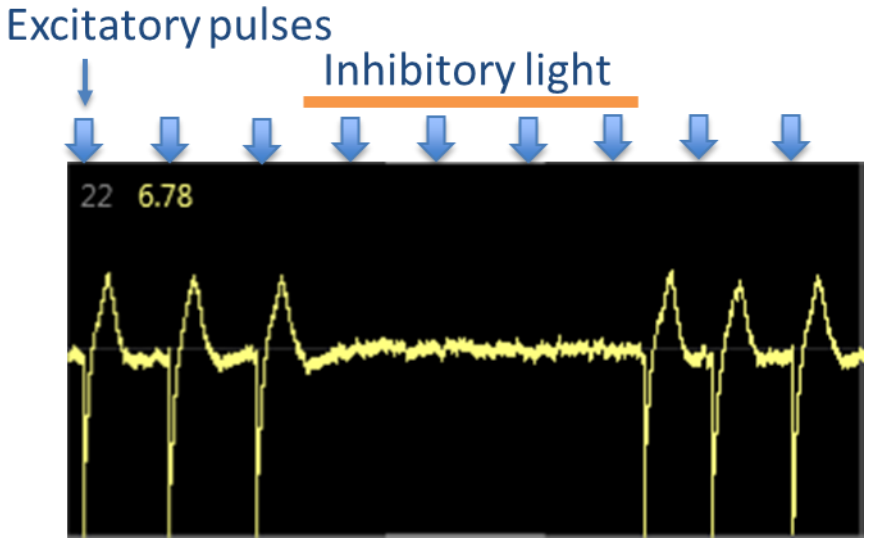

Figure 5.1: Example trace of dual expression of ChR2 and JAWS in cardiomyocytes allows on/off control of beating. 500ng each of ChR2 and JAWS mRNA were delivered to cardiomyocytes in an MEA plate. The next day, cells were paced using pulsed blue light stimulation (blue arrows). At the same time, orange light was used for several seconds (orange bar) to prevent cardiomyocytes from beating. This shows function of both opsins in a dual transfection.

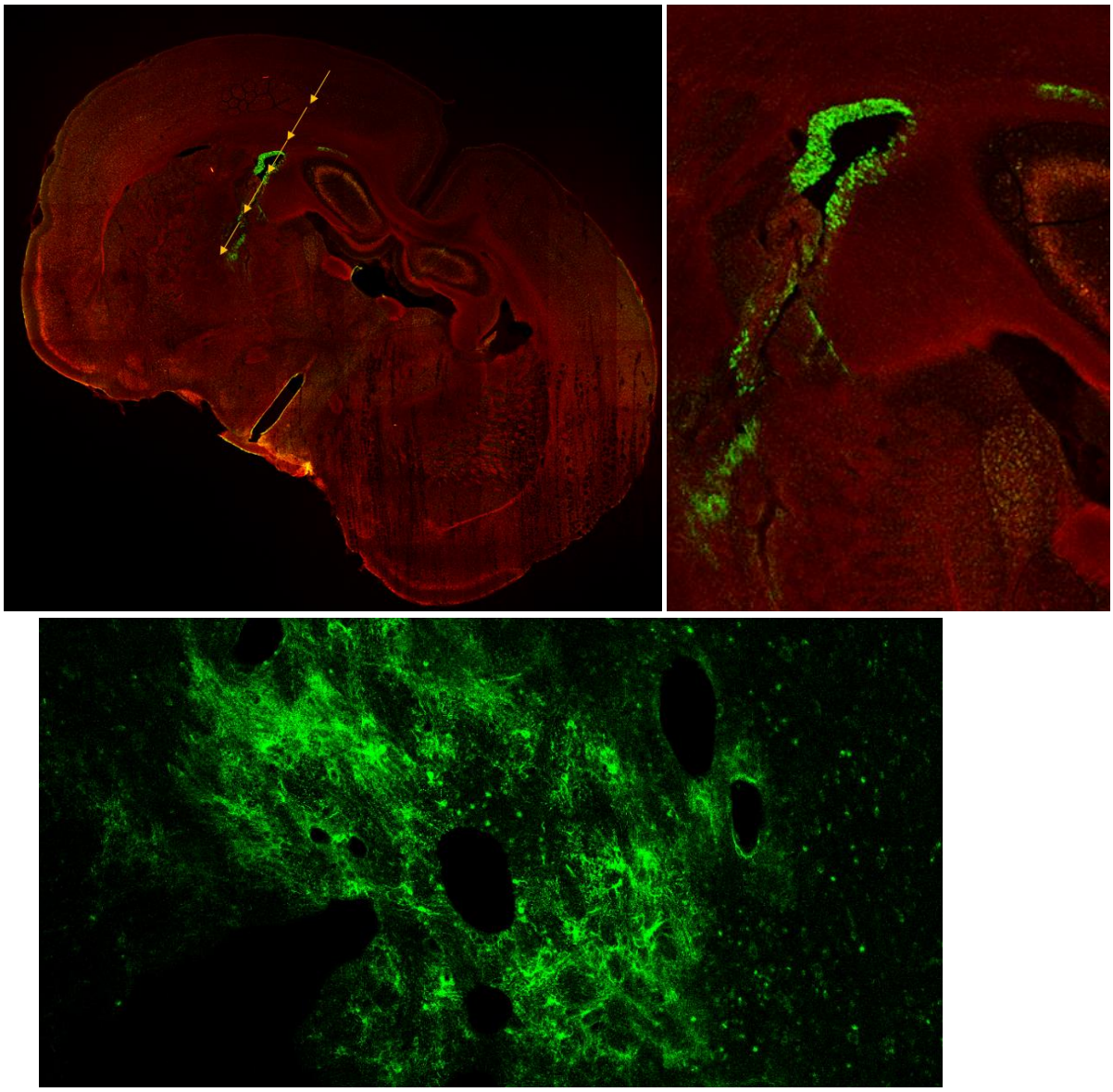

Figure 5.2: Pilot experiment showing protein expression in the rat brain following steoreotaxic injection with ChR2 mRNA. The injection location is depicted by yellow arrows in the left panel. Protein expression (green) is visible along the injection site and along the left ventricle. Nissl stain (red) is used to show neuronal cell types as well as provide contrast. Left panel and right side blow up was taken with 5x objective on a Zeiss LSM 710 confocal microscope. Lower panel was taken at 20x magnification.

REFERENCES

1. Lorenz, C., Fotin-Mleczek, M., Roth, G., Becker, C., Dam, T.C., Verdurmen, W.P.R., Brock, R., Probst, J. and Schlake, T. (2011) Protein expression from exogenous mRNA: Uptake by receptor-mediated endocytosis and trafficking via the lysosomal pathway. *RNA Biology*, **8**, 627-636.

2. Bire, S., Gosset, D., Jegot, G., Midoux, P., Pichon, C. and Rouleux-Bonnin, F. (2013) Exogenous mRNA delivery and bioavailability in gene transfer mediated by piggyBac transposition. *Bmc Biotechnol*, **13**.

3. Kormann, M.S., Hasenpusch, G., Aneja, M.K., Nica, G., Flemmer, A.W., Herber-Jonat, S., Huppmann, M., Mays, L.E., Illenyi, M., Schams, A. *et al.* (2011) Expression of therapeutic proteins after delivery of chemically modified mRNA in mice. *Nat Biotechnol*, **29**, 154-157.

4. Karikó, K., Ni, H., Capodici, J., Lamphier, M. and Weissman, D. (2004) mRNA Is an Endogenous Ligand for Toll-like Receptor 3. *Journal of Biological Chemistry*, **279**, 12542-12550.

5. Muzio, M., Bosisio, D., Polentarutti, N., D'amico, G., Stoppacciaro, A., Mancinelli, R., van't Veer, C., Penton-Rol, G., Ruco, L.P., Allavena, P. *et al.* (2000) Differential expression and regulation of toll-like receptors (TLR) in human leukocytes: Selective expression of TLR3 in dendritic cells. *Journal of Immunology*, **164**, 5998-6004.

6. Diebold, S.S., Kaisho, T., Hemmi, H., Akira, S. and Reis e Sousa, C. (2004) Innate antiviral responses by means of TLR7-mediated recognition of single-stranded RNA. *Science*, **303**, 1529-1531.

7. Larange, A., Antonios, D., Pallardy, M. and Kerdine-Romer, S. (2009) TLR7 and TLR8 agonists trigger different signaling pathways for human dendritic cell maturation. *Journal of Leukocyte Biology*, **85**, 673-683.

8. Rettig, L., Haen, S.P., Bittermann, A.G., von Boehmer, L., Curioni, A., Kramer, S.D., Knuth, A. and Pascolo, S. (2010) Particle size and activation threshold: a new dimension of danger signaling. *Blood*, **115**, 4533-4541.

9. Nair, S.K., Boczkowski, D., Morse, M., Cumming, R.I., Lyerly, H.K. and Gilboa, E. (1998) Induction of primary carcinoembryonic antigen (CEA)-specific cytotoxic T lymphocytes in vitro using human dendritic cells transfected with RNA. *Nat Biotech*, **16**, 364-369.

10. Weissman, D., Ni, H., Scales, D., Dude, A., Capodici, J., McGibney, K., Abdool, A., Isaacs, S.N., Cannon, G. and Karikó, K. (2000) HIV Gag mRNA Transfection of Dendritic Cells (DC) Delivers Encoded Antigen to MHC Class I and II Molecules, Causes DC Maturation, and Induces a Potent Human In Vitro Primary Immune Response. *The Journal of Immunology*, **165**, 4710-4717.

11. Kariko, K., Buckstein, M., Ni, H. and Weissman, D. (2005) Suppression of RNA recognition by Toll-like receptors: the impact of nucleoside modification and the evolutionary origin of RNA. *Immunity*, **23**, 165-175.

12. Hornung, V., Ellegast, J., Kim, S., Brzózka, K., Jung, A., Kato, H., Poeck, H., Akira, S., Conzelmann, K.-K., Schlee, M. *et al.* (2006) 5'-Triphosphate RNA Is the Ligand for RIG-I. *Science*, **314**, 994-997.

13. Nallagatla, S.R. and Bevilacqua, P.C. (2008) Nucleoside modifications modulate activation of the protein kinase PKR in an RNA structure-specific manner. *RNA*, **14**, 1201-1213.

14. Anderson, B.R., Muramatsu, H., Nallagatla, S.R., Bevilacqua, P.C., Sansing, L.H., Weissman, D. and Kariko, K. (2010) Incorporation of pseudouridine into mRNA enhances translation by diminishing PKR activation. *Nucleic Acids Res*, **38**, 5884-5892.

15. Anderson, B.R., Muramatsu, H., Jha, B.K., Silverman, R.H., Weissman, D. and Kariko, K. (2011) Nucleoside modifications in RNA limit activation of 2'-5'-oligoadenylate synthetase and increase resistance to cleavage by RNase L. *Nucleic Acids Research*, **39**, 9329-9338.

16. Karikó, K., Muramatsu, H., Ludwig, J. and Weissman, D. (2011) Generating the optimal mRNA for therapy: HPLC purification eliminates immune activation and improves translation of nucleoside-modified, protein-encoding mRNA. *Nucleic Acids Research*, **39**, e142.

17. Kariko, K., Muramatsu, H., Keller, J.M. and Weissman, D. (2012) Increased Erythropoiesis in Mice Injected With Submicrogram Quantities of Pseudouridine-containing mRNA Encoding Erythropoietin. *Mol Ther*, **20**, 948-953.

18. Koch, S.D., Hong, H., Feyerabend, S., Retz, M., Kuebler, H., Heidenreich, A., van Erps, T., Schroeder, A., Scheel, B., Reus, V. *et al.* (2014) A randomized, double-blind, placebo-controlled, Phase I/II trial of RNActive(®)-vaccine cv9104 in patients with metastatic castrate-refractory prostate cancer (mcrpc): first results of the Phase I part. *Journal for Immunotherapy of Cancer*, **2**, P85-P85.

19. Fotin-Mleczek, M., Zanzinger, K., Heidenreich, R., Lorenz, C., Thess, A., Duchardt, K.M. and Kallen, K.-J. (2012) Highly potent mRNA based cancer vaccines represent an attractive platform for combination therapies supporting an improved therapeutic effect. *The Journal of Gene Medicine*, **14**, 428-439.

20. Rausch, S., Schwentner, C., Stenzl, A. and Bedke, J. (2014) mRNA vaccine CV9103 and CV9104 for the treatment of prostate cancer. *Human Vaccines & Immunotherapeutics*, **10**, 3146-3152.

21. Warren, L., Manos, P.D., Ahfeldt, T., Loh, Y.H., Li, H., Lau, F., Ebina, W., Mandal, P.K., Smith, Z.D., Meissner, A. *et al.* (2010) Highly efficient reprogramming to pluripotency and directed differentiation of human cells with synthetic modified mRNA. *Cell Stem Cell*, **7**, 618-630.

22. Zangi, L., Lui, K.O., von Gise, A., Ma, Q., Ebina, W., Ptaszek, L.M., Spater, D., Xu, H., Tabebordbar, M., Gorbatov, R. *et al.* (2013) Modified mRNA directs the fate of heart progenitor cells and induces vascular regeneration after myocardial infarction. *Nat Biotech*, **31**, 898-907.

23. Tabor, S. and Boyle, A. (2001), *Current Protocols in Immunology*. John Wiley & Sons, Inc.

24. Alexander, S.C., Busby, K.N., Cole, C.M., Zhou, C.Y. and Devaraj, N.K. (2015) Site-Specific Covalent Labeling of RNA by Enzymatic Transglycosylation. *Journal of the American Chemical Society*, **137**, 12756-12759.

25. Rombouts, K., Braeckmans, K. and Remaut, K. (2016) Fluorescent Labeling of Plasmid DNA and mRNA: Gains and Losses of Current Labeling Strategies. *Bioconjugate Chemistry*, **27**, 280-297.

26. Monroy-Contreras, R. and Vaca, L. (2011) Molecular Beacons: Powerful Tools for Imaging RNA in Living Cells. *Journal of Nucleic Acids*, **2011**, 15.

27. Schlake, T., Thess, A., Fotin-Mleczek, M. and Kallen, K.-J. (2012) Developing mRNA-vaccine technologies. *RNA Biology*, **9**, 1319-1330.

28. Nallagatla, S.R. and Bevilacqua, P.C. (2008) Nucleoside modifications modulate activation of the protein kinase PKR in an RNA structure-specific manner. *RNA*, **14**, 1201-1213.

29. Weil, T.T., Parton, R.M. and Davis, I. (2010) Making the message clear: visualizing mRNA localization. *Trends in Cell Biology*, **20**, 380-390.

30. Ligon, T.S., Leonhardt, C. and Rädler, J.O. (2014) Multi-Level Kinetic Model of mRNA Delivery via Transfection of Lipoplexes. *PLoS ONE*, **9**, e107148.

31. Leonhardt, C., Schwake, G., Stögbauer, T.R., Rappl, S., Kuhr, J.-T., Ligon, T.S. and Rädler, J.O. (2014) Single-cell mRNA transfection studies: Delivery, kinetics and statistics by numbers. *Nanomedicine: Nanotechnology, Biology and Medicine*, **10**, 679-688.

32. Sahay, G., Querbes, W., Alabi, C., Eltoukhy, A., Sarkar, S., Zurenko, C., Karagiannis, E., Love, K., Chen, D., Zoncu, R. *et al.* (2013) Efficiency of siRNA

delivery by lipid nanoparticles is limited by endocytic recycling. *Nat Biotech*, **31**, 653-658.

33. Wittrup, A., Ai, A., Liu, X., Hamar, P., Trifonova, R., Charisse, K., Manoharan, M., Kirchhausen, T. and Lieberman, J. (2015) Visualizing lipid-formulated siRNA release from endosomes and target gene knockdown. *Nat Biotech*, **33**, 870-876.

34. Alonas, E., Lifland, A.W., Gudheti, M., Vanover, D., Jung, J., Zurla, C., Kirschman, J., Fiore, V.F., Douglas, A., Barker, T.H. *et al.* (2014) Combining Single RNA Sensitive Probes with Subdiffraction-Limited and Live-Cell Imaging Enables the Characterization of Virus Dynamics in Cells. *ACS Nano*, **8**, 302-315.

35. Lifland, A.W., Zurla, C. and Santangelo, P.J. (2010) Single Molecule Sensitive Multivalent Polyethylene Glycol Probes for RNA Imaging. *Bioconjugate Chemistry*, **21**, 483-488.

36. Lifland, A.W., Zurla, C., Yu, J. and Santangelo, P.J. (2011) Dynamics of native β-actin mRNA transport in the cytoplasm. *Traffic (Copenhagen, Denmark)*, **12**, 1000-1011.

37. Santangelo, P.J., Lifland, A.W., Curt, P., Sasaki, Y., Bassell, G.J., Lindquist, M.E. and Crowe, J.E. (2009) Single molecule-sensitive probes for imaging RNA in live cells. *Nat Meth*, **6**, 347-349.

38. Weibrecht, I., Lundin, E., Kiflemariam, S., Mignardi, M., Grundberg, I., Larsson, C., Koos, B., Nilsson, M. and Soderberg, O. (2013) In situ detection of individual mRNA molecules and protein complexes or post-translational modifications using padlock probes combined with the in situ proximity ligation assay. *Nat Protoc*, **8**, 355-372.

39. Jung, J., Lifland, A.W., Zurla, C., Alonas, E.J. and Santangelo, P.J. (2013) Quantifying RNA–protein interactions in situ using modified-MTRIPs and proximity ligation. *Nucleic Acids Research*, **41**, e12.

40. Lifland, A.W., Jung, J., Alonas, E., Zurla, C., Crowe, J.E. and Santangelo, P.J. (2012) Human Respiratory Syncytial Virus Nucleoprotein and Inclusion Bodies Antagonize the Innate Immune Response Mediated by MDA5 and MAVS. *Journal of Virology*, **86**, 8245-8258.

41. Wigington, C.P., Jung, J., Rye, E.A., Belauret, S.L., Philpot, A.M., Feng, Y., Santangelo, P.J. and Corbett, A.H. (2015) Post-transcriptional Regulation of Programmed Cell Death 4 (PDCD4) mRNA by the RNA-binding Proteins Human Antigen R (HuR) and T-cell Intracellular Antigen 1 (TIA1). *Journal of Biological Chemistry*, **290**, 3468-3487.

42. Cui, S., Wang, B., Zhao, Y., Chen, H., Ding, H., Zhi, D. and Zhang, S. (2014) Transmembrane routes of cationic liposome-mediated gene delivery using human throat epidermis cancer cells. *Biotechnology Letters*, **36**, 1-7.

43. Buxbaum, A.R., Haimovich, G. and Singer, R.H. (2015) In the right place at the right time: visualizing and understanding mRNA localization. *Nat Rev Mol Cell Biol*, **16**, 95-109.

44. Rejman, J., Bragonzi, A. and Conese, M. (2005) Role of clathrin- and caveolae-mediated endocytosis in gene transfer mediated by lipo- and polyplexes. *Mol Ther*, **12**, 468-474.

45. Soderberg, O., Gullberg, M., Jarvius, M., Ridderstrale, K., Leuchowius, K.J., Jarvius, J., Wester, K., Hydbring, P., Bahram, F., Larsson, L.G. *et al.* (2006) Direct observation of individual endogenous protein complexes in situ by proximity ligation. *Nat Methods*, **3**, 995-1000.

46. Koos, B., Andersson, L., Clausson, C.M., Grannas, K., Klaesson, A., Cane, G. and Soderberg, O. (2014) Analysis of protein interactions in situ by proximity ligation assays. *Curr Top Microbiol Immunol*, **377**, 111-126.

47. Leuchowius, K.J., Weibrecht, I. and Soderberg, O. (2011) In situ proximity ligation assay for microscopy and flow cytometry. *Curr Protoc Cytom*, **Chapter 9**, Unit 9 36.

48. Soderberg, O., Leuchowius, K.J., Gullberg, M., Jarvius, M., Weibrecht, I., Larsson, L.G. and Landegren, U. (2008) Characterizing proteins and their interactions in cells and tissues using the in situ proximity ligation assay. *Methods*, **45**, 227-232.

49. Jung, J., Lifland, A.W., Alonas, E.J., Zurla, C. and Santangelo, P.J. (2013) Characterization of mRNA-Cytoskeleton Interactions <italic>In Situ</italic> Using FMTRIP and Proximity Ligation. *PLoS ONE*, **8**, e74598.

50. Wasungu, L. and Hoekstra, D. (2006) Cationic lipids, lipoplexes and intracellular delivery of genes. *Journal of Controlled Release*, **116**, 255-264.

51. Vaughan, E.E. and Dean, D.A. (2006) Intracellular trafficking of plasmids during transfection is mediated by microtubules. *Molecular therapy : the journal of the American Society of Gene Therapy*, **13**, 422-428.

52. Heinicke, L.A., Nallagatla, S.R., Hull, C.M. and Bevilacqua, P.C. (2011) RNA helical imperfections regulate activation of the protein kinase PKR: effects of bulge position, size, and geometry. *RNA*, **17**, 957-966.

53. Toroney, R. and Bevilacqua, P.C. (2009) PKR and the ribosome compete for mRNA. *Nat Chem Biol*, **5**, 873-874.

54. Toroney, R., Hull, C.M., Sokoloski, J.E. and Bevilacqua, P.C. (2012) Mechanistic characterization of the 5'-triphosphate-dependent activation of PKR: lack of 5'-end nucleobase specificity, evidence for a distinct triphosphate binding site, and a critical role for the dsRBD. *RNA*, **18**, 1862-1874.

55. Toroney, R., Nallagatla, S.R., Boyer, J.A., Cameron, C.E. and Bevilacqua, P.C. (2010) Regulation of PKR by HCV IRES RNA: importance of domain II and NS5A. *J Mol Biol*, **400**, 393-412.

56. Anderson, P. and Kedersha, N. (2008) Stress granules: the Tao of RNA triage. *Trends in Biochemical Sciences*, **33**, 141-150.

57. Buchan, J.R., Kolaitis, R.-M., Taylor, J.P. and Parker, R. (2013) Eukaryotic stress granules are cleared by granulophagy and Cdc48/VCP function. *Cell*, **153**, 1461-1474.

58. Buchan, J.R. and Parker, R. (2009) Eukaryotic Stress Granules: The Ins and Out of Translation. *Molecular cell*, **36**, 932.

59. Zurla, C., Lifland, A.W. and Santangelo, P.J. (2011) Characterizing mRNA Interactions with RNA Granules during Translation Initiation Inhibition. *PLoS ONE*, **6**, e19727.

60. Mayor, S. and Pagano, R.E. (2007) Pathways of clathrin-independent endocytosis. *Nat Rev Mol Cell Biol*, **8**, 603-612.

61. Loomis, K., Smith, B., Feng, Y., Garg, H., Yavlovich, A., Campbell-Massa, R., Dimitrov, D.S., Blumenthal, R., Xiao, X. and Puri, A. (2010) Specific targeting to B cells by lipid-based nanoparticles conjugated with a novel CD22-ScFv. *Exp Mol Pathol*, **88**, 238-249.

62. Roberts, R.L., Barbieri, M.A., Ullrich, J. and Stahl, P.D. (2000) Dynamics of rab5 activation in endocytosis and phagocytosis. *Journal of Leukocyte Biology*, **68**, 627-632.

63. Bampton, E.T., Goemans, C.G., Niranjan, D., Mizushima, N. and Tolkovsky, A.M. (2005) The dynamics of autophagy visualized in live cells: from autophagosome formation to fusion with endo/lysosomes. *Autophagy*, **1**, 23-36.

64. Das, S. and Pellett, P.E. (2011) Spatial Relationships between Markers for Secretory and Endosomal Machinery in Human Cytomegalovirus-Infected Cells versus Those in Uninfected Cells. *Journal of Virology*, **85**, 5864-5879.

65. Loomis, K.H., Kirschman, J.L., Bhosle, S., Bellamkonda, R.V. and Santangelo, P.J. (2016) Strategies for modulating innate immune activation and protein production of in vitro transcribed mRNAs. *Journal of Materials Chemistry B*, **4**, 1619-1632.

66. Mehier-Humbert, S. and Guy, R.H. (2005) Physical methods for gene transfer: Improving the kinetics of gene delivery into cells. *Advanced Drug Delivery Reviews*, **57**, 733-753.

67. Santangelo, P.J., Alonas, E., Jung, J., Lifland, A.W. and Zurla, C. (2012) Probes for intracellular RNA imaging in live cells. *Methods in enzymology*, **505**, 383.

68. Muller-McNicoll, M. and Neugebauer, K.M. (2013) How cells get the message: dynamic assembly and function of mRNA-protein complexes. *Nat Rev Genet*, **14**, 275-287.

69. Gonatopoulos-Pournatzis, T. and Cowling, Victoria H. (2014) Cap-binding complex (CBC). *Biochemical Journal*, **457**, 231-242.

70. Gerstberger, S., Hafner, M. and Tuschl, T. (2014) A census of human RNA-binding proteins. *Nat Rev Genet*, **15**, 829-845.

71. Blower, M.D. (2013) Molecular insights into intracellular RNA localization. *International review of cell and molecular biology*, **302**, 1-39.

72. Reid, D.W. and Nicchitta, C.V. (2012) Primary Role for Endoplasmic Reticulum-bound Ribosomes in Cellular Translation Identified by Ribosome Profiling. *The Journal of biological chemistry*, **287**, 5518-5527.

73. Zheng, G.Q., Dahl, J.A., Niu, Y.M., Fu, Y., Klungland, A., Yang, Y.G. and He, C. (2013) Sprouts of RNA epigenetics The discovery of mammalian RNA demethylases. *Rna Biology*, **10**, 915-918.

74. Andries, O., Mc Cafferty, S., De Smedt, S.C., Weiss, R., Sanders, N.N. and Kitada, T. (2015) N1-methylpseudouridine-incorporated mRNA outperforms pseudouridine-incorporated mRNA by providing enhanced protein expression and reduced immunogenicity in mammalian cell lines and mice. *Journal of Controlled Release*, **217**, 337-344.

75. Thess, A., Grund, S., Mui, B.L., Hope, M.J., Baumhof, P., Fotin-Mleczek, M. and Schlake, T. (2015) Sequence-engineered mRNA Without Chemical Nucleoside Modifications Enables an Effective Protein Therapy in Large Animals. *Molecular Therapy*, **23**, 1456-1464.

76. Brennan, C.M. and Steitz*, J.A. (2001) HuR and mRNA stability. *Cellular and Molecular Life Sciences CMLS*, **58**, 266-277.

77. Xu, Y.Z., Di Marco, S., Gallouzi, I., Rola-Pleszczynski, M. and Radzioch, D. (2005) RNA-Binding Protein HuR Is Required for Stabilization of SLC11A1 mRNA and SLC11A1 Protein Expression. *Molecular and Cellular Biology*, **25**, 8139-8149.

78. Schlake, T., Thess, A., Fotin-Mleczek, M. and Kallen, K.J. (2012) Developing mRNA-vaccine technologies. *RNA Biol*, **9**, 1319-1330.

79. Duan, J.B., Shi, J.X., Ge, X.J., Dolken, L., Moy, W., He, D.L., Shi, S., Sanders, A.R., Ross, J. and Gejman, P.V. (2013) Genome-wide survey of interindividual differences of RNA stability in human lymphoblastoid cell lines. *Sci Rep-Uk*, **3**.

80. Saunders, R. and Deane, C.M. (2010) Synonymous codon usage influences the local protein structure observed. *Nucleic Acids Research*, **38**, 6719-6728.

81. Plotkin, J.B. and Kudla, G. (2011) Synonymous but not the same: the causes and consequences of codon bias. *Nat Rev Genet*, **12**, 32-42.

82. Ngumbela, K.C., Ryan, K.P., Sivamurthy, R., Brockman, M.A., Gandhi, R.T., Bhardwaj, N. and Kavanagh, D.G. (2008) Quantitative Effect of Suboptimal Codon Usage on Translational Efficiency of mRNA Encoding HIV-1 gag in Intact T Cells. *Plos One*, **3**.

83. Fath, S., Bauer, A.P., Liss, M., Spriestersbach, A., Maertens, B., Hahn, P., Ludwig, C., Schafer, F., Graf, M. and Wagner, R. (2011) Multiparameter RNA and Codon Optimization: A Standardized Tool to Assess and Enhance Autologous Mammalian Gene Expression. *Plos One*, **6**.

84. Gustafsson, C., Govindarajan, S. and Minshull, J. (2004) Codon bias and heterologous protein expression. *Trends Biotechnol*, **22**, 346-353.

85. Gustafsson, C., Minshull, J., Govindarajan, S., Ness, J., Villalobos, A. and Welch, M. (2012) Engineering genes for predictable protein expression. *Protein Expres Purif*, **83**, 37-46.

86. Griswold, K.E., Mahmood, N.A., Iverson, B.L. and Georgiou, G. (2003) Effects of codon usage versus putative 5 '-mRNA structure on the expression of Fusarium solani cutinase in the Escherichia coli cytoplasm. *Protein Expres Purif*, **27**, 134-142.

87. Lindquist, M.E., Mainou, B.A., Dermody, T.S. and Crowe, J.E. (2011) Activation of protein kinase R is required for induction of stress granules by respiratory syncytial virus but dispensable for viral replication. *Virology*, **413**, 103-110.

88. Xiao, J., Tan, Y., Li, Y. and Luo, Y. (2016) The Specific Protein Kinase R (PKR) Inhibitor C16 Protects Neonatal Hypoxia-Ischemia Brain Damages by Inhibiting Neuroinflammation in a Neonatal Rat Model. *Medical Science Monitor : International Medical Journal of Experimental and Clinical Research*, **22**, 5074-5081.

89. Démoulins, T., Milona, P., Englezou, P.C., Ebensen, T., Schulze, K., Suter, R., Pichon, C., Midoux, P., Guzmán, C.A., Ruggli, N. *et al.* (2016) Polyethylenimine-based polyplex delivery of self-replicating RNA vaccines. *Nanomedicine: Nanotechnology, Biology and Medicine*, **12**, 711-722.

90. Zhao, Q.-Q., Chen, J.-L., Lv, T.-F., He, C.-X., Tang, G.-P., Liang, W.-Q., Tabata, Y. and Gao, J.-Q. (2009) N/P Ratio Significantly Influences the Transfection Efficiency and Cytotoxicity of a Polyethylenimine/Chitosan/DNA Complex. *Biological and Pharmaceutical Bulletin*, **32**, 706-710.

91. Jovičić, A., Roshan, R., Moisoi, N., Pradervand, S., Moser, R., Pillai, B. and Luthi-Carter, R. (2013) Comprehensive Expression Analyses of Neural Cell-Type-Specific miRNAs Identify New Determinants of the Specification and Maintenance of Neuronal Phenotypes. *The Journal of Neuroscience*, **33**, 5127-5137.

92. Entcheva, E. (2013) Cardiac optogenetics. *American Journal of Physiology - Heart and Circulatory Physiology*, **304**, H1179-H1191.

93. Ambrosi, C.M. and Entcheva, E. (2014) In Radisic, M. and Black Iii, L. D. (eds.), *Cardiac Tissue Engineering: Methods and Protocols*. Springer New York, New York, NY, pp. 215-228.

94. Whitmire, C.J., Waiblinger, C., Schwarz, C. and Stanley, G.B. (2016) Information Coding Through Adaptive Gating of Synchronized Thalamic Bursting. *Cell reports*, **14**, 795-807.

95. Lin, J.Y. (2012) Optogenetic excitation of neurons with channelrhodopsins. *Progress in Brain Research*, **196**, 29-47.

96. Mattis, J., Tye, K.M., Ferenczi, E.A., Ramakrishnan, C., O'Shea, D.J., Prakash, R., Gunaydin, L.A., Hyun, M., Fenno, L.E., Gradinaru, V. *et al.* (2012) Principles for applying optogenetic tools derived from direct comparative analysis of microbial opsins. *Nature methods*, **9**, 159-172.

97. Chuong, A.S., Miri, M.L., Busskamp, V., Matthews, G.A.C., Acker, L.C., Sorensen, A.T., Young, A., Klapoetke, N.C., Henninger, M.A., Kodandaramaiah, S.B. *et al.* (2014) Noninvasive optical inhibition with a red-shifted microbial rhodopsin. *Nat Neurosci*, **17**, 1123-1129.

98. Kleinlogel, S., Feldbauer, K., Dempski, R.E., Fotis, H., Wood, P.G., Bamann, C. and Bamberg, E. (2011) Ultra light-sensitive and fast neuronal activation with the Ca2+-permeable channelrhodopsin CatCh. *Nat Neurosci*, **14**, 513-518.

99. Johanning, F.W., Conry, R.M., LoBuglio, A.F., Wright, M., Sumerel, L.A., Pike, M.J. and Curiel, D.T. (1995) A Sindbis virus mRNA polynucleotide vector achieves prolonged and high level heterologous gene expression in vivo. *Nucleic Acids Research*, **23**, 1495-1501.